Cell

HLA export by melanoma cells decoys cytotoxic T cells to promote immune evasion

Graphical abstract

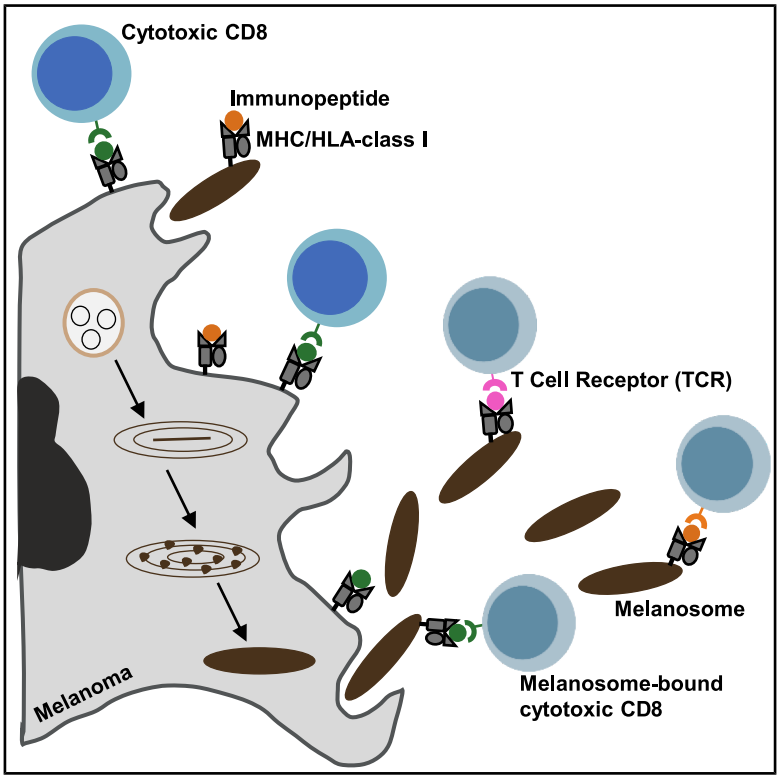

Highlights

- Melanoma melanosomes display MHC molecules that directly engage CD8$^+$ T cell receptors
- Melanosomes carry potent MHC-tumor antigens that compete with tumor cells for TCR binding
- Melanosome-TCR engagement drives T cell mitochondrial dysfunction and apoptosis
- Blocking melanosome release enhances CD8$^+$ T cell infiltration and limits tumor growth

Authors

Yoav Chemla, Orit Itzhaki, Stav Melamed, ..., Shivang Parikh, Yardena Samuels, Carmit Levy

Correspondence

mehdi.khaled@gustaveroussy.fr (M.K.), pierre.close@uliege.be (P.C.), ronnie.shapira@sheba.health.gov.il (R.S.), sebastien.apcher@gustaveroussy.fr (S.A.), asafmadi@tauex.tau.ac.il (A.M.), mitchell.levesque@usz.ch (M.P.L.), francesca.rapino@uliege.be (F.R.), yaroncarmi@gmail.com (Y.C.), ssparikh@mgh.harvard.edu (S.P.), carmitlevy@tauex.tau.ac.il (C.L.), yardena.samuels@weizmann.ac.il (Y.S.)

In brief

Melanoma cells escape immune surveillance by releasing MHC-antigen-loaded large EVs, known as melanosomes, that directly engage and impair CD8$^+$ T cell receptors.

Chemla et al., 2026, Cell *189*, 1–19
January 8, 2026
https://doi.org/10.1016/j.cell.2025.11.020

CellPress

Please cite this article in press as: Chemla et al., HLA export by melanoma cells decoys cytotoxic T cells to promote immune evasion, Cell (2026), https://doi.org/10.1016/j.cell.2025.11.020

Cell

CellPress
OPEN ACCESS

Article

HLA export by melanoma cells decoys cytotoxic T cells to promote immune evasion

Yoav Chemla,[1,30] Orit Itzhaki,[1,2,30] Stav Melamed,[1,30] Chen Weller,[3,30] Yuval Sade,[1,30] Paulee Manich,[1,30] Keren Reshef,[4,30] Nicolas Xenidis,[1,30] Avishai Maliah,[1,30] Gilad Levy,[5,31] Roma Parikh,[1,31] Osnat Bartok,[3,31] Opal Levy,[1,31] Itay Tal,[1,31] Gal Aziel,[1,31] Abraham Nissani,[2,31] Sharon Yunger,[2,31] Daniela Likonen,[6,31] Vitaly Kliminsky,[6,31] Tamar Golan,[1,31] Coralie Capron,[7,31] Valentina Ace,[1,31] Ronen Levy,[3,31] Diana Rasoulouniriana,[4] Zohar Eyal,[8] Yuval Barzilay,[8] Roi Balaban,[9] Aseel Khateeb,[4] Rami Khosravi,[10] Amir Grau,[11] Tamar Ziv,[12] Polina Greenberg,[3] Dvir Netanely,[13] Hananya Vaknin,[14] Xunwei Wu,[15] Yael Amitay,[16] Ronen Brenner,[14] Julia María Martínez Gómez,[7]

(Author list continued on next page)

[1]Department of Human Genetics and Biochemistry, Gray Faculty of Medical and Health Sciences, Tel Aviv University, Tel Aviv 69978, Israel
[2]Ella Lemelbaum Institute for Immuno-Oncology and Melanoma, Sheba Medical Center, Ramat Gan 52621, Israel
[3]Department of Molecular Cell Biology, Weizmann Institute of Science, Rehovot, Israel
[4]Department of Pathology, Gray Faculty of Medical and Health Sciences, Tel Aviv University, Tel Aviv 69978, Israel
[5]Sagol School of Neuroscience, Tel Aviv University, Tel Aviv, Israel
[6]Department of Dermatology, Sheba Medical Center, Ramat Gan, Israel
[7]Laboratory of Cancer Stemness, GIGA Institute, University of Liège, Liège, Belgium
[8]Department of Molecular Genetics, Weizmann Institute of Science, Rehovot 76100, Israel
[9]Department of Clinical Microbiology and Immunology, Gray Faculty of Medical and Health Sciences, Tel Aviv University, Tel Aviv, Israel
[10]Single Cell Genomics Core, Gray Faculty of Medical and Health Sciences, Tel Aviv University, Tel Aviv, Israel
[11]Biomedical Core Facility, Rappaport Faculty of Medicine, Technion-Israel Institute of Technology, Haifa, Israel
[12]Smoler Proteomics Center, Lokey Interdisciplinary Center for Life Sciences & Engineering, Technion-Israel Institute of Technology, Haifa, Israel
[13]Blavatnik School of Computer Science and Artificial Intelligence, Tel Aviv University, Tel Aviv, Israel
[14]Institute of Oncology, E. Wolfson Medical Center, Holon, Israel
[15]Department of Dermatology, Massachusetts General Hospital, Boston, MA, USA
[16]Department of Molecular Cell Biology, Weizmann Institute of Science, Tel Aviv, Israel
[17]Institute of Pathology, Tel Aviv Sourasky Medical Center, Tel Aviv, Israel
[18]Metabolic Center, Sheba Medical Center, Tel-Hashomer, Ramat Gan, Israel
[19]Bio-Imaging Unit, Hebrew University, Jerusalem 91904, Israel
[20]Department of Immunology and Regenerative Biology, Weizmann Institute of Science, Rehovot, Israel
[21]Hadassah Cancer Research Institute, Hadassah Hebrew University Hospital, Jerusalem, Israel
[22]The School of Psychological Sciences, Tel Aviv University, Tel Aviv, Israel

(Affiliations continued on next page)

SUMMARY

While melanoma cells often express a high burden of mutated proteins, the infiltration of reactive T cells rarely results in tumor-eradicating immunity. We discovered that large extracellular vesicles, known as melanosomes, secreted by melanoma cells are decorated with major histocompatibility complex (MHC) molecules that stimulate $CD8^+$ T cells through their T cell receptor (TCR), causing T cell dysfunction and apoptosis. Immunopeptidomic and T cell receptor sequencing (TCR-seq) analyses revealed that these melanosomes carry MHC-bound tumor-associated antigens with higher affinity and immunogenicity, which compete with their tumor cell of origin for direct TCR-MHC interactions. Analysis of biopsies from melanoma patients confirmed that melanosomes trap infiltrating lymphocytes, induce partial activation, and decrease $CD8^+$ T cell cytotoxicity. Inhibition of melanosome secretion *in vivo* significantly reduced tumor immune evasion. These findings suggest that MHC export protects melanoma from the cytotoxic effects of T cells. Our study highlights a novel immune evasion mechanism and proposes a therapeutic avenue to enhance tumor immunity.

INTRODUCTION

Cytotoxic T cell infiltration into the tumor microenvironment (TME) correlates with improved clinical outcomes, and immunotherapies aim to harness this immunity.[1,2] Current strategies include expansion of tumor-infiltrating lymphocytes (TILs),[3] engineered T cells,[4,5] and checkpoint blockade.[6,7]

Please cite this article in press as: Chemla et al., HLA export by melanoma cells decoys cytotoxic T cells to promote immune evasion, Cell (2026), https://doi.org/10.1016/j.cell.2025.11.020

Dov Hershkovitz,[17] Tal Yardeni,[18] Valentina Zemser-Werner,[17] Oren Kobiler,[9] Yael Friedmann,[19] David Bassan,[20] Ron Shamir,[13] Lea Eisenbach,[20] Nadine Santana-Magal,[4] Michael Milyavsky,[4] Galit Eisenberg,[21] Leeat Keren,[16] Merav Cohen,[9] Dvir Gur,[8] Boaz Barak,[5,22] Michal Lotem,[21] David Sprinzak,[23] Shoshana Greenberger,[9] David Fisher,[15] Michal J. Besser,[2,9,24,25] Mehdi Khaled,[26,*] Pierre Close,[27,*] Ronnie Shapira,[2,*] Sebastien Apcher,[26,*] Asaf Madi,[4,*] Mitchell P. Levesque,[28,*] Francessca Rapino,[7,*] Yaron Carmi,[4,*] Shivang Parikh,[1,29,*] Yardena Samuels,[3,*] and Carmit Levy[1,32,*]

[23]School of Neurobiology, Biochemistry and Biophysics, George S. Wise Faculty of Life Sciences, Tel Aviv University, Tel Aviv 6997801, Israel
[24]Samueli Integrative Pioneering Institute and Davidoff Center, Rabin Medical Center, Petach Tikva, Israel
[25]Felsenstein Cancer Research Center, Gray Faculty of Medical and Health Sciences, Tel Aviv University, Tel Aviv, Israel
[26]Gustave Roussy Cancer Campus, INSERM U1015, Universite Paris-Saclay, 114 rue Edouard Vaillant, 94800 Villejuif, France
[27]Laboratory of Cancer Signaling, GIGA Institute, University of Liège, Liège, Belgium
[28]University of Zurich, Faculty of Medicine, University Hospital of Zurich, Department of Dermatology, Schlieren 8952, Switzerland
[29]Ragon Institute of Mass General, MIT and Harvard, Cambridge, MA, USA
[30]Senior author
[31]These authors contributed equally
[32]Lead contact
*Correspondence: mehdi.khaled@gustaveroussy.fr (M.K.), pierre.close@uliege.be (P.C.), ronnie.shapira@sheba.health.gov.il (R.S.), sebastien.apcher@gustaveroussy.fr (S.A.), asafmadi@tauex.tau.ac.il (A.M.), mitchell.levesque@usz.ch (M.P.L.), francesca.rapino@uliege.be (F.R.), yaroncarmi@gmail.com (Y.C.), ssparikh@mgh.harvard.edu (S.P.), yardena.samuels@weizmann.ac.il (Y.S.), carmitlevy@tauex.tau.ac.il (C.L.)
https://doi.org/10.1016/j.cell.2025.11.020

Melanoma, the deadliest human skin cancer, with 100,000 new cases per year,[8,9] remains the prototypical model for cancer immunotherapy.[10] Yet, ~50% of patients are resistant to treatment,[11–14] despite tumor expression of altered or neoantigens[15,16] recognized by TILs.[17] The mechanisms underlying this immune evasion remain incompletely understood.

Melanosomes, large extracellular vesicles (200–500 nm) unique to melanocytes,[18] transport melanin pigment to neighboring cells as a key protector of skin cells against UV-induced DNA damage.[19,20] Melanosomes differ from exosomes in lineage restriction and cargo composition.[21] We previously showed that melanoma-derived melanosomes drive fibroblast transformation, lymphomagenesis, macrophage diversification, and drug resistance.[21–24] Further, melanosomes contribute to melanoma drug resistance by exporting chemotherapeutic agents.[25] Clinically, melanosome production varies with disease stage,[26] active melanogenesis reduces survival,[27–29] and melanosome proteins are recognized by T cells in vitiligo.[30–33] Yet, whether melanosomes directly modulate T cell function is unknown.

Memory or naive $CD8^+$ T cells express T cell receptors (TCRs) that recognize tumor-associated or neoantigen peptides displayed by major histocompatibility complex (MHC) class I molecules.[34] In humans, the human leukocyte antigen (HLA)-A, HLA-B, and HLA-C loci encode the heavy chains of class I MHCs, while in mice the homologs are encoded by the H2K, H2D, and H2L loci.[35,36] T cell activation involves three signals: signal 1 is the interaction between the TCR and MHC class I) on an antigen-presenting cell or a tumor cell, and signal 2 is the interaction of CD28 on the T cell with B7-1/B7-2 (also known as CD80 and CD86) on the antigen-presenting cell or tumor cell,[37] and once signal 2 occurs, T cells secrete granzyme B and interleukin-2 (IL-2), collectively known as signal 3. If the interaction with B7-1/B7-2 is weak or absent, or if PD-1 or CTLA-4 bind B7-1/B7-2 instead of CD28, T cells undergo tolerance, anergy, or apoptosis.[38–40]

In this study, we identify a novel mechanism of melanoma immune evasion. Melanosomes bind $CD8^+$ T cells and suppress their activity in a TCR/antigen-dependent manner. Non-responder TILs were surrounded by pigment, unlike those of responders. In co-culture, melanosomes blocked interferon (IFN)γ and granzyme B secretion, reducing T cell cytotoxicity, while inhibition of melanosome release in mice enhanced $CD8^+$ infiltration and restrained tumor growth. Proteomic, imaging, and immunopeptidomic analyses revealed that melanoma melanosomes are enriched in immune-related proteins and carry HLA molecules, enabling melanoma to secrete HLA that engages TCRs and competes with tumor cells for T cell recognition. TCR sequencing (TCR-seq) further showed that TILs from non-responders share more clonotypes between melanosomes and melanoma cells compared with responders, indicating direct competition between melanosomes and tumor cells for T cell engagement. Mechanistically, melanosomes delivered incomplete activation signals, reduced mitochondrial activity, and induced $CD8^+$ T cell apoptosis. These findings identify melanoma-derived melanosomes as active mediators of immune evasion and potential therapeutic targets.

RESULTS

The presence of melanosomes correlates with poor prognosis, lack of response to immunotherapy, and decreased T cell cytotoxicity

We previously showed that melanosomes are secreted near melanoma cells and that expression of melanosome-associated enzymes correlates with poor prognosis in melanoma patients,[21] a finding corroborated by others.[28] Using TCGA data,[41] we identified a melanosome-related gene signature (n = 384 genes) whose expression was inversely correlated with recurrence and survival (Figures S1A and S1B; Table S1). Analysis of published transcriptomic data[27] further revealed that melanin production and melanosome-related processes are significantly

Please cite this article in press as: Chemla et al., HLA export by melanoma cells decoys cytotoxic T cells to promote immune evasion, Cell (2026), https://doi.org/10.1016/j.cell.2025.11.020

CellPress
OPEN ACCESS

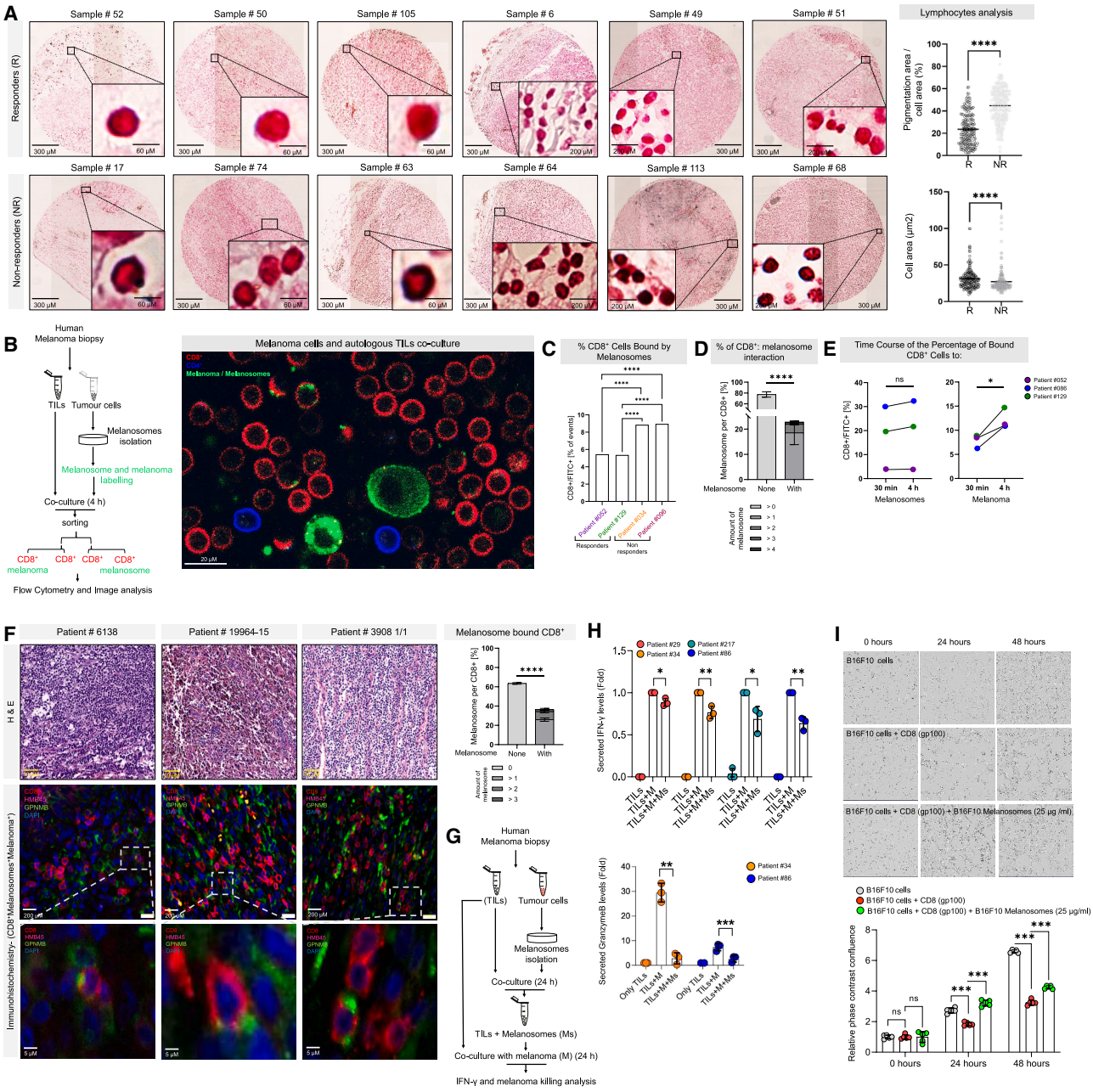

Figure 1. The presence of melanosomes correlates with poor prognosis, lack of response to immunotherapy, and decreased T cell cytotoxicity

(A) Left: images of melanin-stained FFPE tissue from representative responders (R) and non-responders (NR) melanoma patients. Right: percent of pigmentation area per cell area and cell area (μm^2). $^{****}p < 0.0001$; two-tailed *t* tests.

(B) Left: experimental scheme. Right: representative confocal microscopy shows $CD8^+$ (red) and $CD4^+$ (blue) T cells and tumor cells or melanosomes (both labeled green). Scale bar, 20 µM.

(C) Percent of $CD8^+$ T cells (by FACS) bound by melanosomes isolated from human melanoma biopsies of responder and non-responder patients co-cultured as in (B). $n = 4$. $^{****}p < 0.0001$; chi-square tests.

(D) Percent of $CD8^+$ T cells (by confocal microscopy) bound by melanosomes isolated from human melanoma biopsy patients co-cultured as in (B). Shades of gray: number of melanosomes per one $CD8^+$ T cell. $n = 3$ patients. $^{****}p < 0.0001$; Kruskal-Wallis test. Error bars ± SEM.

(E) Percent of $CD8^+$ T cells (by flow cytometry) bound by melanoma cells or melanosomes after 30 min and 4 h co-culturing. ($n = 3$). $^{*}p < 0.05$; paired *t* test.

(legend continued on next page)

Please cite this article in press as: Chemla et al., HLA export by melanoma cells decoys cytotoxic T cells to promote immune evasion, Cell (2026), https://doi.org/10.1016/j.cell.2025.11.020

downregulated in patients responding to immune checkpoint inhibitors (Figures S1E and S1F; Table S2).

We next evaluated pigment distribution in metastatic melanoma samples (n = 69) (Table S3) and found significantly more pigment-loaded T cells in poor immunotherapy responders than in good responders ($p < 0.0001$) (Figures 1A and S1C). Melanin-associated T cells in non-responders were also smaller, consistent with T cell exhaustion.[42] Supporting this, spatial proteomics data[43] (n = 18) showed that higher tumor expression of Melan-A (melanosome marker[44]) correlated with increased TIM3$^+$ exhausted T cells (R = 0.43, p = 0.07), whereas SOX10, a neural crest protein and a melanoma marker that is not present on melanosomes,[8] expression did not (R = 0.17, p = 0.49) (Figure S1D). Together, these data suggest that melanosomes directly interact with lymphocytes in the TME and impair their function.

Since the abundance and spatial distribution of tumor-infiltrating CD8$^+$ T cells reflect immune response effectiveness,[45] we hypothesized that melanosomes might specifically interact with CD8$^+$ T cells. To test this, we analyzed melanosome-bound T cells in TIL therapy responders and non-responders using patient samples from the Biobank of the Ella Lemelbaum Institute, Sheba Medical Center (Figure 1B, right). Melanosomes isolated from melanoma cultures (Figure S1G) were incubated with autologous TILs for 4 h. Consistent with pathology findings, a significantly greater percentage of TILs were bound by melanosomes in non-responders than in responders (Figures 1C and S1H). Imaging and fluorescence-activated cell sorting (FACS) analyses showed that 15%–35% of TILs carried melanosomes (Figures 1B and S1I–S1K), typically 1–4 melanosomes per CD8$^+$ T cell (Figures 1D, 1F, right, S1L, and S1O). As immune synapse formation occurs within 30 min,[46] we examined interaction dynamics and found that melanosomes bound CD8$^+$ T cells within 30 min and remained stable over 4 h, whereas binding to melanoma cells increased gradually (Figures 1E and S1M). We further estimated that a melanoma cell secretes ~40 melanosomes per day (Figure S1N). Thus, melanosome-CD8$^+$ interactions resemble immunologic synapse dynamics and may be more efficient than direct CD8$^+$ T cell-melanoma interactions.

To examine melanosome-CD8$^+$ T cell interactions in the TME, we immunostained lymph node metastases from six melanoma patients for melanoma cells (HMB-45), melanosomes (GPNMB^a), and CD8$^+$ T cells. Melanosomes were detected on the surfaces of infiltrating CD8$^+$ T cells (Figures 1F, left, and S1O), but only a subset of TILs was bound (Figures 1D, 1F, right, S1I–S1L, and S1O).

To test whether melanosomes affect TIL cytotoxicity, we established autologous melanoma-TIL cultures. TILs pre-exposed to melanosomes secreted significantly less IFNγ and granzyme B, while melanoma cells released less lactate dehydrogenase (LDH), indicating reduced apoptosis (Figures 1G, 1H, and S1P).

Next, we evaluated whether melanosomes alter the cytotoxic function of CD8$^+$ T cells. As models, we used CD8$^+$ T cells from gp-100 mice, which express a TCR specific for a Pmel-17-derived epitope homologous to human gp-100,[47] and from OT-1 mice, which express a TCR engineered to recognize ovalbumin ($OVA_{257-264}$).[48] CD8$^+$ T cells were activated with IL2 for 24 h and co-cultured with B16 or B16-OVA melanoma cells in the presence or absence of melanosomes derived from B16F10 or B16F10-OVA cells. In both models, melanosomes markedly reduced melanoma cell killing and T cell cytotoxicity compared with cultures without melanosomes (Figures 1I and S1Q–S1T). These results suggest that melanosomes directly interact with CD8$^+$ T cells and impair their effector function.

Inhibition of melanosome secretion by melanoma cells blocks tumor progression and induces infiltration of CD8$^+$ T cells

To test melanoma development when melanosome secretion is inhibited, we used the depigmentation agent kojic acid,[49–52] which blocks tyrosinase, the rate-limiting enzyme of melanogenesis.[53] Kojic acid significantly reduced melanoma pigmentation and melanosome secretion compared with vehicle and forskolin controls (Figures 2A, 2B, and S2B) but did not affect melanoma proliferation (Figure 2C). Because antigen presentation requires MHC class I,[54] we examined MHC class I expression and found that kojic acid, unlike IFNγ,[55] had no effect (Figure 2D). Kojic acid also did not alter proliferation or apoptosis of activated CD8$^+$ T cells (Figures 2E, 2F, S2C, and S2D), indicating that its hypopigmentation effect is specific and independent of MHC class I regulation.

After confirming that kojic acid does not directly affect melanoma growth or CD8$^+$ T cell survival, we tested it in a mouse melanoma model. C57/BL6J mice were injected subcutaneously with B16-F10-luciferase cells and, 1 week post melanoma cell injection, treated intratumorally with kojic acid or DMSO every other day for 16 days (Figure S2G). Kojic acid significantly reduced tumor growth (Figures 2H and S2A), confirmed by H&E staining, tumor volume, and weight analyses (Figures 2I

(F) Representative images from melanoma specimens from human patients stained with H&E (upper panels) and for CD8 (T lymphocytes, red), HMB45 (melanoma, pink), and GPNMB (melanosomes, green) and with DAPI (nuclei, blue) (middle and lower panels). Scale bars, 200 μM (middle panel) and 5 μM (lower panel).The graph represents image analysis: the percent of CD8$^+$ T cells bound by melanosomes. Shades of gray: number of melanosomes per one CD8$^+$ T cell. ****$p < 0.0001$; Kruskal-Wallis test. Error bars ± SEM.

(G) Experimental scheme. Melanosomes, Ms; melanoma, M.

(H) Fold change in IFNγ (upper panel) or granzyme B (lower panel) secretion from TILs isolated from melanoma biopsy tissue from indicated patients and co-cultured as in (G). Plotted are means ± standard deviations of three independent experiments. Statistical analysis performed via unpaired t test; *$p < 0.05$, **$p < 0.01$, and ***$p < 0.001$; error bars ± SEM.

(I) Upper: bright-field images of B16F10 melanoma cells co-cultured with CD8$^+$ cells of gp-100 mice (1:5 cell ratio) with or without melanosomes for the indicated time points. Lower: confluence, measured as relative phase contrast, as a function of time for indicated cultures. n = 5 replicates. ns indicates not significant, ***$p < 0.001$; two-tailed paired t tests. Error bars ± SEM.

See also Figure S1.

Please cite this article in press as: Chemla et al., HLA export by melanoma cells decoys cytotoxic T cells to promote immune evasion, Cell (2026), https://doi.org/10.1016/j.cell.2025.11.020

CellPress
OPEN ACCESS

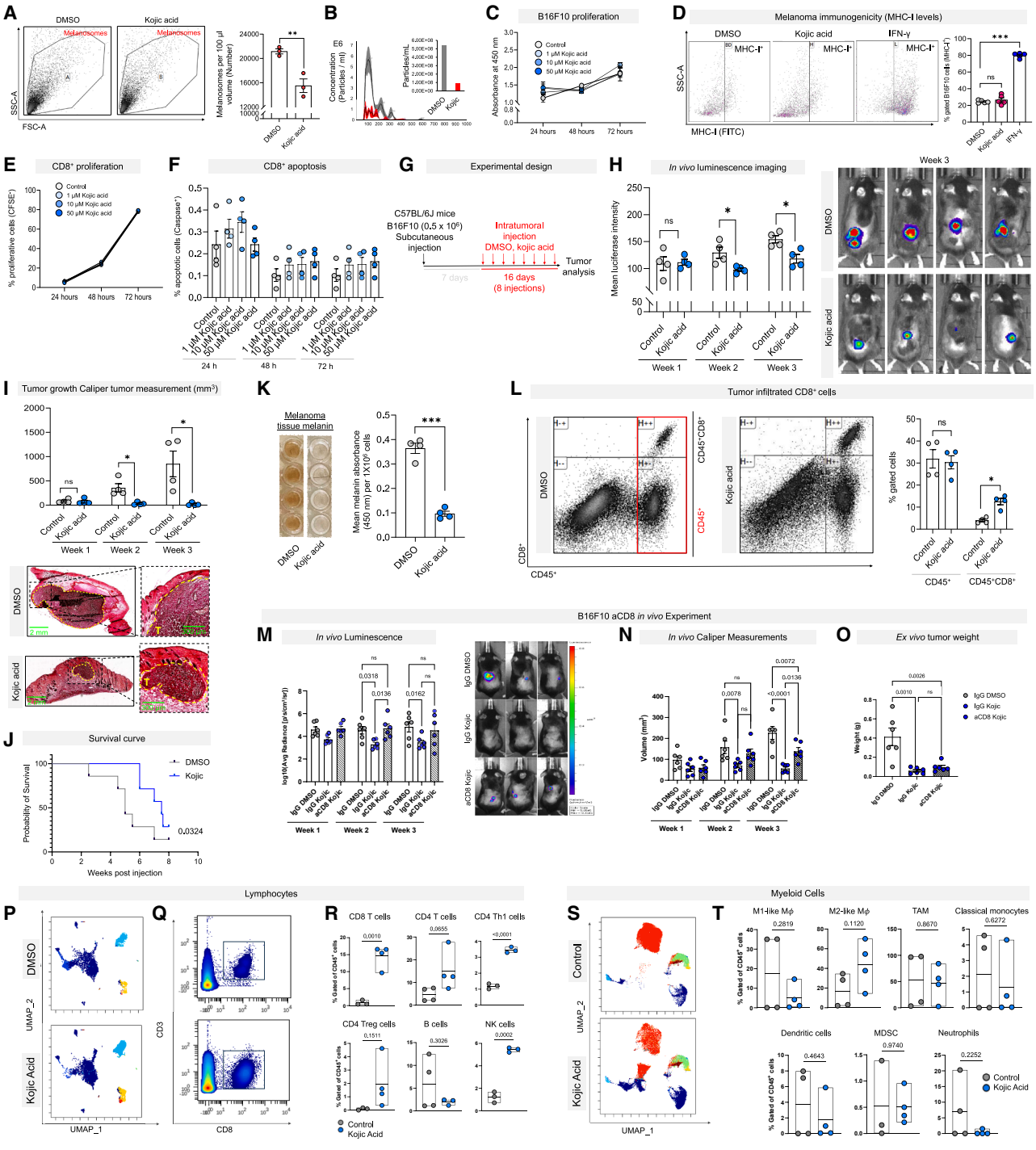

Figure 2. Inhibition of melanosome secretion by melanoma cells blocks tumor progression and induces infiltration of CD8⁺ T cells

(A) Left: representative FACS dot plots. Right: quantification of melanosomes from B16F10 cell media upon indicated conditions for 72 h. $n = 3$. Statistical analysis performed via unpaired t test; $^{**}p < 0.01$. Error bars ± SEM.

(B) Representative Nanosight traces and particles per ml from B16F10 cell media upon indicated conditions for 72 h. $n = 3$.

(C) B16F10 melanoma cell proliferation as monitored by mean absorbance over time under indicated conditions. $n = 4$.

(D) Left: representative FACS dot plots. Right: percent MHC class I⁺ B16F10 cells following 48 h treatment with DMSO (vehicle), kojic acid (50 µM), or IFNγ (100 ng/ml). $n = 5$. ns indicates not significant, $^{***}p < 0.001$; two-tailed unpaired t test. Error bars ± SEM.

(E) CD8⁺ T cell proliferation (%CFSE-stained) after indicated treatments. $n = 4$.

(F) Percent apoptotic caspase-stained CD8⁺ T cells after indicated treatments. $n = 4$. Error bars ± SEM.

(legend continued on next page)

Please cite this article in press as: Chemla et al., HLA export by melanoma cells decoys cytotoxic T cells to promote immune evasion, Cell (2026), https://doi.org/10.1016/j.cell.2025.11.020

and S2E). Survival was significantly improved (Figure 2J), tumor pigmentation was significantly reduced (Figure 2K), and $CD8^+$ T cell infiltration was increased (Figure 2L). The $CD45^+/CD8^+$ ratio further supported an inverse correlation between pigmentation and immune response, consistent with our previous findings[22] (Figure S2F).

To test $CD8^+$ dependence, wild-type C57/BL6J mice were treated with anti-CD8α antibody, which blunts $CD8^+$ T cell function,[56–59] or with immunoglobulin G (IgG) control (Figure S2G). Kojic acid's antitumor effect was markedly reduced with CD8 depletion (Figures 2M–2O and S2H–S2J). In a syngeneic non-melanoma model (MC38), kojic acid had no impact on tumor growth, size, or weight (Figures S2K–S2O), supporting a melanoma-specific effect. Finally, CRISPR-Cas9 knockout of tyrosinase in B16-F10 cells phenocopied kojic acid treatment, confirming that its action is mediated through melanosome inhibition (Figures S2P–S2S).

To assess the impact of melanosomes on immune players in the TME, we performed mass cytometry of tumor-infiltrating $CD45^+$ cells from C57/BL6J mice bearing B16-F10-luciferase melanomas treated with kojic acid or DMSO (Figure 2G). 3 weeks post injection, tumors were harvested, and $CD45^+$ cells were divided into lymphoid ($CD45^+CD11b^-CD11c^-Gr1^-$) and myeloid ($CD45^+CD11b^+IgM^-CD3^-$) compartments and analyzed by UMAP (Figures 2P and 2S). Kojic acid significantly increased $CD8^+$ cytotoxic T cells (Figures 2Q and 2R), consistent with FACS data (Figure 2L), and also raised natural killer (NK) cell frequencies and shifted $CD4^+$ T cells toward a Th1 phenotype (Figure 2R). No effects were observed on Treg or B cells, findings supported by unsupervised clustering (Figures S2T, S2V, and S2W). FlowSOM clustering and supervised analysis of the myeloid compartment confirmed no major changes in dendritic cells (DCs), macrophages, myeloid-derived suppressor cells (MDSCs), neutrophils, or tumor-associated macrophages (TAMs) after melanosome depletion (Figures 2T, S2U, and S2X–S2Z).

Taken together, our data indicate that inhibition of melanosome secretion from melanoma cells enhances $CD8^+$ T cell infiltration into the TME and reduces tumor growth, suggesting that blocking melanosome secretion enhances the activity and effectiveness of tumor-infiltrating $CD8^+$ T cells.

MHC class I on melanosome membranes binds to the TCR on $CD8^+$ T cells

To investigate how melanosomes interact with T cells, we isolated melanosomes and exosomes from human (MNT1) and mouse (B16F10) melanoma cultures and analyzed them by mass spectrometry. NanoSight confirmed their expected sizes (melanosomes 200–500 nm, exosomes 30–100 nm[60]) (Figure S3A). Proteomic profiling revealed distinct, non-overlapping signatures: melanosomes were enriched in canonical melanosome proteins (e.g., tyrosinase and Pmel),[60] while exosomes contained the marker Eno1,[61] excluding cross-contamination (Figures 3A and S3A). Compared with exosomes, melanosomes were significantly enriched in immune-related proteins,[62] including membrane-associated proteins linked to T cell signaling and MHC class I antigen presentation (Figures 3B, S3C, and S3D). Extending the analysis to melanosomes from normal melanocytes (n = 3 donors) and melanoma lines (MNT-1, WM3526, WM1716, and WM3314) revealed melanogenesis enrichment in both, but the MHC class I antigen pathway was present only in melanoma-derived melanosomes and absent in the normal melanosome sample (Figures 3C and S3E; Table S4).

To confirm the presence of MHC class I/HLA molecules on melanosomes, we used an MHC class I/HLA-specific antibody and found binding on both mouse B16F10 and human MNT-1 melanoma cells, as well as on their secreted melanosomes

(G) Experimental scheme.
(H) Left: mean *in vivo* luminescence intensity post tumor cell implantation. Statistical analysis performed via unpaired t test; ns indicates not significant, $^{***}p < 0.001$; error bars ± SEM. Right: representative images at the final time point.
(I) Upper: tumor volumes (mm^3). Statistical analysis performed via unpaired t test; ns indicates not significant, $^{*}p < 0.05$. Error bars ± SEM. Lower: representative H&E-stained sections of primary tumors. Tumor area is marked with yellow dashed lines. Scale bars, 2 mm (left) and 300 μM (right).
(J) Survival curve of mice post-indicated treatment. Statistical significance by Gehan-Breslow-Wilcoxon long-rank test.
(K) Left: bright-field images. Right: mean melanin absorbance (450 nm) of tumor cells extracted from mice treated as indicated. Statistical analysis performed via unpaired t test; $^{***}p < 0.001$. Error bars ± SEM.
(L) Left: representative FACS dot plots. Right: percent gated $CD45^+$ and $CD8^+$ cells isolated from tumors of mice treated as indicated. n = 4. ns indicates not significant, $^{*}p < 0.05$; two-tailed unpaired t tests. Error bars ± SEM.
(M–O) Similar procedure as in (G). In addition, after 1 week, mice were intraperitoneally injected with anti-CD8 (aCD8) or IgG (control) every 4 days. n = 6 mice per group. The experimental design is shown in Figure S2G. Statistical analysis was performed via two-way ANOVA (M and N) or one-way ANOVA (O). ns indicates not significant. Error bars ± SEM.
(M) Left: photon quantification of bioluminescence via IVIS of tumors *in vivo* over the experimental time plotted as $\log_{10}$ of the average radiance. ns indicates not significant. Error bars ± SEM. Right: representative bioluminescent images.
(N) Calculated average tumor volume (mm^3) per group over the experimental time. ns indicates not significant. Error bars ± SEM.
(O) *Ex vivo* tumor weight quantification (gr). ns indicates not significant. Error bars ± SEM.
(P–T) CyTOF mass-cytometry analysis of tumors treated with DMSO or kojic acid as in (G) (n = 4 mice per group).
(P) Representative supervised UMAPs of TILs population ($CD45^+CD11b^-CD11c^-Gr1^-$).
(Q) Representative dot plot of the $CD8^+$ T cell populations.
(R) Percentage of each lymphocyte population from the total $CD45^+$ population. Statistical analysis performed via unpaired t test.
(S) Representative unsupervised UMAP of myeloid cells ($CD45^+CD11b^+IgM^-CD3^-$).
(T) Percentage of each myeloid population from the total $CD45^+$ population in kojic acid or DMSO-treated tumors, using FlowSOM clustering. n = 4 mice per group. Statistical significance was determined by using a two-tailed t test.
See also Figure S2.

Please cite this article in press as: Chemla et al., HLA export by melanoma cells decoys cytotoxic T cells to promote immune evasion, Cell (2026), https://doi.org/10.1016/j.cell.2025.11.020

CellPress
OPEN ACCESS

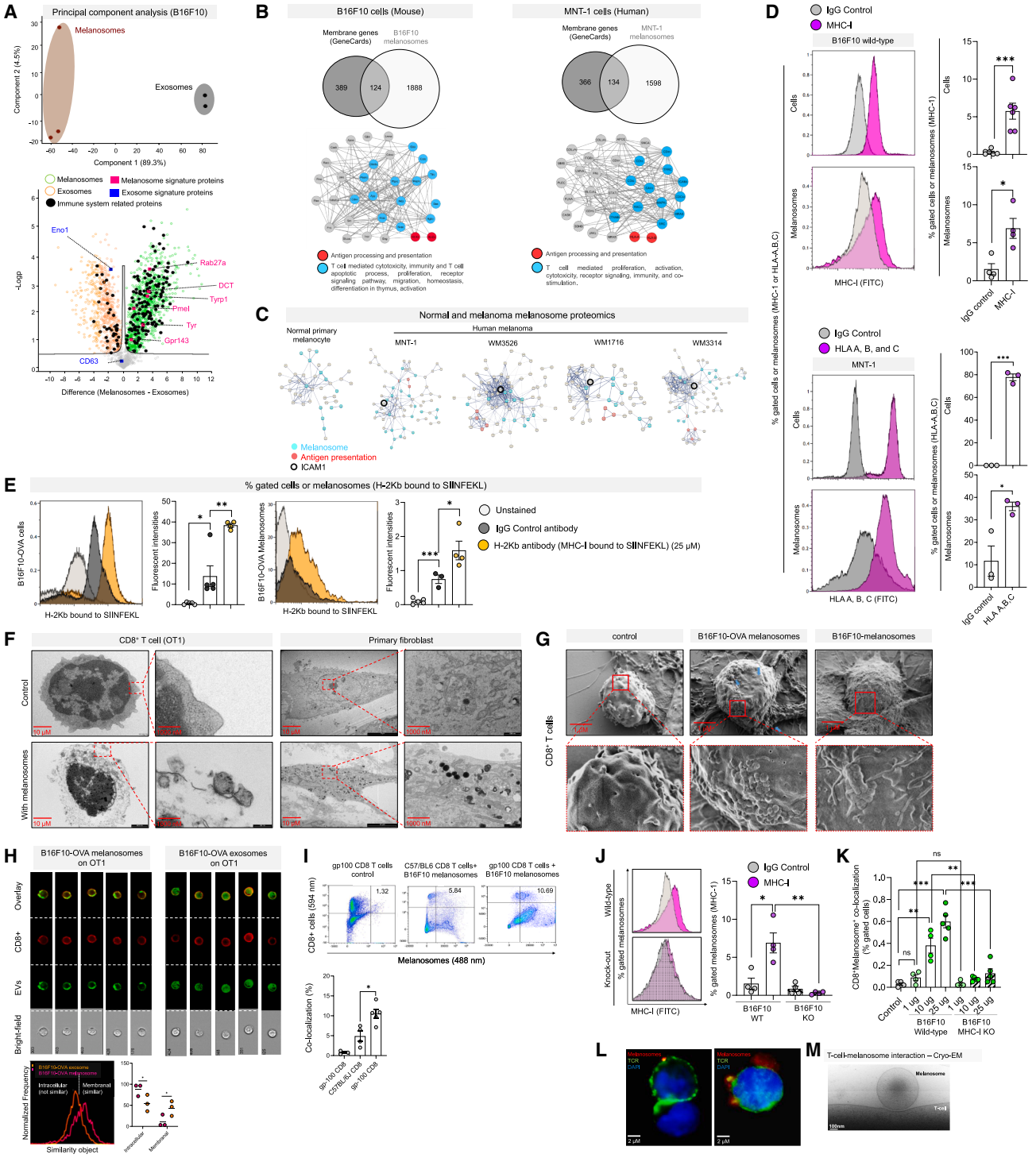

Figure 3. MHC class I on melanosome membranes binds to the TCR on CD8⁺ T cells

(A) Upper: principal-component analysis (PCA) of proteomes of melanosomes and exosomes secreted from B16F10 melanoma cells. Each point denotes a sample (n = 3 melanosome and n = 2 exosome samples). Lower: volcano plot comparing proteomes of secreted melanosomes (green) and exosomes (orange) from the B16F10 cells (false discovery rate [FDR] q value < 0.05). Black dots indicate the proteins involved in immune system-related biological processes, pink squares the melanosome signature proteins, blue squares the exosome signature proteins, and gray dots the non-significant proteins.

(B) Upper: Venn diagrams of overlaps between membrane genes from GeneCards and the proteomes of secreted melanosomes from B16F10 mouse melanoma cells (left) and MNT-1 human melanoma cells (right). Lower: string plots of overlapping factors reveal significant enrichment of the T cell-mediated biological processes (blue) and the antigen processing and presentation biological processes genes (red).

(legend continued on next page)

Please cite this article in press as: Chemla et al., HLA export by melanoma cells decoys cytotoxic T cells to promote immune evasion, Cell (2026), https://doi.org/10.1016/j.cell.2025.11.020

(Figures 3D and S3B). Since IFNγ induces HLA expression,[55] we observed a significant increase in MHC class I on cells and melanosomes following IFNγ treatment (Figure 3D). To test whether melanosomal MHC class I molecules are peptide-loaded, we isolated melanosomes from B16F10-OVA cells and used an antibody specific for the MHC class I complex bound to the OVA peptide SIINFEKL ($OVA_{257-264}$).[63] The MHC class I/peptide complex was detected on both B16F10-OVA cells and their melanosomes (Figures 3E and S3G), indicating that melanosomal MHC class I is correctly loaded and capable of interacting with TCRs.

To further examine melanosome-$CD8^+$ T cell interactions, we incubated melanosomes from B16F10-OVA cells with $CD8^+$ T cells from OT-1 mice or with primary skin fibroblasts. Electron microscopy showed membrane-to-membrane contacts with OT-1 T cells, whereas fibroblasts internalized the melanosomes (Figures 3F and S3F). These contacts resembled immune synapses. High-resolution scanning electron microscopy (SEM) further revealed that B16-OVA melanosomes bound to OT-1 $CD8^+$ T cells, while B16-F10 melanosomes lacking the OVA antigen did not (Figure 3G). These findings support that melanosome-$CD8^+$ T cell binding occurs through MHC-peptide-TCR interactions.

To test specificity, we exposed OT-1 $CD8^+$ T cells to exosomes and melanosomes from B16-F10 and B16-F10 OVA cells. ImageStream analysis showed that B16-F10 OVA melanosomes co-localized with the membrane of OT-1 T cells, whereas B16-F10 OVA exosomes were internalized (Figures 3H and S3I). OVA melanosomes bound OT-1 T cells significantly more than B16-F10 melanosomes (Figure S3H), though a small fraction of B16-F10 melanosomes also bound, suggesting additional binding mechanisms. As controls, 3T3-L1 fibroblasts, known to internalize exosomes[64] and melanosomes,[21] took up both vesicle types equally (Figure S3J). Finally, B16-F10 OVA melanosomes co-localized more strongly with OT-1 T cells than with C57BL/6 T cells (Figure S3L), supporting OVA-specific peptide-mediated interaction.

To extend our observations to an endogenous system, we examined interactions between B16-F10 melanoma melanosomes and $CD8^+$ T cells from gp-100 or wild-type C57BL/6J mice. Melanosomes co-localized significantly more with gp-100 T cells than with wild-type T cells (Figure 3I). When melanosomes from MHC class I-deficient B16-F10 cells[65] were co-cultured with gp-100 T cells, interactions were significantly reduced compared with wild-type B16-F10 melanosomes (Figures 3J, 3K, S3K, S3M, and S3N). High-resolution microscopy further confirmed co-localization of gp-100 TCRs with B16-F10 melanosomes (Figures 3L, 3M, and S3O). Together, these findings demonstrate that melanosome binding to $CD8^+$ T cells depends on MHC class I/peptide-TCR interactions.

Human melanoma melanosome MHC immunopeptidomic analysis reveals that melanosomes carry TAAs and neoantigens

To explore the mechanistic role of MHC molecules on melanosomes, we performed an unbiased, high-throughput analysis of the immunopeptidome[66] presented by melanosomes to evaluate its overlap with the cellular MHC class I landscape and to assess its contribution to T cell recognition. We utilized human melanoma cells (WM3526) and their secreted melanosomes, with or without IFNγ stimulation (Figures 4A and 4B; Table S5), to assess the characteristics of the melanosomes' immunopeptidome landscape and analyze the properties of the identified peptides. First, we examined several quality control features, comparing the melanosomes to the cell line. Overall, MHC class I-bound peptides presented by melanosomes had properties similar to

(C) Proteome of secreted melanosomes isolated from normal human melanocytes and various melanoma cells. String plot shows melanosomes' proteome (top 500) crossed with predicted membrane protein genes from The Human Protein Atlas (5,571 genes). Significant enrichment of antigen presentation (red), melanosome-related proteins (blue), and immune synapses (ICAM1; black circle).

(D) Left: MHC class I or HLA-A, -B, and -C and IgG (control) expression in melanosomes secreted from B16F10 or MNT-1 by FACS analysis. Right: density plots of fluorescence intensities of IgG (gray) and MHC class I or HLA (pink) vs. percentage of gated cells or melanosomes. $n \geq 3$ independent samples for each experimental condition. $^*p < 0.05$, and $^{***}p < 0.001$; two-tailed unpaired *t* tests. Error bars ± SEM.

(E) FACS analyses of B16F10-OVA cells (left) and melanosomes (right) incubated with $OVA_{257-264}$ peptide; unstained cells (light gray); IgG control (dark gray); H-2Kb (the anti-OVA peptide antibody) (yellow). Plots show fluorescent intensities vs. percentage of gated cells or melanosomes. $n \geq 3$ independent samples for each experimental condition. $^*p < 0.05$, $^{**}p < 0.01$, and $^{***}p < 0.001$; two-tailed unpaired *t* test. Error bars ± SEM.

(F) Transmission electron microscopy of $CD8^+$ T cells from OT1 mice (left) or primary fibroblasts (right) co-cultured overnight with or without melanosomes isolated from B16F10 OVA cells. Scale bars, 10 μM and 1,000 nM.

(G) SEM of $CD8^+$ T cells from OT1 mice co-cultured overnight without melanosomes, with B16F10-OVA melanosomes, and with B16F10 melanosomes. Scale bar, 1 μM.

(H) Upper: ImageStream analyses of $CD8^+$ T cells (red) from OT1 mice co-cultured overnight with labeled melanosomes (left) or exosomes (right) (green). Lower: percent of EV localization intracellularly or on the membrane. Analysis considered 5×10^3 $CD8^+$ T cells from three independent experiments. $^*p < 0.05$; two-tailed paired *t* test.

(I) Upper: representative FACS dot plots. Lower: quantification of interactions of T cells from gp-100 or wild-type mice with B16F10 melanosomes. $n = 2$ independent experiments. $^*p < 0.05$; two-tailed unpaired *t* test. Error bars ± SEM.

(J) FACS plots (left) and quantification (right) of interactions between melanosomes from wild-type B16F10 and B16F10 cells lacking MHC class I stained for the IgG (control, gray) and anti-MHC class I antibodies (pink). $n = 4$ independent samples for each experimental condition. $^*p < 0.05$, and $^{**}p < 0.01$; two-tailed unpaired *t* test. Error bars ± SEM.

(K) Quantification of co-localization of T cells isolated from gp-100 mice or wild-type mice with the melanosomes from wild-type B16F10 cells or cells lacking MHC class I. $n = 4$ independent experiments. ns indicates not significant, $^{**}p < 0.01$ and $^{***}p < 0.001$; two-tailed unpaired *t* test. Error bars ± SEM.

(L) Representative high-resolution microscopy images of gp-100 $CD8^+$ T cells TCR (green) and B16F10 melanosomes (stained for GPNMB, red). Nuclei were stained with DAPI (blue). Scale bar, 2 μM.

(M) Representative high-resolution Cryo-EM image of $CD8^+$ T cell interacting with a melanosome isolated from a human melanoma biopsy. Scale bar, 100 nM. See also Figure S3.

Please cite this article in press as: Chemla et al., HLA export by melanoma cells decoys cytotoxic T cells to promote immune evasion, Cell (2026), https://doi.org/10.1016/j.cell.2025.11.020

CellPress
OPEN ACCESS

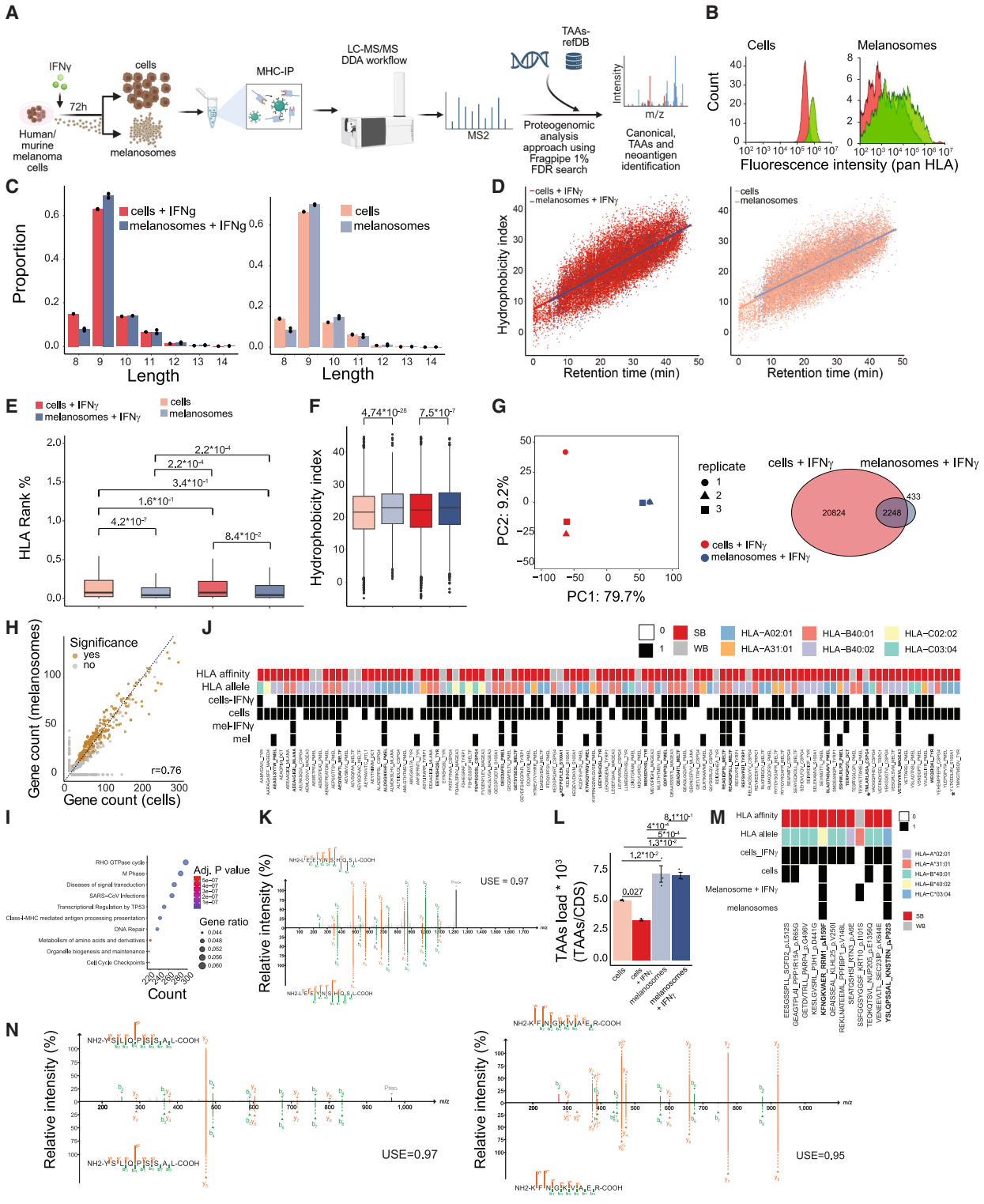

Figure 4. Human melanoma melanosome MHC immunopeptidomic analysis reveals that melanosomes carry TAAs and neoantigens

(A) Experimental scheme of the proteogenomic immunopeptidome analysis workflow, outlining the isolation of melanoma cells (B16F10 and WM3526) and their derived melanosomes, followed by MHC class I immunoprecipitation and liquid chromatography-tandem mass spectrometry (LC-MS/MS) analysis of eluted peptides.

(legend continued on next page)

Please cite this article in press as: Chemla et al., HLA export by melanoma cells decoys cytotoxic T cells to promote immune evasion, Cell (2026), https://doi.org/10.1016/j.cell.2025.11.020

those presented at the cell surface, including comparable peptide length distributions (Figure 4C) and a linear relationship between retention time and hydrophobicity (Figure 4D). Notably, predicted MHC-binding affinity and hydrophobicity, features previously associated with increased immunogenic potential,[67–69] were significantly higher among peptides identified in the melanosome samples than in the cell samples (Figures 4E and 4F).

Melanoma cells and melanosomes had distinct MHC class I ligandome profiles (Figure 4G), but a substantial proportion of the melanosome-derived peptide repertoire overlapped with that of the parent cells (83.8%), implying derivation from the total cellular ligandome (Figure 4G). Pathway enrichment analysis of the immunopeptidome landscape revealed a positive correlation between pathways enriched in cells and their corresponding melanosomes, with substantial overlaps in functional categories such as class I MHC-mediated antigen processing and presentation, DNA repair, and cell cycle regulation (Figures 4H and 4I). Given the observed MHC class I-dependent, peptide-specific suppression of $CD8^+$ T cell activity by melanosomes, we hypothesized that melanosomes present immunogenic peptides. Indeed, we have identified 25 tumor-associated antigens (TAAs) in melanosome samples (Figure 4J) with high-confidence peptide identifications (Figure 4K). These TAAs are predicted to bind a variety of HLA alleles with high affinity. Strikingly, the majority of these peptides were also detected in the corresponding melanoma cell samples (Figure 4J). Notably, melanosomes exhibited a statistically significant enrichment in TAA presentation compared with melanoma cells, regardless of IFNγ treatment (Figure 4L).

Finally, we used whole-exome sequencing to generate a custom proteomic database for proteogenomic analysis of neopeptides/neoantigens. This approach identified three mutation-derived neoantigens within the human melanosome immunopeptidome, two of which were also present in the cellular MHC class I repertoire (Figures 4M and 4N). Importantly, we analyzed the murine B16F10 cells and secreted melanosome immunopeptidomic data, which recapitulated most of our findings in human cells (Figures S4A–S4J). Together, these findings suggest that melanosomes, by carrying immunogenic peptides, including TAAs and neoantigens, compete with melanoma cells for $CD8^+$ T cell recognition, thereby contributing to their immunomodulatory effects.

The majority of melanosome-bound $CD8^+$ TILs' TCRs are shared with those of melanoma-bound $CD8^+$ TILs

To comprehensively elucidate the mechanism of melanosome-T cell interaction, we isolated and labeled (PKH67) secreted melanosomes and their originating melanoma cells from patient samples ($n = 4$) and incubated them with autologous T cells. The samples were then sorted via FACS into melanosome-bound, melanoma-bound, and free $CD8^+$ TILs, which were subjected to single-cell TCR sequencing (Figures 5A–5C, S1H, and S5A). For each patient, we identified shared TCR clones between $CD8^+$ TILs bound to melanosomes and those bound to melanoma (Figures 5D and S5B; Table S6). While melanosome-bound $CD8^+$ TILs contained unique TCRs, the shared clones and melanoma-unique clones represented the most expanded populations (Figure 5E; Table S6). Notably, in non-responders, the fraction of melanoma-unique TCR clones was much lower than in responders (~25% vs. ~4%) (Figure 5E; Table S6). No clones were shared across patients regardless of $CD8^+$ TIL binding condition (Figure 5F). To better understand the transcriptional state of the shared clones, we performed single-cell RNA sequencing (RNA-seq) of melanosome-bound versus unbound $CD8^+$ TILs. Shared TCR clones showed no strong bias toward any transcriptional state defined

(B) Histograms depicting HLA-I surface levels on WM3526 cells (left) and secreted melanosomes (right), measured by flow cytometry.
(C) Bar charts present the length distribution of MHC class I-bound peptides identified in IFNγ-treated WM3526 cells and their derived melanosomes (left) or in untreated samples (right). Mean ± SEM.
(D) Scatterplots of retention time versus hydrophobicity index of MHC class I-bound peptides identified in IFNγ-treated WM3526 cells and their derived melanosomes (left; r = 0.77 and r = 0.8, respectively) or untreated samples (right; r = 0.767 and r = 0.762, respectively).
(E) Boxplot of the rank percent of peptides predicted to bind MHC class I alleles. *p* values were obtained by pairwise *t* test followed by Bonferroni correction. Boxes represent the interquartile range (IQR) and median rank percent, and whiskers extend ±1.5-fold the IQR (dots correspond to individual peptides).
(F) Boxplots of the hydrophobicity index of each peptide detected in WM5326 samples. *p* values were obtained using pairwise *t* test followed by Bonferroni correction. Boxes represent the IQR and median rank percent, and whiskers extend to ±1.5 IQR.
(G) Principal-component analysis (PCA) of IFNγ-treated WM3526 cells and their derived melanosomes (left) and a Venn diagram of MHC class I-bound peptides identified in IFNγ-treated WM3526 cells and their derived melanosomes (right).
(H) Scatterplot of enriched pathway counts in WM5326 cells and their derived melanosomes. Pearson correlation (r) between the groups is indicated. Significantly enriched pathways ($p_{adj} < 0.05$), as identified by the Reactome pathway analysis pipeline, are highlighted in orange.
(I) Dot plot of the top 10 enriched pathways identified in WM3526 cells and their derived melanosomes, including both IFNγ-treated and untreated conditions, based on Reactome pathway analysis.
(J) Heatmap of tumor-associated antigen (TAA) identifications. Black and white squares indicate presence or absence in each group. Asterisks highlight peptides previously detected in the HLA benign ligand ATLAS.[70] Binding affinity is color-coded: strong binders (SBs) in red, weak binders (WBs) in gray. The best predicted HLA allele binding is also indicated by color.
(K) Representative mirror plot of a TAA-derived MHC class I-bound peptide, identified in WM3526 cells and their derived melanosomes. The upper spectrum shows the experimentally identified peptide, and the lower spectrum shows the predicted peptide. Unweighted spectral entropy (USE) is indicated.
(L) Bar plot showing the TAA load in each sample. *p* values were obtained by pairwise *t* test followed by Bonferroni correction. Mean ± SEM.
(M) Heatmap of neoantigen-derived peptides identified in WM3526 samples. Each column represents a peptide. Top annotation row shows peptide identification status in individual samples (black, detected; white, not detected). Bottom annotation row indicates whether peptides were identified in WM3526 cells only (black) or in both cells and melanosomes (magenta). Predicted binding affinity is color-coded (SBs in red; WBs in gray), and the best predicted MHC class I allele is shown by color.
(N) Representative mirror plot of a neoantigen MHC class I-bound peptide, identified in WM3526 cells and their derived melanosomes. USE is shown. Upper spectrum: experimentally identified peptide; lower spectrum: predicted peptide.
See also Figure S4.

Please cite this article in press as: Chemla et al., HLA export by melanoma cells decoys cytotoxic T cells to promote immune evasion, Cell (2026), https://doi.org/10.1016/j.cell.2025.11.020

CellPress
OPEN ACCESS

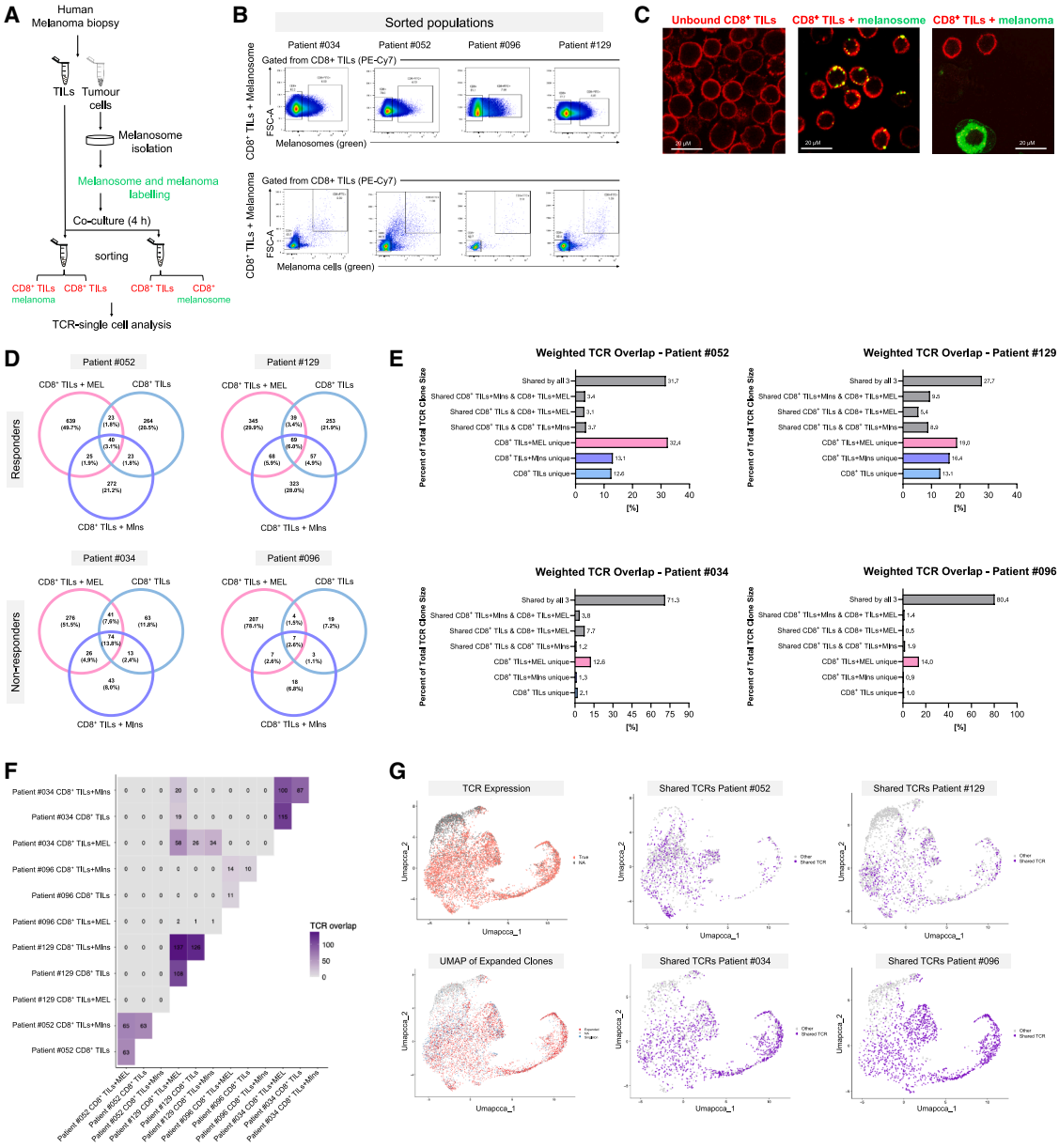

Figure 5. The majority of melanosome-bound CD8⁺ TILs' TCRs are shared with those of melanoma-bound CD8⁺ TILs

(A) Experimental Scheme; *n* = 4 patients; responders and NR.

(B) FACS plots showing the sorted populations: CD8⁺ TILs bound by melanosomes or by melanoma cells (CD8⁺FITC⁺) and unbound CD8⁺ TILs (CD8⁺).

(C) Representative confocal microscopy images of each sorted population: CD8⁺ TILs (red); autologous melanosomes or melanoma cells (green). Scale bar, 20 μM.

(D) Venn diagrams illustrating shared TCR clonotypes between CD8⁺ TILs that were bound by melanosomes, bound by melanoma, or free, shown per patient.

(E) Bars show the proportion of unique and shared TCR clonotypes by frequency.

(F) Visualization of shared clonotypes across all pairwise sample comparisons.

(G) Left: UMAP plots of single-cell TCR-seq data showing TCR expression and clonal expansion status across individual cells. Right: UMAP plots of single-cell RNA-seq data showing clustering of cells from individual patients based on shared TCR clones (purple) across all samples.

See also Figure S5.

by clustering (Figure 5G). Together, these findings suggest that melanosomes and melanoma share a highly overlapping peptide repertoire for engaging CD8⁺ TILs. We therefore hypothesize that melanosomes compete with melanoma for CD8⁺ TIL binding, acting as a physical barrier between T cells and tumor cells.

Melanosome binding to CD8⁺ T cells induces a non-optimal transcriptional profile, reduces TCR signaling and mitochondrial activity, and leads to apoptosis

Clustering analysis showed transcriptomic changes in TILs after melanosome treatment (Figure 6A), including enrichment of IFNγ

Please cite this article in press as: Chemla et al., HLA export by melanoma cells decoys cytotoxic T cells to promote immune evasion, Cell (2026), https://doi.org/10.1016/j.cell.2025.11.020

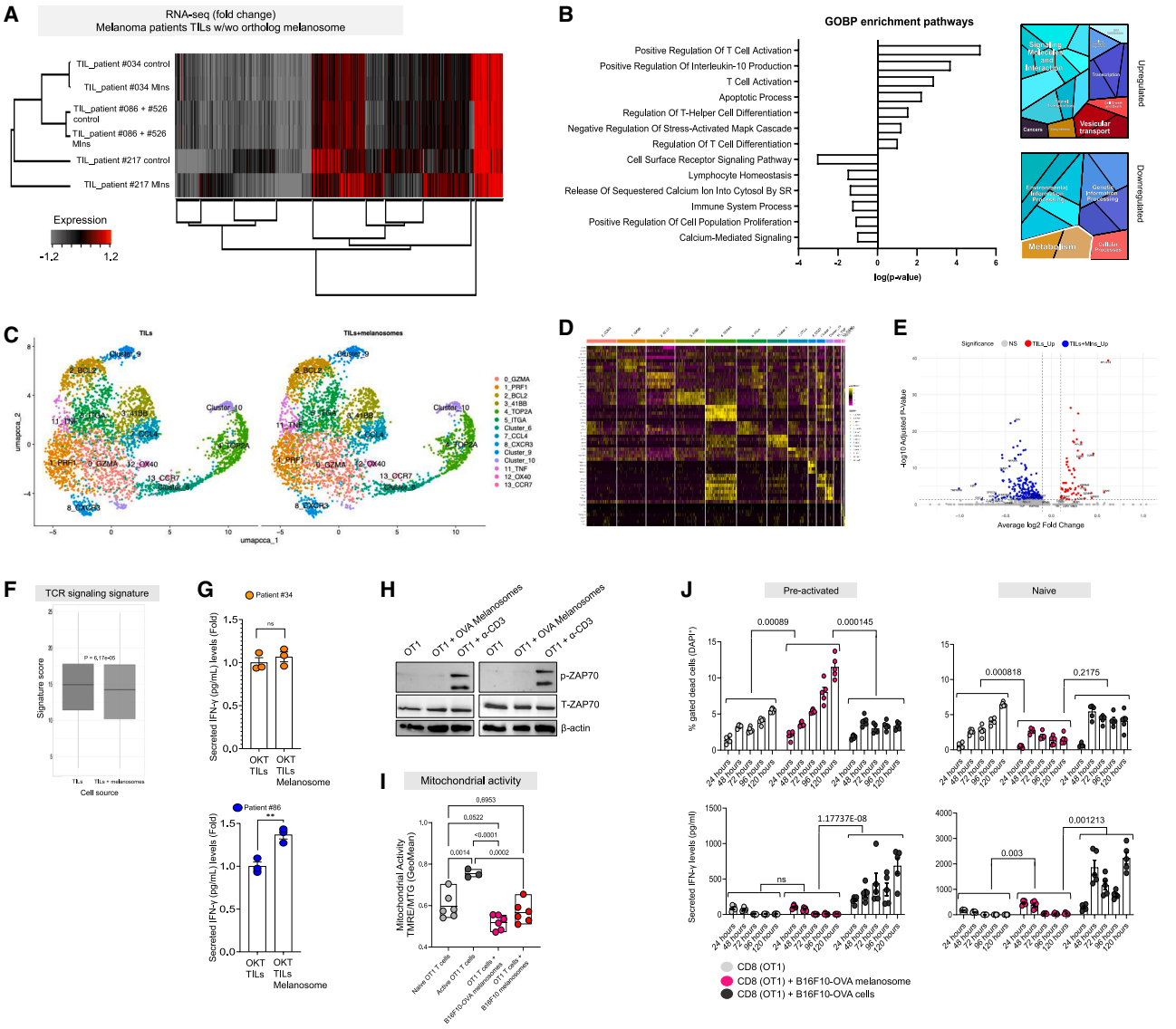

Figure 6. Melanosome binding to CD8⁺ T cells induces a non-optimal transcriptional profile, reduces TCR signaling and mitochondrial activity, and leads to apoptosis

(A) Heatmap of differential expression of genes in TILs from three patients with melanoma before and after incubation with autologous melanosomes.

(B) Left: Gene Ontology biological processes (GOBP) enrichment of top 500 differentially expressed genes in melanosome-treated TILs demonstrating positive and negative regulation of immune response. Right: proteomap of enriched phenotypes in up- and downregulated genes.

(C) UMAP plot visualizing clustering of melanosome-bound CD8⁺ TILs or unbound CD8⁺ TILs sorted cells.

(D) Heatmap representing the top differentially expressed genes in each cluster, as shown in (C).

(E) Volcano plot representing the top differentially expressed genes comparing melanosome-bound CD8⁺ TILs (TILs+MIns up) or unbound CD8⁺ TILs (TILs up).

(F) Boxplot of signature scores for TCR downstream signaling. *p* value calculated with the Wilcoxon test.

(G) IFNγ secretion (pg/ml normalized to fold change) by human TILs treated with anti-CD3 antibody (OKT-3) with and without culture with autologous melanosomes. $n = 2$ different patients, 3 repeats. ns indicates not significant, ** $p < 0.01$; two-tailed unpaired *t* test. Error bars ± SEM.

(H) Protein level by western blot analysis for phospo-ZAP70 (pZAP70), total phospo-ZAP70 (T-ZAP70), and B-actin in indicated conditions.

(I) Mitochondrial activity under indicated conditions. $n = 6$ (naive, B16F10-OVA melanosomes, B16F10 melanosomes); $n = 3$ (activated). Two-way ANOVA test. Error bars ± SEM.

(J) Quantification of cell death (upper) and IFNγ secretion (lower; pg/ml, fold change normalized) in OVA-OT1 CD8⁺ T cells (partially activated or naive) co-cultured with B16F10-OVA-derived melanosomes or with B16F10-OVA cells lacking melanosomes. $n = 5$. ns indicates not significant; two-tailed unpaired *t* test. Error bars ± SEM.

See also Figure S6.

Please cite this article in press as: Chemla et al., HLA export by melanoma cells decoys cytotoxic T cells to promote immune evasion, Cell (2026), https://doi.org/10.1016/j.cell.2025.11.020

mRNA, a T cell activation marker,[71] and factors involved in TNF signaling, which can drive CD8$^+$ T cell death[72,73] (Figure S6A; Table S7). To explore the mechanism of cytotoxic inhibition, we performed single-cell RNA-seq and profiled transcriptomes of TILs isolated from biopsy samples of three melanoma patients before and after 24 h incubation with autologous melanosomes (Table S7). Globally, melanosome-bound TILs upregulated granzyme family genes and mitochondrial genes (Figure 6B).

Next, we identified 14 transcriptionally distinct clusters of TILs; however, because the CD8$^+$ T cell states were not very distinct, annotation was based on marker genes for each cluster (Figures 6C and 6D). The distribution of TILs varied between groups, with notable shifts in cell population proportions (Figure S6D). Clusters 2_BCL2, 5_ITGA, and 11_TNF, related to anti-apoptotic, adhesive, and inflammatory phenotypes,[37,74] were enriched in melanosome-bound TILs, whereas clusters 3_41BB and 4_TOP2A, associated with proliferation and inflammatory states,[75,76] were more common in unbound TILs (Figure 6D). TCR signaling signature was significantly reduced in melanosome-bound cells (Figures 6E and 6F), although these TILs produced slightly more IFNγ than controls (Figure 6G). Accordingly, ZAP70 phosphorylation, a marker of TCR activation,[77] was absent after melanosome interaction with CD8$^+$ T cells compared with CD3 activation (Figure 6H). Mitochondrial function was significantly reduced in CD8$^+$ T cells after melanosome treatment (Figure 6I), consistent with impaired TCR signaling and an exhausted-like state.[78,79] However, no increase in secreted granzyme B or IFNγ was observed (Figures 1H, 6J, lower, and S6D), and classical exhaustion markers (PD1, TIM3, LAG3, and 41BB)[75,76] were not induced (Figure S6B) compared with direct co-culture with autologous melanoma cells. In line with bulk RNA-seq (Figure 6A), this mixed T cell state prompted us to test TCR signaling enrichment. Together with evidence that melanosome interaction ultimately leads to CD8$^+$ T cell death (Figures 6J, upper, and S6C), these findings suggest that melanosome binding reshapes the TIL transcriptional profile, creating a "confused" state characterized by reduced TCR signaling, reduced mitochondrial activity, and increased apoptosis.

DISCUSSION

Melanoma is the most lethal skin cancer, with 50% of patients resistant to immunotherapy.[11–14] Although extracellular vesicles (EVs) have been studied in immune responses, work has focused mainly on exosomes,[80,81] which, for example, can activate T and B cells through DCs.[81–86] We found that melanoma immune escape involves direct interaction of CD8$^+$ T cells with large melanoma EVs: while TME cells internalize melanosomes,[21,23,24] CD8$^+$ T cells interact with their surfaces. Mouse melanoma B16-OVA exosomes are internalized by CD8$^+$ T cells, whereas human metastatic melanoma exosomes remain surface-associated.[87] Melanosomes mask CD8$^+$ T cells, leading to partial activation, while melanoma-derived circulating exosomes expressing PD-L1 induce checkpoint responses.[88] Additionally, organ-specific EV interactions are driven by integrin patterns on melanoma exosomes, enabling lung cell targeting.[89] Together, these findings highlight that EV-cell interactions are cell-state-, cell-type-, and EV-type-dependent and underscore the need for systematic mapping to develop strategies that modulate EV activity.

Melanosomes upregulate IFNγ or granzyme B mRNA in T cells without inducing IFNγ secretion, likely due to posttranscriptional regulation seen in exhaustion or chronic inflammation,[87,90,91] or nuclear retention of IFNγ transcripts as in NK cells requiring dual IL-12/IL-2 stimulation.[92] We hypothesize that melanosome interaction lacks a necessary secondary signal or induces post-translational degradation, explaining the absence of IFNγ secretion and warranting further study.

Melanosome biogenesis proceeds through four intracellular steps[93] and may share pathways with MHC class II biogenesis,[94] though the stage at which HLA is acquired remains unknown. While intracellular melanosomes are membrane-bound,[95,96] their membrane status after secretion is unclear,[93] and they may be released as melanocores via exocytosis or as single-membrane vesicles.[93,97] Thus, the HLA source of melanosomes likely depends on the secretion mode and requires further investigation.

TILs in the TME contain TCR repertoires that reflect the functional state of each T cell clone and influence disease progression. High TCR diversity (i.e., clonality) correlates with longer overall survival and response to PD-1 blockade immunotherapy.[98,99] However, how antigens are distributed in melanoma tumors, and whether they are expressed by all tumor cells or restricted to specific clones, remains unclear. Clinically, since melanosomes carry distinct antigens, it may be beneficial to exclude melanosome-reactive TILs before reinfusion in adoptive T cell therapy.

Limitations of the study

Our findings reveal that melanoma-derived large extracellular vesicles, known as melanosomes, are decorated with MHC molecules that act as decoys for CD8$^+$ T cells by engaging their TCRs, leading to T cell dysfunction and apoptosis. We combined immunopeptidomics of melanosomes and melanoma cells with single-cell TCR sequencing of TILs bound by either. A high degree of antigenic overlap supports the idea that melanosomes compete with melanoma cells for CD8$^+$ T cell engagement.

Although we identified three neoantigens presented by melanosomes, their ability to elicit a functional CD8$^+$ T cell response remains unconfirmed. Further, the origin of melanosomal MHC is also unclear, whether it is acquired from their tumor cell of origin or loaded via intrinsic machinery. Finally, while melanosomes impair T cell mitochondrial function and viability, the exact mechanism of cell death remains unknown. We cannot rule out the presence of an unidentified inhibitory molecule.

RESOURCE AVAILABILITY

Lead contact

Requests for further information and resources should be directed to and will be fulfilled by the lead contact, Carmit Levy (carmitlevy@tauex.tau.ac.il).

Materials availability

All unique/stable reagents generated in this study are available from the lead contact without restriction.

Data and code availability

- Single-cell RNA-seq, single-cell TCR-seq, and WM3526 whole-exome sequencing (WES) data have been deposited at NCBI GEO and are

publicly available as of the date of publication. Accession numbers are listed in the key resources table.
- The mass spectrometry proteomics data have been deposited to the ProteomeXchange Consortium via the PRIDE partner repository with the dataset identifiers PXD068867, PXD068870, and PXD069094.
- Any additional information required to reanalyze the data reported in this paper is available from the lead contact upon request.

ACKNOWLEDGMENTS

C.L. acknoledges that this work was funded by the European Research Council (ERC) under the European Union's Horizon 2020 research and innovation program European Union. Views and opinions expressed are, however, those of the author(s) only and do not necessarily reflect those of the European Union or the ERCEA. Neither the European Union nor the granting authority can be held responsible for them (C.L., grant agreement no. 726225). C.L. acknowledges the Tel Aviv University Gray Medical School core facility, Medina and Elisha with endless gratitude, and Yuval and Omer for exponential joy. D.F. acknowledges the NIH grants NCI P01 CA163222 and NIAMS R01 AR043369-27 and the Dr. Miriam and Sheldon G. Adelson Medical Research Foundation. A.M. acknowledges the Mantoux Bioinformatics Institute of the Nancy and Stephen Grand Israel National Center for Personalized Medicine and specifically Dr. Avital Sarusi Portuguez.

AUTHOR CONTRIBUTIONS

S.M., data curation, formal analysis, investigation, methodology, project administration, validation, visualization, and writing – review & editing; O.I., conceptualization, data curation, formal analysis, methodology, investigation, and resources; P.M., data curation, formal analysis, investigation, validation, visualization, and writing – review & editing; Y. Sade, data curation, formal analysis, investigation, validation, visualization, and writing – review & editing; C.W., data curation, formal analysis, investigation, and visualization; Y. Chemla, data curation, formal analysis, and investigation; N.X., investigation; K.R., data curation, formal analysis, investigation, and visualization; A. Maliah, data curation, formal analysis, investigation, and methodology. G.L., data curation, formal analysis, and investigation; R.P., data curation, formal analysis, and investigation; O.B., data curation, formal analysis, and investigation; O.L., formal analysis and investigation; I.T., investigation; G.A., formal analysis and investigation; A.N., data curation, formal analysis, investigation, and methodology; S.Y., data curation, formal analysis, and investigation; D.L., resources, methodology; V.K., resources and methodology; T.G., conceptualization, data curation, formal analysis, and investigation; C.C., formal analysis; V.A., data curation, formal analysis, and investigation; R.L., data curation, formal analysis, and investigation; D.R., data curation, formal analysis, investigation, and visualization; Z.E., data curation, formal analysis, and investigation; Y.B., data curation, formal analysis, and investigation; R. Balaban, data curation and supervision; A.K., investigation; R.K., formal analysis, investigation, resources, and supervision; A.G., formal analysis, investigation, resources, and supervision; T.Z., formal analysis, investigation, resources, and supervision; P.G., formal analysis; D.N., formal analysis; H.V., investigation; X.W., investigation; R. Brenner, resources; J.M.M.G., formal analysis; D.H., resources; T.Y., investigation, resources, and supervision; V.Z.-W., investigation and resources; O.K., resources; Y.F., formal analysis and investigation; D.B., methodology and resources; R. Shapira, resources and supervision; L.E., methodology and resources; N.S.-M., investigation; M.M., supervision and resources; G.E., resources; L.K., investigation and resources; Y.A., investigation and resources; M.C., resources and supervision; D.G., resources and supervision; B.B., resources and supervision; M.L., resources and supervision; D.S., resources; S.G., resources and supervision; D.F., supervision; M.J.B., supervision; M.K., resources and supervision; P.C., investigation, resources, and supervision; R. Shamir, resources and supervision; S.A., resources and supervision; A. Madi, resources, supervision, and writing – review & editing; M.P.L., investigation, resources, and visualization; F.R., resources and supervision; Y. Carmi, conceptualization, methodology, resources, and supervision; S.P., conceptualization, data curation, formal analysis, investigation, methodology, project administration, supervision, validation, visualization, and writing – original draft; Y. Samuels, conceptualization, methodology, resources, supervision, and writing – original draft; C.L., conceptualization, funding acquisition, investigation, methodology, project administration, resources, supervision, visualization, writing – original draft, and writing – review & editing.

DECLARATION OF INTERESTS

D.F. has a financial interest in Soltego & Company developing salt-inducible kinase inhibitors for topical skin-darkening treatments that might be used for a broad set of human applications. The interests of D.F. were reviewed and are managed by Massachusetts General Hospital and Partners Healthcare in accordance with their conflict-of-interest policies. D.F. also declares equity and/or consulting relationships with Tasca, Pierre Fabre, Biocoz, Swiss Rockets, and Coherent Medicines.

STAR★METHODS

Detailed methods are provided in the online version of this paper and include the following:

- KEY RESOURCES TABLE
- EXPERIMENTAL MODEL AND STUDY PARTICIPANT DETAILS
  - Melanoma tissue array
  - Human patient samples
  - Melanoma specimens
  - Mice
  - Cell culture
- METHOD DETAILS
  - In vivo tumor growth models
  - Bioluminescent assays
  - In vivo tumor treatment
  - Primary cell isolation
  - Survival curve
  - In vitro CD3 activation
  - Melanosome isolation
  - Exosome isolation
  - Labeling of melanosome and exosome membranes
  - Mouse melanoma model
  - Isolation and activation of mononuclear cells from mouse spleens
  - Image analysis of melanoma Tissue Micro Array (TMA)
  - Hematoxylin and eosin staining
  - Immunofluorescence analyses
  - Nanosight analyses
  - Transmission electron microscopy analyses
  - Scanning electron microscopy
  - Mass spectrometry
  - Flow cytometry
  - Analyses of TILs from mouse tumors
  - Immunopeptidome sample processing and LC-MS/MS
  - Co-culture survival assay of $CD8^+$ T cells
  - Melanosome $CD8^+$ T cells binding assay
  - Killing assay
  - ImageStream cytometry
  - Apoptosis assay
  - Proliferation assays
  - RNA sequencing
  - Analyses of secreted $IFN\gamma$ levels
  - Analyses of secreted GranzymeB levels
  - T cell interaction with melanoma or melanosomes assays
  - Cryo Electron Microscopy
  - Confocal microscopy
  - Quantification of melanosomes secretion amount
  - Expression of activation and exhaustion markers in TIL
  - CRISPR
  - CyTOF
  - Mitochondrial activity assay
  - Spatial proteomics

- QUANTIFICATION AND STATISTICAL ANALYSIS
  - Statistics
  - Immunopeptidomics statistical analyses
  - Proteomics Gene Ontology enrichment analysis
  - RNA-seq data analysis
  - Melanogenesis-related gene enrichment
  - TCGA data
  - MHC-I peptidomics immunogenicity analyses

SUPPLEMENTAL INFORMATION

Supplemental information can be found online at https://doi.org/10.1016/j.cell.2025.11.020.

Received: January 8, 2025
Revised: August 16, 2025
Accepted: November 17, 2025

REFERENCES

1. Galon, J., Costes, A., Sanchez-Cabo, F., Kirilovsky, A., Mlecnik, B., Lagorce-Pagès, C., Tosolini, M., Camus, M., Berger, A., Wind, P., et al. (2006). Type, density, and location of immune cells within human colorectal tumors predict clinical outcome. Science *313*, 1960–1964. https://doi.org/10.1126/science.1129139.
2. Fridman, W.H., Pagès, F., Sautès-Fridman, C., and Galon, J. (2012). The immune contexture in human tumours: impact on clinical outcome. Nat. Rev. Cancer *12*, 298–306. https://doi.org/10.1038/nrc3245.
3. Restifo, N.P., Dudley, M.E., and Rosenberg, S.A. (2012). Adoptive immunotherapy for cancer: harnessing the T cell response. Nat. Rev. Immunol. *12*, 269–281. https://doi.org/10.1038/nri3191.
4. Gross, G., Gorochov, G., Waks, T., and Eshhar, Z. (1989). Generation of effector T cells expressing chimeric T cell receptor with antibody type-specificity. Transplant. Proc. *21*, 127–130.
5. Kalos, M., Levine, B.L., Porter, D.L., Katz, S., Grupp, S.A., Bagg, A., and June, C.H. (2011). T cells with chimeric antigen receptors have potent antitumor effects and can establish memory in patients with advanced leukemia. Sci. Transl. Med. *3*, 95ra73. https://doi.org/10.1126/scitranslmed.3002842.
6. Pardoll, D.M. (2012). The blockade of immune checkpoints in cancer immunotherapy. Nat. Rev. Cancer *12*, 252–264. https://doi.org/10.1038/nrc3239.
7. Hodi, F.S., O'Day, S.J., McDermott, D.F., Weber, R.W., Sosman, J.A., Haanen, J.B., Gonzalez, R., Robert, C., Schadendorf, D., Hassel, J.C., et al. (2010). Improved survival with ipilimumab in patients with metastatic melanoma. N. Engl. J. Med. *363*, 711–723. https://doi.org/10.1056/NEJMoa1003466.
8. Bell, R.E., and Levy, C. (2011). The three M's: melanoma, microphthalmia-associated transcription factor and microRNA. Pigment Cell Melanoma Res. *24*, 1088–1106. https://doi.org/10.1111/j.1755-148X.2011.00931.x.
9. Hodis, E., Watson, I.R., Kryukov, G.V., Arold, S.T., Imielinski, M., Theurillat, J.-P., Nickerson, E., Auclair, D., Li, L., Place, C., et al. (2012). A landscape of driver mutations in melanoma. Cell *150*, 251–263. https://doi.org/10.1016/j.cell.2012.06.024.
10. Carlino, M.S., Larkin, J., and Long, G.V. (2021). Immune checkpoint inhibitors in melanoma. Lancet *398*, 1002–1014. https://doi.org/10.1016/S0140-6736(21)01206-X.
11. Harel, M., Ortenberg, R., Varanasi, S.K., Mangalhara, K.C., Mardamshina, M., Markovits, E., Baruch, E.N., Tripple, V., Arama-Chayoth, M., Greenberg, E., et al. (2019). Proteomics of melanoma response to immunotherapy reveals mitochondrial dependence. Cell *179*, 236–250.e18. https://doi.org/10.1016/j.cell.2019.08.012.
12. Gide, T.N., Wilmott, J.S., Scolyer, R.A., and Long, G.V. (2018). Primary and acquired resistance to immune checkpoint inhibitors in metastatic melanoma. Clin. Cancer Res. *24*, 1260–1270. https://doi.org/10.1158/1078-0432.CCR-17-2267.
13. Schadendorf, D., Hodi, F.S., Robert, C., Weber, J.S., Margolin, K., Hamid, O., Patt, D., Chen, T.-T., Berman, D.M., and Wolchok, J.D. (2013). Pooled analysis of long-term survival data from phase II and phase III trials of ipilimumab in metastatic or locally advanced, unresectable melanoma. J. Clin. Oncol. *33*, 1889–1894. https://doi.org/10.1200/JCO.2014.56.2736.
14. Topalian, S.L., Sznol, M., McDermott, D.F., Kluger, H.M., Carvajal, R.D., Sharfman, W.H., Brahmer, J.R., Lawrence, D.P., Atkins, M.B., Powderly, J.D., et al. (2023). Survival, Durable Tumor Remission, and Long-Term Safety in Patients With Advanced Melanoma Receiving Nivolumab. J. Clin. Oncol. *41*, 943–954. https://doi.org/10.1200/JCO.22.02272.
15. Schumacher, T.N., and Schreiber, R.D. (2015). Neoantigens in cancer immunotherapy. Science *348*, 69–74. https://doi.org/10.1126/science.aaa4971.
16. Vogelstein, B., Papadopoulos, N., Velculescu, V.E., Zhou, S., Diaz, L.A., and Kinzler, K.W. (2013). Cancer genome landscapes. Science *339*, 1546–1558. https://doi.org/10.1126/science.1235122.
17. Straetemans, T., Berrevoets, C., Coccoris, M., Treffers-Westerlaken, E., Wijers, R., Cole, D.K., Dardalhon, V., Sewell, A.K., Taylor, N., Verweij, J., and Debets, R. (2015). Recurrence of melanoma following T cell treatment: continued antigen expression in a tumor that evades T cell recruitment. Mol. Ther. *23*, 396–406. https://doi.org/10.1038/mt.2014.215.
18. Raposo, G., and Marks, M.S. (2007). Melanosomes–dark organelles enlighten endosomal membrane transport. Nat. Rev. Mol. Cell Biol. *8*, 786–797. https://doi.org/10.1038/nrm2258.
19. Malcov-Brog, H., Alpert, A., Golan, T., Parikh, S., Nordlinger, A., Netti, F., Sheinboim, D., Dror, I., Thomas, L., Cosson, C., et al. (2018). UV-Protection Timer Controls Linkage between Stress and Pigmentation Skin Protection Systems. Mol. Cell *72*, 444–456.e7. https://doi.org/10.1016/j.molcel.2018.09.022.
20. Peinado, H., Alečković, M., Lavotshkin, S., Matei, I., Costa-Silva, B., Moreno-Bueno, G., Hergueta-Redondo, M., Williams, C., García-Santos, G., Ghajar, C., et al. (2012). Melanoma exosomes educate bone marrow progenitor cells toward a pro-metastatic phenotype through MET. Nat. Med. *18*, 883–891. https://doi.org/10.1038/nm.2753.
21. Dror, S., Sander, L., Schwartz, H., Sheinboim, D., Barzilai, A., Dishon, Y., Apcher, S., Golan, T., Greenberger, S., Barshack, I., et al. (2016). Melanoma miRNA trafficking controls tumour primary niche formation. Nat. Cell Biol. *18*, 1006–1017. https://doi.org/10.1038/ncb3399.
22. Netanely, D., Leibou, S., Parikh, R., Stern, N., Vaknine, H., Brenner, R., Amar, S., Factor, R.H., Perluk, T., Frand, J., et al. (2021). Classification of node-positive melanomas into prognostic subgroups using keratin, immune, and melanogenesis expression patterns. Oncogene *40*, 1792–1805. https://doi.org/10.1038/s41388-021-01665-0.
23. Leichner, G.S., Schweitzer, I., Dror, S., Levin, L., Geva, P., Golan, T., Zaremba, L., Shapira, G., Parikh, R., Shomron, N., et al. (2023). Primary Melanoma miRNA Trafficking Induces Lymphangiogenesis. J. Investig. Dermatol. *143*, 1788–1798.e7. https://doi.org/10.1016/j.jid.2023.02.030.
24. Parikh, R., Parikh, S., Berzin, D., Vaknine, H., Ovadia, S., Likonen, D., Greenberger, S., Scope, A., Elgavish, S., Nevo, Y., et al. (2024). Recycled melanoma-secreted melanosomes regulate tumor-associated macrophage diversification. EMBO J. *43*, 3553–3586. https://doi.org/10.1038/s44318-024-00103-7.
25. Chen, K.G., Valencia, J.C., Lai, B., Zhang, G., Paterson, J.K., Rouzaud, F., Berens, W., Wincovitch, S.M., Garfield, S.H., Leapman, R.D., et al. (2006). Melanosomal sequestration of cytotoxic drugs contributes to the intractability of malignant melanomas. Proc Natl. Acad. Sci. USA *103*, 9903–9907. https://doi.org/10.1073/pnas.0600213103.
26. Pinner, S., Jordan, P., Sharrock, K., Bazley, L., Collinson, L., Marais, R., Bonvin, E., Goding, C., and Sahai, E. (2009). Intravital imaging reveals

transient changes in pigment production and Brn2 expression during metastatic melanoma dissemination. Cancer Res. *69*, 7969–7977. https://doi.org/10.1158/0008-5472.CAN-09-0781.

27. Riaz, N., Havel, J.J., Makarov, V., Desrichard, A., Urba, W.J., Sims, J.S., Hodi, F.S., Martín-Algarra, S., Mandal, R., Sharfman, W.H., et al. (2017). Tumor and Microenvironment Evolution during Immunotherapy with Nivolumab. Cell *171*, 934–949.e16. https://doi.org/10.1016/j.cell.2017.09.028.
28. Brożyna, A.A., Jóźwicki, W., Carlson, J.A., and Slominski, A.T. (2013). Melanogenesis affects overall and disease-free survival in patients with stage III and IV melanoma. Hum. Pathol. *44*, 2071–2074. https://doi.org/10.1016/j.humpath.2013.02.022.
29. Slominski, A., Zbytek, B., and Slominski, R. (2009). Inhibitors of melanogenesis increase toxicity of cyclophosphamide and lymphocytes against melanoma cells. Int. J. Cancer *124*, 1470–1477. https://doi.org/10.1002/ijc.24005.
30. Du, J., Miller, A.J., Widlund, H.R., Horstmann, M.A., Ramaswamy, S., and Fisher, D.E. (2003). MLANA/MART1 and SILV/PMEL17/GP100 are transcriptionally regulated by MITF in melanocytes and melanoma. Am. J. Pathol. *163*, 333–343. https://doi.org/10.1016/S0002-9440(10)63657-7.
31. Lo, J.A., Kawakubo, M., Juneja, V.R., Su, M.Y., Erlich, T.H., LaFleur, M.W., Kemeny, L.V., Rashid, M., Malehmir, M., Rabi, S.A., et al. (2021). Epitope spreading toward wild-type melanocyte-lineage antigens rescues suboptimal immune checkpoint blockade responses. Sci. Transl. Med. *13*, eabd8636. https://doi.org/10.1126/scitranslmed.abd8636.
32. Godefroy, E., Scotto, L., Souleimanian, N.E., Ritter, G., Old, L.J., Jotereau, F., Valmori, D., and Ayyoub, M. (2006). Identification of two Melan-A CD4+ T cell epitopes presented by frequently expressed MHC class II alleles. Clin. Immunol. *121*, 54–62. https://doi.org/10.1016/j.clim.2006.05.007.
33. Cochlovius, B., Linnebacher, M., Zewe-Welschof, M., and Zöller, M. (1999). Recombinant gp100 protein presented by dendritic cells elicits a T-helper-cell response in vitro and in vivo. Int. J. Cancer *83*, 547–554. https://doi.org/10.1002/(sici)1097-0215(19991112)83:4<547::aid-ijc18>3.0.co;2-6.
34. Peri, A., Salomon, N., Wolf, Y., Kreiter, S., Diken, M., and Samuels, Y. (2023). The landscape of T cell antigens for cancer immunotherapy. Nat. Cancer *4*, 937–954. https://doi.org/10.1038/s43018-023-00588-x.
35. Rudd, C.E. (2023). $CD8^+$ T cell killing of MHC class I-deficient tumors. Nat. Cancer *4*, 1214–1216. https://doi.org/10.1038/s43018-023-00606-y.
36. Watts, C., and Powis, S. (1999). Pathways of antigen processing and presentation. Rev. Immunogenet. *1*, 60–74. https://pubmed.ncbi.nlm.nih.gov/11256573/.
37. Friedmann-Morvinski, D., Bendavid, A., Waks, T., Schindler, D., and Eshhar, Z. (2005). Redirected primary T cells harboring a chimeric receptor require costimulation for their antigen-specific activation. Blood *105*, 3087–3093. https://doi.org/10.1182/blood-2004-09-3737.
38. Sugiura, D., Okazaki, I.M., Maeda, T.K., Maruhashi, T., Shimizu, K., Arakaki, R., Takemoto, T., Ishimaru, N., and Okazaki, T. (2022). PD-1 agonism by anti-CD80 inhibits T cell activation and alleviates autoimmunity. Nat. Immunol. *23*, 399–410. https://doi.org/10.1038/s41590-021-01125-7.
39. Haile, S.T., Dalal, S.P., Clements, V., Tamada, K., and Ostrand-Rosenberg, S. (2013). Soluble CD80 restores T cell activation and overcomes tumor cell programmed death ligand 1-mediated immune suppression. J. Immunol. *191*, 2829–2836. https://doi.org/10.4049/jimmunol.1202777.
40. Waldman, A.D., Fritz, J.M., and Lenardo, M.J. (2020). A guide to cancer immunotherapy: from T cell basic science to clinical practice. Nat. Rev. Immunol. *20*, 651–668. https://doi.org/10.1038/s41577-020-0306-5.
41. Cancer; Genome; Atlas Network (2015). Genomic classification of cutaneous melanoma. Cell *161*, 1681–1696. https://doi.org/10.1016/j.cell.2015.05.044.
42. Wherry, E.J., Ha, S.J., Kaech, S.M., Haining, W.N., Sarkar, S., Kalia, V., Subramaniam, S., Blattman, J.N., Barber, D.L., and Ahmed, R. (2007). Molecular signature of CD8+ T cell exhaustion during chronic viral infection. Immunity *27*, 670–684. https://doi.org/10.1016/j.immuni.2007.09.006.
43. Amitay, Y., Milo, I., Haran, T.K., Deis, S., Truzman, G., Elhanani, O., Salame, T.-M., Azimov, M., Stein, I., Cohen, J.E., et al. (2025). Immune organization in sentinel lymph nodes of melanoma patients is prognostic of distant metastases. Preprint at bioRxiv. https://www.biorxiv.org/content/10.1101/2024.11.24.625041v1.
44. Sakai, C., Kawakami, Y., Law, L.W., Furumura, M., and Hearing, V.J., Jr. (1997). Melanosomal proteins as melanoma-specific immune targets. Melanoma Res. *7*, 83–95. https://doi.org/10.1097/00008390-199704000-00001.
45. Chen, J., He, Q., Liu, J., Xiao, Y., Xiao, C., Chen, K., Xie, D., and Zhang, X. (2018). CD8+ tumor-infiltrating lymphocytes as a novel prognostic biomarker in lung sarcomatoid carcinoma, a rare subtype of lung cancer. Cancer Manag. Res. *10*, 3505–3511. https://doi.org/10.2147/CMAR.S169074.
46. O'Keefe, J.P., Blaine, K., Alegre, M.L., and Gajewski, T.F. (2004). Formation of a central supramolecular activation cluster is not required for activation of naive CD8+ T cells. Proc. Natl. Acad. Sci. USA *101*, 9351–9356. https://doi.org/10.1073/pnas.0305965101.
47. Smith, F.O., Downey, S.G., Klapper, J.A., Yang, J.C., Sherry, R.M., Royal, R.E., Kammula, U.S., Hughes, M.S., Restifo, N.P., Levy, C.L., et al. (2008). Treatment of metastatic melanoma using interleukin-2 alone or in conjunction with vaccines. Clin. Cancer Res. *14*, 5610–5618. https://doi.org/10.1158/1078-0432.CCR-08-0116.
48. Hogquist, K.A., Jameson, S.C., Heath, W.R., Howard, J.L., Bevan, M.J., and Carbone, F.R. (1994). T cell receptor antagonist peptides induce positive selection. Cell *76*, 17–27. https://doi.org/10.1016/0092-8674(94)90169-4.
49. Zilles, J.C., Dos Santos, F.L., Kulkamp-Guerreiro, I.C., and Contri, R.V. (2022). Biological activities and safety data of kojic acid and its derivatives: A review. Exp. Dermatol. *31*, 1500–1521. https://doi.org/10.1111/exd.14662.
50. García-Gavín, J., González-Vilas, D., Fernández-Redondo, V., and Toribio, J. (2010). Pigmented contact dermatitis due to kojic acid. A paradoxical side effect of a skin lightener. Contact Derm. *62*, 63–64. https://doi.org/10.1111/j.1600-0536.2009.01673.x.
51. Lajis, A.F.B., Hamid, M., and Ariff, A.B. (2012). Depigmenting effect of Kojic acid esters in hyperpigmented B16F1 melanoma cells. J. Biomed. Biotechnol. *2012*, 952452. https://doi.org/10.1155/2012/952452.
52. Azumi, J., Takeda, T., Shimada, Y., Aso, H., and Nakamura, T. (2019). The Organogermanium Compound THGP Suppresses Melanin Synthesis via Complex Formation with L-DOPA on Mushroom Tyrosinase and in B16 4A5 Melanoma Cells. Int. J. Mol. Sci. *20*, 4785. https://doi.org/10.3390/ijms20194785.
53. Saeedi, M., Eslamifar, M., and Khezri, K. (2019). Kojic acid applications in cosmetic and pharmaceutical preparations. Biomed. Pharmacother. *110*, 582–593. https://doi.org/10.1016/j.biopha.2018.12.006.
54. Calis, J.J.A., Maybeno, M., Greenbaum, J.A., Weiskopf, D., De Silva, A.D., Sette, A., Keşmir, C., and Peters, B. (2013). Properties of MHC class I presented peptides that enhance immunogenicity. PLoS Comput. Biol. *9*, e1003266. https://doi.org/10.1371/journal.pcbi.1003266.
55. Rosa, F.M., and Fellous, M. (1988). Regulation of HLA-DR gene by IFN-gamma. Transcriptional and post-transcriptional control. J. Immunol. *140*, 1660–1664. https://doi.org/10.4049/jimmunol.140.5.1660.
56. Balogh, K.N., Templeton, D.J., and Cross, J.V. (2018). Macrophage Migration Inhibitory Factor protects cancer cells from immunogenic cell death and impairs anti-tumor immune responses. PLoS One *13*, e0197702. https://doi.org/10.1371/journal.pone.0197702.

57. Van der Jeught, K., Joe, P.T., Bialkowski, L., Heirman, C., Daszkiewicz, L., Liechtenstein, T., Escors, D., Thielemans, K., and Breckpot, K. (2014). Intratumoral administration of mRNA encoding a fusokine consisting of IFN-beta and the ectodomain of the TGF-beta receptor II potentiates antitumor immunity. Oncotarget *5*, 10100–10113. https://doi.org/10.18632/oncotarget.2463.

58. Quezada, S.A., Simpson, T.R., Peggs, K.S., Merghoub, T., Vider, J., Fan, X., Blasberg, R., Yagita, H., Muranski, P., Antony, P.A., et al. (2010). Tumor-reactive CD4(+) T cells develop cytotoxic activity and eradicate large established melanoma after transfer into lymphopenic hosts. J. Exp. Med. *207*, 637–650. https://doi.org/10.1084/jem.20091918.

59. Kearl, T.J., Jing, W., Gershan, J.A., and Johnson, B.D. (2013). Programmed death receptor-1/programmed death receptor ligand-1 blockade after transient lymphodepletion to treat myeloma. J. Immunol. *190*, 5620–5628. https://doi.org/10.4049/jimmunol.1202005.

60. Le, L., Sirés-Campos, J., Raposo, G., Delevoye, C., and Marks, M.S. (2021). Melanosome Biogenesis in the Pigmentation of Mammalian Skin. Integr. Comp. Biol. *61*, 1517–1545. https://doi.org/10.1093/icb/icab078.

61. Jiang, K., Dong, C., Yin, Z., Li, R., Mao, J., Wang, C., Zhang, J., Gao, Z., Liang, R., Wang, Q., and Wang, L. (2020). Exosome-derived ENO1 regulates integrin α6β4 expression and promotes hepatocellular carcinoma growth and metastasis. Cell Death Dis. *11*, 972. https://doi.org/10.1038/s41419-020-03179-1.

62. Tyanova, S., Temu, T., Sinitcyn, P., Carlson, A., Hein, M.Y., Geiger, T., Mann, M., and Cox, J. (2016). The Perseus computational platform for comprehensive analysis of (prote)omics data. Nat. Methods *13*, 731–740. https://doi.org/10.1038/nmeth.3901.

63. Dersh, D., Yewdell, J.W., and Wei, J. (2019). A SIINFEKL-Based System to Measure MHC Class I Antigen Presentation Efficiency and Kinetics. Methods Mol. Biol. *1988*, 109–122. https://doi.org/10.1007/978-1-4939-9450-2_9.

64. Feng, D., Zhao, W.L., Ye, Y.Y., Bai, X.C., Liu, R.Q., Chang, L.F., Zhou, Q., and Sui, S.F. (2010). Cellular internalization of exosomes occurs through phagocytosis. Traffic *11*, 675–687. https://doi.org/10.1111/j.1600-0854.2010.01041.x.

65. Das, K., Eisel, D., Lenkl, C., Goyal, A., Diederichs, S., Dickes, E., Osen, W., and Eichmüller, S.B. (2017). Generation of murine tumor cell lines deficient in MHC molecule surface expression using the CRISPR/Cas9 system. PLoS One *12*, e0174077. https://doi.org/10.1371/journal.pone.0174077.

66. Kalaora, S., Barnea, E., Merhavi-Shoham, E., Qutob, N., Teer, J.K., Shimony, N., Schachter, J., Rosenberg, S.A., Besser, M.J., Admon, A., and Samuels, Y. (2016). Use of HLA peptidomics and whole exome sequencing to identify human immunogenic neo-antigens. Oncotarget *7*, 5110–5117. https://doi.org/10.18632/oncotarget.6960.

67. Zhou, C., Wei, Z., Zhang, Z., Zhang, B., Zhu, C., Chen, K., Chuai, G., Qu, S., Xie, L., Gao, Y., and Liu, Q. (2019). pTuneos: prioritizing tumor neoantigens from next-generation sequencing data. Genome Med. *11*, 67. https://doi.org/10.1186/s13073-019-0679-x.

68. Chowell, D., Krishna, S., Becker, P.D., Cocita, C., Shu, J., Tan, X., Greenberg, P.D., Klavinskis, L.S., Blattman, J.N., and Anderson, K.S. (2015). TCR contact residue hydrophobicity is a hallmark of immunogenic CD8+ T cell epitopes. Proc. Natl. Acad. Sci. USA *112*, E1754–E1762. https://doi.org/10.1073/pnas.1500973112.

69. Krokhin, O.V., Craig, R., Spicer, V., Ens, W., Standing, K.G., Beavis, R.C., and Wilkins, J.A. (2004). An improved model for prediction of retention times of tryptic peptides in ion pair reversed-phase HPLC: its application to protein peptide mapping by off-line HPLC-MALDI MS. Mol. Cell. Proteomics *3*, 908–919. https://doi.org/10.1074/mcp.M400031-MCP200.

70. Marcu, A., Bichmann, L., Kuchenbecker, L., Kowalewski, D.J., Freudenmann, L.K., Backert, L., Mühlenbruch, L., Szolek, A., Lübke, M., Wagner, P., et al. (2021). HLA Ligand Atlas: a benign reference of HLA-presented peptides to improve T-cell-based cancer immunotherapy. J. Immunother. Cancer *9*, e002071. https://doi.org/10.1136/jitc-2020-002071.

71. Refaeli, Y., Van Parijs, L., Alexander, S.I., and Abbas, A.K. (2002). Interferon gamma is required for activation-induced death of T lymphocytes. J. Exp. Med. *196*, 999–1005. https://doi.org/10.1084/jem.20020666.

72. Otano, I., Alvarez, M., Minute, L., Ochoa, M.C., Migueliz, I., Molina, C., Azpilikueta, A., de Andrea, C.E., Etxeberria, I., Sanmamed, M.F., et al. (2020). Human CD8 T cells are susceptible to TNF-mediated activation-induced cell death. Theranostics *10*, 4481–4489. https://doi.org/10.7150/thno.41646.

73. Bertrand, F., Rochotte, J., Colacios, C., Montfort, A., Andrieu-Abadie, N., Levade, T., Benoist, H., and Ségui, B. (2016). Targeting TNF alpha as a novel strategy to enhance CD8+ T cell-dependent immune response in melanoma? Oncoimmunology *5*, e1068495. https://doi.org/10.1080/2162402X.2015.1068495.

74. Harding, F.A., McArthur, J.G., Gross, J.A., Raulet, D.H., and Allison, J.P. (1992). CD28-mediated signalling co-stimulates murine T cells and prevents induction of anergy in T-cell clones. Nature *356*, 607–609. https://doi.org/10.1038/356607a0.

75. Croft, M. (2003). Co-stimulatory members of the TNFR family: keys to effective T-cell immunity? Nat. Rev. Immunol. *3*, 609–620. https://doi.org/10.1038/nri1148.

76. Wherry, E.J. (2011). T cell exhaustion. Nat. Immunol. *12*, 492–499. https://doi.org/10.1038/ni.2035.

77. Courtney, A.H., Lo, W.L., and Weiss, A. (2018). TCR Signaling: Mechanisms of Initiation and Propagation. Trends Biochem. Sci. *43*, 108–123. https://doi.org/10.1016/j.tibs.2017.11.008.

78. Yu, Y.R., Imrichova, H., Wang, H., Chao, T., Xiao, Z., Gao, M., Rincon-Restrepo, M., Franco, F., Genolet, R., Cheng, W.C., et al. (2020). Disturbed mitochondrial dynamics in CD8+ TILs reinforce T cell exhaustion. Nat. Immunol. *21*, 1540–1551. https://doi.org/10.1038/s41590-020-0793-3.

79. Maliah, A., Santana-Magal, N., Parikh, S., Gordon, S., Reshef, K., Sade, Y., Khateeb, A., Richter, A., Gutwillig, A., Parikh, R., et al. (2024). Cross-linking of Ly6a metabolically reprograms CD8 T cells for cancer immunotherapy. Nat. Commun. *15*, 8354. https://doi.org/10.1038/s41467-024-52079-x.

80. Raposo, G., Nijman, H.W., Stoorvogel, W., Liejendekker, R., Harding, C.V., Melief, C.J., and Geuze, H.J. (1996). B lymphocytes secrete antigen-presenting vesicles. J. Exp. Med. *183*, 1161–1172. https://doi.org/10.1084/jem.183.3.1161.

81. Buzas, E.I. (2023). The roles of extracellular vesicles in the immune system. Nat. Rev. Immunol. *23*, 236–250. https://doi.org/10.1038/s41577-022-00763-8.

82. Théry, C., Duban, L., Segura, E., Véron, P., Lantz, O., and Amigorena, S. (2002). Indirect activation of naive CD4+ T cells by dendritic cell-derived exosomes. Nat. Immunol. *3*, 1156–1162. https://doi.org/10.1038/ni854.

83. Vincent-Schneider, H., Stumptner-Cuvelette, P., Lankar, D., Pain, S., Raposo, G., Benaroch, P., and Bonnerot, C. (2002). Exosomes bearing HLA-DR1 molecules need dendritic cells to efficiently stimulate specific T cells. Int. Immunol. *14*, 713–722. https://doi.org/10.1093/intimm/dxf048.

84. Guan, S., Li, Q., Liu, P., Xuan, X., and Du, Y. (2014). Umbilical cord blood-derived dendritic cells loaded with BGC823 tumor antigens and DC-derived exosomes stimulate efficient cytotoxic T-lymphocyte responses and antitumor immunity in vitro and in vivo. Cent. Eur. J. Immunol. *39*, 142–151. https://doi.org/10.5114/ceji.2014.43713.

85. Nakayama, M. (2014). Antigen Presentation by MHC-Dressed Cells. Front. Immunol. *5*, 672. https://doi.org/10.3389/fimmu.2014.00672.

86. Théry, C., Ostrowski, M., and Segura, E. (2009). Membrane vesicles as conveyors of immune responses. Nat. Rev. Immunol. *9*, 581–593. https://doi.org/10.1038/nri2567.

87. Khabar, K.S.A., and Young, H.A. (2007). Post-transcriptional control of the interferon system. Biochimie *89*, 761–769. https://doi.org/10.1016/j.biochi.2007.02.008.

88. Chen, G., Huang, A.C., Zhang, W., Zhang, G., Wu, M., Xu, W., Yu, Z., Yang, J., Wang, B., Sun, H., et al. (2018). Exosomal PD-L1 contributes to immunosuppression and is associated with anti-PD-1 response. Nature *560*, 382–386. https://doi.org/10.1038/s41586-018-0392-8.

89. Hoshino, A., Costa-Silva, B., Shen, T.L., Rodrigues, G., Hashimoto, A., Tesic Mark, M., Molina, H., Kohsaka, S., Di Giannatale, A., Ceder, S., et al. (2015). Tumour exosome integrins determine organotropic metastasis. Nature *527*, 329–335. https://doi.org/10.1038/nature15756.

90. Tang, M.L., Varigos, G., and Kemp, A.S. (1994). Reduced interferon-gamma (IFN-gamma) secretion with increased IFN-gamma mRNA expression in atopic dermatitis: evidence for a post-transcriptional defect. Clin. Exp. Immunol. *97*, 483–490. https://doi.org/10.1111/j.1365-2249.1994.tb06114.x.

91. Savan, R. (2014). Post-transcriptional regulation of interferons and their signaling pathways. J. Interferon Cytokine Res. *34*, 318–329. https://doi.org/10.1089/jir.2013.0117.

92. Hodge, D.L., Martinez, A., Julias, J.G., Taylor, L.S., and Young, H.A. (2002). Regulation of nuclear gamma interferon gene expression by interleukin 12 (IL-12) and IL-2 represents a novel form of posttranscriptional control. Mol. Cell. Biol. *22*, 1742–1753. https://doi.org/10.1128/MCB.22.6.1742-1753.2002.

93. Benito-Martínez, S., Salavessa, L., Raposo, G., Marks, M.S., and Delevoye, C. (2021). Melanin Transfer and Fate within Keratinocytes in Human Skin Pigmentation. Integr. Comp. Biol. *61*, 1546–1555. https://doi.org/10.1093/icb/icab094.

94. Marks, M.S., Theos, A.C., and Raposo, G. (2003). Melanosomes and MHC class II antigen-processing compartments: a tinted view of intracellular trafficking and immunity. Immunol. Res. *27*, 409–426. https://doi.org/10.1385/IR:27:2-3:409.

95. Hurbain, I., Romao, M., Sextius, P., Bourreau, E., Marchal, C., Bernerd, F., Duval, C., and Raposo, G. (2018). Melanosome distribution in keratinocytes in different skin types: melanosome clusters are not degradative organelles. J. Investig. Dermatol. *138*, 647–656. https://doi.org/10.1016/j.jid.2017.09.039.

96. Tarafder, A.K., Bolasco, G., Correia, M.S., Pereira, F.J.C., Iannone, L., Hume, A.N., Kirkpatrick, N., Picardo, M., Torrisi, M.R., Rodrigues, I.P., et al. (2014). Rab11b mediates melanin transfer between donor melanocytes and acceptor keratinocytes via coupled exo/endocytosis. J. Investig. Dermatol. *134*, 1056–1066. https://doi.org/10.1038/jid.2013.432.

97. Delevoye, C., Marks, M.S., and Raposo, G. (2019). Lysosome-related organelles as functional adaptations of the endolysosomal system. Curr. Opin. Cell Biol. *59*, 147–158. https://doi.org/10.1016/j.ceb.2019.05.003.

98. Barras, D., Ghisoni, E., Chiffelle, J., Orcurto, A., Dagher, J., Fahr, N., Benedetti, F., Crespo, I., Grimm, A.J., Morotti, M., et al. (2024). Response to tumor-infiltrating lymphocyte adoptive therapy is associated with preexisting CD8+ T-myeloid cell networks in melanoma. Sci. Immunol. *9*, eadg7995. https://doi.org/10.1126/sciimmunol.adg7995.

99. Valpione, S., Mundra, P.A., Galvani, E., Campana, L.G., Lorigan, P., De Rosa, F., Gupta, A., Weightman, J., Mills, S., Dhomen, N., and Marais, R. (2021). The T cell receptor repertoire of tumor infiltrating T cells is predictive and prognostic for cancer survival. Nat. Commun. *12*, 4098. https://doi.org/10.1038/s41467-021-24343-x.

100. Hugo, W., Zaretsky, J.M., Sun, L., Song, C., Moreno, B.H., Hu-Lieskovan, S., Berent-Maoz, B., Pang, J., Chmielowski, B., Cherry, G., et al. (2016). Genomic and Transcriptomic Features of Response to Anti-PD-1 Therapy in Metastatic Melanoma. Cell *165*, 35–44. https://doi.org/10.1016/j.cell.2016.02.065.

101. Amitay, Y., Milo, I., Haran, T.K., Deis, S., Truzman, G., Elhanani, O., Salame, T.-M., Azimov, M., Stein, I., Cohen, J.E., et al. (2024). Immune organization in sentinel lymph nodes of melanoma patients is prognostic of distant metastases. Preprint at bioRxiv. https://doi.org/10.1101/2024.11.24.625041.

102. Itzhaki, O., Hovav, E., Ziporen, Y., Levy, D., Kubi, A., Zikich, D., Hershkovitz, L., Treves, A.J., Shalmon, B., Zippel, D., et al. (2011). Establishment and large-scale expansion of minimally cultured "young" tumor infiltrating lymphocytes for adoptive transfer therapy. J. Immunother. *34*, 212–220. https://doi.org/10.1097/CJI.0b013e318209c94c.

103. Farhat-Younis, L., Na, M., Zarfin, A., Khateeb, A., Santana-Magal, N., Richter, A., Gutwillig, A., Rasoulouniriana, D., Gleiberman, A., Beck, L., et al. (2024). Expression of modified FcγRI enables myeloid cells to elicit robust tumor-specific cytotoxicity. eLife *12*, RP91999. https://doi.org/10.7554/eLife.91999.

104. Wang, K., Liu, C., Di, C.J., Ma, C., Han, C.G., Yuan, M.R., Li, P.F., Li, L., and Liu, Y.X. (2014). Kojic acid protects C57BL/6 mice from gamma-irradiation induced damage. Asian Pac. J. Cancer Prev. *15*, 291–297. https://doi.org/10.7314/apjcp.2014.15.1.291.

105. Elkoshi, N., Parikh, S., Malcov-Brog, H., Parikh, R., Manich, P., Netti, F., Maliah, A., Elkoshi, H., Haj, M., Rippin, I., et al. (2023). Ataxia Telangiectasia Mutated Signaling Delays Skin Pigmentation upon UV Exposure by Mediating MITF Function toward DNA Repair Mode. J. Investig. Dermatol. *143*, 2494–2506.e4. https://doi.org/10.1016/j.jid.2023.03.1686.

106. Sheinboim, D., Parikh, S., Manich, P., Markus, I., Dahan, S., Parikh, R., Stubbs, E., Cohen, G., Zemser-Werner, V., Bell, R.E., et al. (2022). An exercise-induced metabolic shield in distant organs blocks cancer progression and metastatic dissemination. Cancer Res. *82*, 4164–4178. https://doi.org/10.1158/0008-5472.CAN-22-0237.

107. Cox, J., Hein, M.Y., Luber, C.A., Paron, I., Nagaraj, N., and Mann, M. (2014). Accurate proteome-wide label-free quantification by delayed normalization and maximal peptide ratio extraction, termed MaxLFQ. Mol. Cell. Proteomics *13*, 2513–2526. https://doi.org/10.1074/mcp.M113.031591.

108. Kong, A.T., Leprevost, F.V., Avtonomov, D.M., Mellacheruvu, D., and Nesvizhskii, A.I. (2017). MSFragger: ultrafast and comprehensive peptide identification in mass spectrometry-based proteomics. Nat. Methods *14*, 513–520. https://doi.org/10.1038/nmeth.4256.

109. Yang, K.L., Yu, F., Teo, G.C., Li, K., Demichev, V., Ralser, M., and Nesvizhskii, A.I. (2023). MSBooster: improving peptide identification rates using deep learning-based features. Nat. Commun. *14*, 4539. https://doi.org/10.1038/s41467-023-40129-9.

110. Weller, C., Bartok, O., McGinnis, C.S., Palashati, H., Chang, T.G., Malko, D., Shmueli, M.D., Nagao, A., Hayoun, D., Murayama, A., et al. (2025). Translation dysregulation in cancer as a source for targetable antigens. Cancer Cell *43*, 823–840.e18. https://doi.org/10.1016/j.ccell.2025.03.003.

111. Reynisson, B., Alvarez, B., Paul, S., Peters, B., and Nielsen, M. (2020). NetMHCpan-4.1 and NetMHCIIpan-4.0: improved predictions of MHC antigen presentation by concurrent motif deconvolution and integration of MS MHC eluted ligand data. Nucleic Acids Res. *48*, W449–W454. https://doi.org/10.1093/nar/gkaa379.

112. Pitcovski, J., Shahar, E., Aizenshtein, E., and Gorodetsky, R. (2017). Melanoma antigens and related immunological markers. Crit. Rev. Oncol. Hematol. *115*, 36–49. https://doi.org/10.1016/j.critrevonc.2017.05.001.

113. Durinck, S., Spellman, P.T., Birney, E., and Huber, W. (2009). Mapping identifiers for the integration of genomic datasets with the R/Bioconductor package biomaRt. Nat. Protoc. *4*, 1184–1191. https://doi.org/10.1038/nprot.2009.97.

114. Durinck, S., Moreau, Y., Kasprzyk, A., Davis, S., De Moor, B., Brazma, A., and Huber, W. (2005). BioMart and Bioconductor: a powerful link between biological databases and microarray data analysis. Bioinformatics *21*, 3439–3440. https://doi.org/10.1093/bioinformatics/bti525.

115. Li, H., and Durbin, R. (2009). Fast and accurate short read alignment with Burrows-Wheeler transform. Bioinformatics *25*, 1754–1760. https://doi.org/10.1093/bioinformatics/btp324.

116. Van der Auwera, G.A., Carneiro, M.O., Hartl, C., Poplin, R., Del Angel, G., Levy-Moonshine, A., Jordan, T., Shakir, K., Roazen, D., Thibault, J., et al. (2013). From FastQ data to high confidence variant calls: the Genome Analysis Toolkit best practices pipeline. Curr. Protoc. Bioinform. *43*, 11.10.1–11.10.33. https://doi.org/10.1002/0471250953.bi1110s43.

117. Wang, K., Li, M., and Hakonarson, H. (2010). ANNOVAR: functional annotation of genetic variants from high-throughput sequencing data. Nucleic Acids Res. *38*, e164. https://doi.org/10.1093/nar/gkq603.

118. Chen, S., Francioli, L.C., Goodrich, J.K., Collins, R.L., Kanai, M., Wang, Q., Alföldi, J., Watts, N.A., Vittal, C., Gauthier, L.D., et al. (2024). A genomic mutational constraint map using variation in 76,156 human genomes. Nature *625*, 92–100. https://doi.org/10.1038/s41586-023-06045-0.

119. Ferreira, H.J., Stevenson, B.J., Pak, H., Yu, F., Almeida Oliveira, J., Huber, F., Taillandier-Coindard, M., Michaux, J., Ricart-Altimiras, E., Kraemer, A.I., et al. (2024). Immunopeptidomics-based identification of naturally presented non-canonical circRNA-derived peptides. Nat. Commun. *15*, 2357. https://doi.org/10.1038/s41467-024-46408-3.

120. Mitchell, J., Milite, S., Bartram, J., Walker, S., Volkova, N., Yavorska, O., Zarowiecki, M., Chalker, J., Thomas, R., Vago, L., et al. (2024). Clinical application of tumour-in-normal contamination assessment from whole genome sequencing. Nat. Commun. *15*, 323. https://doi.org/10.1038/s41467-023-44158-2.

121. Li, Y., Kind, T., Folz, J., Vaniya, A., Mehta, S.S., and Fiehn, O. (2021). Spectral entropy outperforms MS/MS dot product similarity for small-molecule compound identification. Nat. Methods *18*, 1524–1531. https://doi.org/10.1038/s41592-021-01331-z.

122. Stuart, T., Butler, A., Hoffman, P., Hafemeister, C., Papalexi, E., Mauck, W.M., 3rd, Hao, Y., Stoeckius, M., Smibert, P., and Satija, R. (2019). Comprehensive Integration of Single-Cell Data. Cell *177*, 1888–1902.e21. https://doi.org/10.1016/j.cell.2019.05.031.

123. Kurtulus, S., Madi, A., Escobar, G., Klapholz, M., Nyman, J., Christian, E., Pawlak, M., Dionne, D., Xia, J., Rozenblatt-Rosen, O., et al. (2019). Checkpoint Blockade Immunotherapy Induces Dynamic Changes in PD-1(-)CD8(+) Tumor-Infiltrating T Cells. Immunity *50*, 181–194.e6. https://doi.org/10.1016/j.immuni.2018.11.014.

124. Bolger, A.M., Lohse, M., and Usadel, B. (2014). Trimmomatic: a flexible trimmer for Illumina sequence data. Bioinformatics *30*, 2114–2120. https://doi.org/10.1093/bioinformatics/btu170.

125. Dobin, A., Davis, C.A., Schlesinger, F., Drenkow, J., Zaleski, C., Jha, S., Batut, P., Chaisson, M., and Gingeras, T.R. (2013). STAR: ultrafast universal RNA-seq aligner. Bioinformatics *29*, 15–21. https://doi.org/10.1093/bioinformatics/bts635.

126. Baxter, L.L., Watkins-Chow, D.E., Pavan, W.J., and Loftus, S.K. (2019). A curated gene list for expanding the horizons of pigmentation biology. Pigment Cell Melanoma Res. *32*, 348–358. https://doi.org/10.1111/pcmr.12743.

127. Buchfink, B., Reuter, K., and Drost, H.G. (2021). Sensitive protein alignments at tree-of-life scale using DIAMOND. Nat. Methods *18*, 366–368. https://doi.org/10.1038/s41592-021-01101-x.

Please cite this article in press as: Chemla et al., HLA export by melanoma cells decoys cytotoxic T cells to promote immune evasion, Cell (2026), https://doi.org/10.1016/j.cell.2025.11.020

STAR★METHODS

KEY RESOURCES TABLE

REAGENT or RESOURCE	SOURCE	IDENTIFIER
Antibodies		
112Cd Rat Anti mouse CD45	BioLegend	Clone:30-F11; Cat#103120; RRID: AB_312985
113In anti-mouse/human CD44	BioLegend	Clone:IM7; Cat#103014; RRID: AB_312965
115In Rat anti-mouse CD3	BioLegend	Clone: 145-2C11; Cat#100340; RRID: AB_11149115
141Pr Rat anti-mouse CD274	BioLegend	Clone:10F.9G2; Cat#124302; RRID: AB_961228
142Nd Ratr anti-mouse Ly-6G/Ly-6C (Gr-1)	BioLegend	Clone: RB6-8C5; Cat#108449; RRID: AB_2563785
143Nd Ratr anti-mouse CD86	BioLegend	Clone:GL-1; Cat#105002; RRID: AB_313145
144Nd Ratr anti-mouse F4/80	BioLegend	Clone: BM8; Cat#123102; RRID: AB_893506
145Nd Anti mouse CD4	Standard biotools	Clone: RM4-5; Cat#3145002B; RRID: AB_2687832
146Nd Rat anti-mouse CD45R	BioLegend	Clone: RA3-6B2; Cat#103202; RRID: AB_312987
147Sm Rat anti-mouse Ly6c	BioLegend	Clone: HK1.4; Cat#115808; RRID: AB_1134214
148Nd Rat anti-mouse IL-6r (CD126)	BioLegend	Clone: D7715A7; Cat#115808; RRID: AB_313679
149Sm Rat anti-mouse CD8	BioLegend	Clone: 53-6.7; Cat#100746; RRID: AB_11147171
150Nd Rat anti-mouse CD25	Fluidigm Corporation	Clone: 3C7; Cat#3150002B; RRID: AB_2687835
152Sm Hamster anti-mouse TCRγδ	BioLegend	Clone: GL3; Cat#553175; RRID: AB_394686
153Eu Hamster anti-mouse PD-L2	BioLegend	Clone: TY25; Cat#107202; RRID: AB_345250
154Sm Hamster anti-mouse CD11c	BioLegend	Clone: N418; Cat#117302; RRID: AB_313771
155Gd Rat anti-mouse IgM	BioLegend	Clone: RMM-1; Cat#406502; RRID: AB_315052
156Gd Rat anti-mouse CD49b	BioLegend	Clone: DX5; Cat#108902; RRID: AB_313409
157Gd Rat anti-mouse CD19	BioLegend	Clone: 6D5; Cat#115502; RRID: AB_313637
158Gd Anti mouse PD-1 CD279	BioLegend	Clone: RMP1-14; Cat#109113; RRID: AB_2563735
159Tb Rat anti-mouse Ki-67	BioLegend	Clone: 16A8; Cat#652402; RRID: AB_11204254
160Gd Mouse anti mouse/human T-bet	BioLegend	Clone: 4B10; Cat#644802; RRID: AB_1595503
161Dy Mouse anti-mouse CX3CR1	BioLegend	Clone: SA011F11; Cat#149002; RRID: AB_2564313
162Dy Mouse anti-mouse CD64	BioLegend	Clone: X54-5/7.1; Cat#139302; RRID: AB_10613107
163Dy Rat anti-mouse CD127	BioLegend	Clone: A7R34; Cat#135002; RRID: AB_1937287
164Dy Hamster anti-mouse CD28	BioLegend	Clone: 37.51; Cat#102116; RRID: AB_11147170
165Ho anti-mouse/rat/human FOXP3	Fluidigm Corporation	Clone: 150D; Cat#320002; RRID: AB_439746
166Er anti-mouse TCR β chain	BioLegend	Clone: H57-597; Cat#109235; RRID: AB_2562804
167Er Rat anti mouse FR4	BioLegend	Clone: TH6; Cat#125102; RRID: AB_1027724
169Tm Rat anti mouse CXCR2 (CD182)	BioLegend	Clone: SA044G4; Cat#149302; RRID: AB_2565277
170Er Anti-mouse NK-1.1	BioLegend	Clone: PK136; Cat#108702; RRID: AB_313389
171Yb Rat Anti mouse CD195	BD Pharmingen	Clone: Clone C34-3448; Cat#559921; RRID: AB_397375
172Yb Hamster anti mouse CD152	BioLegend	Clone: 9H10; Cat#106202; RRID: AB_313247
173Yb Rat anti mouse Sca-1	BioLegend	Clone: D7; Cat#108102; RRID: AB_313339
174Yb Rat anti mouse Ia-Ie	BioLegend	Clone: M5/114.15.2; Cat#108102; RRID: AB_313340

(*Continued on next page*)

Please cite this article in press as: Chemla et al., HLA export by melanoma cells decoys cytotoxic T cells to promote immune evasion, Cell (2026), https://doi.org/10.1016/j.cell.2025.11.020

Continued

REAGENT or RESOURCE	SOURCE	IDENTIFIER
175Lu Rat anti mouse IgD	BioLegend	Clone: 11-26c.2a; Cat#108102; RRID: AB_313341
176Yb Rat anti mouse CD11b	BioLegend	Clone: M1/70; Cat#108102; RRID: AB_313342
anti-CD3 antibody OKT3 (MACS® GMP CD3 pure)	Miltenyi Biotec	Clone: OKT3; Cat#170-076-124; RRID: AB_2904535
Anti-Mouse H-2Db	SouthrenBiotech	Cat#1910-01; RRID: AB_2795489
APC anti-human CD137 (4-1BB) Antibody	BioLegend	clone: 4B4-1; Cat#309810; RRID: AB_830672
APC anti-human CD25 Antibody	BioLegend	Clone: BC96; Cat#302610; RRID: AB_314280
APC anti-human CD28 Antibody	BioLegend	clone: CD28.2, Cat#302912; RRID: AB_314314
APC anti-human CD3	Millipore, Merck	Clone: HIT3a; Cat#MABF315; RRID: N/A
APC anti-human CD4	BioLegend	Clone: RPA-T4; Cat#300552; RRID: AB_2564153
APC anti-human CD45 Antibody	BioLegend	Clone: 2D1; Cat#368512; RRID: AB_2566372
APC CD45 Antibody, anti-mouse, REAfinity™	Miltenyi Biotec	Clone: REA737 | 30F11; Cat#130-110-798; RRID: AB_2658220
FITC anti-human CD134 (OX40) Antibody	BioLegend	clone: Ber-ACT35 (ACT35); Cat#350006; RRID: AB_10661725
FITC anti-human CD223 (LAG-3) Antibody	BioLegend	clone: 11C3C65; Cat#369308; RRID: AB_2629751
FITC anti-human CD279 (PD-1) Antibody	BioLegend	Clone: EH12.2H7; Cat#329904; RRID: AB_940479
FITC anti-human HLA-A,B,C	BioLegend	Clone: W6/32; Cat#311404; RRID: AB_314873
Human anti-CD8	Cell Marque	Cat#108M-95; RRID: AB_1158206
Human anti-GPNMB	R&D Systems	Cat#AF2550; RRID: AB_416615
Human anti-HMB45	Abcam	Clone: HMB45; Cat#ab732; RRID: AB_305844
InVivoMAb anti-mouse CD8α	BioXCell	Clone: 2.43; Cat#BE0061; RRID: AB_1125541
InVivoMAb anti-mouse MHC Class I (H-2Kb), clone Y-3	BioXCell	Cat#BE0172; RRID: AB_10949300
InVivoMAb rat IgG2b isotype control, anti-keyhole limpet hemocyanin	BioXCell	Clone: LTF-2; Cat#BE0090; RRID: AB_1107780
Pacific Blue™ anti-human CD3 Antibody	BioLegend	clone: SK7; Cat#344824; RRID: AB_2563422
pan-HLA antibody W6/32	ATCC	Cat#ATCC-HB-95; RRID: N/A
PE anti-human CD3 Antibody	BioLegend	Clone: HIT3a; Cat#300308; RRID: AB_314044
PE anti-human CD366 (Tim-3) Antibody	BioLegend	clone: F38-2E2, Cat#345006; RRID: AB_2116576
PE Anti-MHC class I antibody [34-1-2S]	Abcam	Clone:34-1-2S; Cat#ab95571; RRID: AB_10680344
PE CD8a Antibody, anti-mouse	Miltenyi Biotec	Clone: REA734 | HIT8a; Cat#130-102-595; RRID: AB_2659885
PE CD8a Antibody, anti-mouse, REAfinity™	Miltenyi Biotec	Clone: REA601 | 53-6.7; Cat#130-118-946; RRID: AB_2733251
PE CD8a Antibody, anti-mouse, REAfinity™	Miltenyi Biotec	clone: REA601; Cat#130-123-781; RRID: AB_2811550
PE OVA257-264 (SIINFEKL) peptide bound to H-2Kb Monoclonal Antibody	eBioscience	Clone: eBio25-D1.16; Cat#12-5743-82; RRID: AB_925774
PE/Cyanine7 anti-human CD8	BioLegend	Clone: SK1; Cat#344712; RRID: AB_2044008
Purified anti-mouse CD28 Antibody	BioLegend	Clone: 37.51; Cat#102101; RRID: AB_312866
Purified anti-mouse CD3 Antibody	BioLegend	Clone: 17A2; Cat#100201; RRID: AB_312658
Secondary antibody Alexa Fluor 488	Invitrogen	Cat#A-11055; RRID: AB_2534102
Secondary antibody Alexa Fluor 594	Invitrogen	Cat#A-21207; RRID: AB_141637
Secondary antibody Alexa Fluor 647	Invitrogen	Cat#A-31571; RRID: AB_162542
Chemicals, peptides, and recombinant proteins		
0.1M DTT	NEB	Cat#B1222A
2-Mercaptoethanol (β- Mercaptoethanol)	Gibco	Cat#31350-010
Acetonitrile (ACN)	Bio-Lab	Cat#000120410100
Agar	Sigma-Aldrich	Cat#05040
BSA	Thermo Fisher Scientific	Cat#134731000

(*Continued on next page*)

Please cite this article in press as: Chemla et al., HLA export by melanoma cells decoys cytotoxic T cells to promote immune evasion, Cell (2026), https://doi.org/10.1016/j.cell.2025.11.020

Continued

REAGENT or RESOURCE	SOURCE	IDENTIFIER
CD8+ mouse magnetic MicroBeads	Miltenyi Biotech	Cat#130-116-478
Cell Acquisition Solution	Standard BioTools	Cat#201240
Collagenase-II	Worthington-Biochem	Cat#LS004176
Collagenase-IV	Worthington-Biochem	Cat#LS004188
DAPI (4′,6-diamidino-2-phenylindole)	Thermo Fisher Scientific	Cat#D1306
Dimethyl sulfoxide	Sigma-Aldrich	Cat#67-68-5
D-Luciferin, Potassium Salt	Biovision	AB-ab143655-1-B
DNAse-I	Worthington-Biochem	Cat#LS002006
DPX mountant	Sigma-Aldrich	Cat#06522-100ML
Dulbecco's Modified Eagle Medium (1x) with L-Glutamine, 500 mL	Gibco	Cat#41965-039
Dulbecco's Phosphate Buffer Saline (DPBS)	Gibco	Cat#14190-094
Dynabeads Protein-G	Thermo Fisher Scientific	Cat#10003D
EDTA	Promega	Cat#V4231
EDTA	Bio-Lab	Cat#009012233100
Eosin	Sigma-Aldrich	Cat#318906-500ML
Ethanol (denatured)	Sigma-Aldrich	Cat#1.00974
Ethanol-d6	Sigma-Aldrich	Cat#186414
Fontana Masson	Abcam	Cat#ab150669
Foxp3/Transcription Factor Staining Buffer Set	eBioscience	Cat#00-5523-00
Gentamicin, 40mg/mL	DANHSON	Cat#SN: VC253LV3L4CHN7, Gentamicin DS
Glutaraldehyde solution	Sigma-Aldrich	Cat#G7651
Hank's balanced salt solution	Gibco	Cat#14-025-092
heat-inactivated Fetal Bovin Serum, 500 mL	Gibco	Cat#A5256801
Hematoxylin	Sigma-Aldrich	Cat#H3136-25G
HEPES buffer solution, 1M	Gibco	Cat#15630-056
Hexamethyldisilazane	Sigma-Aldrich	Cat#440191-100ML
Histopaque-1077	Sigma-Aldrich	Cat#H8889-100ML
Human serum, Type AB, Heat-Inactivated	BioIVT	Cat#HUMANABSRMP-HI-1
insulin-transferrin-selenium liquid Media Supplement	Sigma-Aldrich	Cat#I3146-5ML
Iodoacetamide	Sigma-Aldrich	Cat#I6125
Ir DNA intercalator	Standard BioTools	Cat#201192B
Isoflurane	Piramal	https://www.piramalcriticalcare.us/products/isoflurane/
Karnovsky fixative buffer	EMS	Cat#15720
kojic acid	Sigma-Aldrich	Cat#501-30-4
Lead(II) nitrate	Sigma-Aldrich	Cat#203580
L-Glutamine Solution, 200mM, 100mL	Gibco	Cat#25030-024
MEM-Eagle non-essential amino acids	Biological Industries	Cat#M7145-100ML
MitoTracker™ Green FM Dye	Thermo Fisher Scientific	Cat#M46750
Mouse IL-2 Recombinant Protein	PeproTech	Cat#212-12
NaOH	Sigma-Aldrich	Cat#72068-100ML
octyl-b-D glucopyranoside	Sigma-Aldrich	Cat#O8001
Osmium tetroxide solution	Sigma-Aldrich	Cat#75632
OVA257-264 (SIINFEKL) peptide	Sigma-Aldrich	Cat#A5503-1G
Paraformaldehyde	Sigma-Aldrich	Cat#158127
Penicillin Streptomycin, 10000 U/mL, 100ml	Gibco	Cat#15140-122

(*Continued on next page*)

Please cite this article in press as: Chemla et al., HLA export by melanoma cells decoys cytotoxic T cells to promote immune evasion, Cell (2026), https://doi.org/10.1016/j.cell.2025.11.020

Continued

REAGENT or RESOURCE	SOURCE	IDENTIFIER
PFA	Electron Microscopy Sciences	Cat#15710
PKH26 Red Fluorescent Cell Linker Kit	Sigma-Aldrich	Cat#PKH26GL; Cat#MINI26
PKH67 Green Fluorescent Cell Linker Kit	Sigma-Aldrich	Cat#PKH67GL; Cat#MINI67
PMSF	Sigma-Aldrich	Cat#78830
Poly-L-lysine hydrobromide	Sigma-Aldrich	Cat# P1399-25MG
Potassium ferricyanide(III)	Sigma-Aldrich	Cat#702587
Proleukin (Aldesleukin, IL-2) 18x106 IU	Megapharm	Cat#HM5420Y
Propylene oxide	Sigma-Aldrich	Cat#56671
Protease Inhibitors Cocktail	Sigma-Aldrich	Cat#P8340
Protein A Resign	Genscript	Cat#L00210
Protein G Resign	Genscript	Cat#L00209
Puromycin	Sigma-Aldrich	Cat#P8833-10MG
Rat Collagen Type I	Merck Millipore	Cat#08-115
Reprosil C18-Aqua	Dr. Maisch GmbH, Germany	Cat#r10.9aqua.
Rhodium solution	Standard BioTools	Cat#201103A
RPMI 1640, with L-Glutamine	Gibco	Cat#21875-034
Sodium cacodylate Buffer	Sigma-Aldrich	Cat#97068
sodium deoxycholate	Sigma-Aldrich	Cat#D6750
Sodium Pyruvate Solution	Sartorius	Cat#03-042-1B
Sucrose	Sigma-Aldrich	Cat#S0389-5KG
Trifluoracetic acid (TFA)	Sigma-Aldrich	Cat#302031
TRIzol™ Reagent	Thermo Fisher Scientific	Cat#15596018
Trypsin-EDTA (0.25%), phenol red	Gibco	Cat#25200056
Uranyl Acetate Solution	EMS	CAS#541-09-3
VECTASHIELD® Antifade Mounting Medium with DAPI	Vector Laboratories	Cat#H-1200-10
Western-Ready™ MES SDS-PAGE Running Buffer (10X)	BioLegend	Cat#426307
Critical commercial assays		
CellEvent™ Caspase-3/7 Detection Reagents	Invitrogen	Cat#C10423
CFSE Cell Division Tracker Kit	BioLegend	Cat#423801
Chromium GEM-X Single Cell 5' Reagent Kit v3	10x Genomics	Cat#PN-1000699
Chromium Single Cell V(D)J Amplification Kit Human	10x Genomics	Cat#PN-1000252
CyQUANT™ XTT Cell Viability Assays	Invitrogen	Cat#X12223
CytoTox 96® Non-Radioactive Cytotoxicity Assay	IM Beit Haemek (Promega)	Cat#G1780
DNeasy Blood & Tissue Kit	Qiagen	Cat#69504
Dual Index Kit TT Set A	10x Genomics	Cat#PN-1000215
Human Granzyme B ELISA MAX Deluxe Set	BioLegend	Cat#439204
Human IFNγ ELISA MAX Deluxe Set	BioLegend	Cat#430104; Cat#430105
MAXPAR™ X8 chelating polymer kit	Standard BioTools	Cat#201144A
MitoTracker™ Green FM	Thermo Fisher Scientific	Cat#M7514
Mouse Interferon gamma ELISA Kit PicoKine	Boster Bio	Cat#EK0375
NEBNext Poly(A) mRNA Magnetic Isolation Module	New England BioLabs	Cat#E7490
NEBNext Ultra II Directional RNA Library Preparation kit	New England BioLabs	Cat#E7760S

(*Continued on next page*)

Continued

REAGENT or RESOURCE	SOURCE	IDENTIFIER
NextSeq 500 system	Illumina	https://emea.support.illumina.com/sequencing/sequencing_instruments/nextseq-500.html
NextSeq 500/550 High Output Kit v2.5 (75 Cycles)	Illumina	Cat#20028870
PCRBIO Taq Mix Red Kit	PCRBIOSYSTEM	Cat#PB10.13-02
QIAquick PCR Purification Kit	Qiagen	Cat#28104
TMRE-Mitochondrial Membrane Potential Assay Kit	Abcam	Cat#ab113852
Deposited data		
Melanoma Cell Lines Mass Spectrometry data (Immunopeptidomics, MAPP and Proteomics)	This paper	PXD069094; PXD068867; PXD068870
scRNA-seq	This paper	GEO: GSE309733
scTCR-seq	This paper	ENA: PRJEB102639
WES data of WM3526	This paper	GEO: PRJNA1322090
Gene Expression from Melanoma Patients Before and After Anti-PD1 Therapy with History of Anti-CTLA4 or Naive to Anti-CTLA4 Therapy	Riaz et al.[27]	GEO: GSE91061
Gene Expression Profile from Melanoma Patients Given Anti- PD1 Therapy	Hugo et al.[100]	GEO: GSE78220
HLA-Ligand ATLAS Mass Spectrometry data	Marcu *et al*.[70]	N/A
Spatial Proteomics of Sentinel Lymph Nodes	Amitay et al.[101]	N/A
Experimental models: Cell lines		
3T3-L1	ATCC	CL-173
B16-F10	ATCC	CRL-6475
B16-F10 MHC-I knock-out	Gift from Prof. Stefan Eichmüller	N/A
B16-F10 tyrosinase knock-out	Gift from Prof. Shoshana Greenberger	N/A
B16-F10-DN	Gift from Prof. Shoshana Greenberger	N/A
B16-F10-OVA	Gift from Prof. Yaron Carmi	N/A
MC-38	Gift from Prof. Yaron Carmi	N/A
MNT-1	ATCC	CRL-3450
WM1716	Gift from Drs. Meenhard Herlyn and Levi Garraway	N/A
WM3314	Gift from Drs. Meenhard Herlyn and Levi Garraway	N/A
WM3526	Gift from Drs. Meenhard Herlyn and Levi Garraway	N/A
WM3682	Gift from Drs. Meenhard Herlyn and Levi Garraway	N/A
Experimental models: Organisms/strains		
Mouse: Wild type: C57BL/6J	Harlan	1BL/626
Mouse: gp-100	The Lotem Laboratory	N/A
Mouse: OT1 TCR C57BK/6 CD45.1+	The Jung Laboratory	N/A
Software and algorithms		
Aperio Digital Pathology Slide Scanner	Leica Biosystems	https://www.leicabiosystems.com/digital-pathology/scan/cytoinsight-gsl-image-analysis-case-management-solution-for-cytogenomics/

(*Continued on next page*)

Please cite this article in press as: Chemla et al., HLA export by melanoma cells decoys cytotoxic T cells to promote immune evasion, Cell (2026), https://doi.org/10.1016/j.cell.2025.11.020

Continued

REAGENT or RESOURCE	SOURCE	IDENTIFIER
Aperio ImageScope software	Leica Biosystems	https://www.leicabiosystems.com/digital-pathology/manage/aperio-imagescope/
BD FACSDiva Software	BD Biosciences	https://www.bdbiosciences.com/en-us/products/software/instrument-software/bd-facsdiva-software
BioRender	BioRender	http://biorender.com/
Code for immunopeptidome data analysis	Weller et al.	https://github.com/YSamuelsLab/MetaPept2
DIAMOND (v.0.9.14)	bioconda	N/A
FASTQC 2022	Babraham Bioinformatics	https://www.bioinformatics.babraham.ac.uk/projects/fastqc/
Flowjo (v10.8.0)	BD Biosciences	https://www.flowjo.com/
FragPipe v.21.1	Nesvilab	https://github.com/Nesvilab/FragPipe/releases
GraphPad Prism	N/A	https://www.graphpad.com/
Helios Software	Standard BioTools	N/A
IDEAS 6.2	AmnisCorp	N/A
ImageJ	National Institutes of Health	RRID:SCR_002285
IncuCyte S3 2019A software	Sartorius	https://www.sartorius.com/en/products/live-cell-imaging-analysis/live-cell-analysis-software/incucyte-software-v2019a
iTEM the Tem imaging platform	Olympus	N/A
IVIS Lumina III system	PerkinElmer	https://www.revvity.com/product/ivis-lumina-x5-imaging-system-cls148590
Jupiter_core 4.9.1	N/A	https://github.com/jupyter/jupyter_core
MaxQuant software version 2.1	Max-Planck-Institute of Biochemistry	https://maxquant.org/
NetMHCpan (v.4.1)	DTU	https://services.healthtech.dtu.dk/services/NetMHCpan-4.1/
NetMHCpan 4.1	DTU Health Tech	https://services.healthtech.dtu.dk/services/NetMHCpan-4.1/
NTA 3.0 software	Malvern Panalytical	N/A
Peptide-PRISM	Erhard *et al*	https://erhard-lab.de/software
Prism (v.8.4.3)+(v.10.0.0)	GraphPad	www.graphpad.com
PyCharm v.2024.1.1 Community edition	JetBrains	https://www.jetbrains.com/pycharm/
R studio v. 2023.12.0+369	N/A	https://cran.rstudio.com
RADIUS software	Emsis	N/A
SIS Megaview III	Olympus	N/A
Trimmomatic	Usadel lab	N/A
ZEN software	Carl Zeiss Microscopy	https://www.zeiss.com/microscopy/en/products/software/zeiss-zen.html
Other		
glow-discharged holey carbon R2/2 Cu 200-mesh grids with a SiO_2 support	Quantifoil	Q2100R2S
Sep-Pak tC18 96-well	Waters	Cat#186002321
Ultra-Micro SpinColumn, C18	Harvard Apparatus	BVD-74-7206

EXPERIMENTAL MODEL AND STUDY PARTICIPANT DETAILS

Melanoma tissue array

A tissue microarray was prepared from FFPE samples from 69 melanoma patients with Stage III and IV metastatic melanoma, who were responders and non-responders to immunotherapy, treated at the University Hospital of Zurich. Samples were obtained under

ethical number #BASEC:2014-0425. For this study, we used the TMA #258. Detailed information on these samples is provided in Table S3.

Images were analyzed in ImageJ by an experimenter blinded to the genotypes. The scale was manually adjusted for each image. For each cell, the pigmented area was manually outlined using the 'Freehand Selection' tool, followed by tracing of the entire cell area. Both pigment and total cell areas were measured using the 'Measure' function. The percentage of pigment relative to total cell area was calculated and reported alongside the absolute cell area measurements.

Human patient samples

Fresh melanoma tissue biopsies from melanoma patients (both male and female) were obtained during surgeries at the Ella Lemelbaum Institute for Immuno-Oncology and Melanoma at Sheba Medical Center. TILs and autologous melanoma lines were isolated from tumor biopsies from patients enrolled in a phase II TIL ACT trial at the Sheba Medical Center (NCT00287131). Patients signed an informed consent approved by the Israeli Ministry of Health (Helsinki approval no. 3518/2004), which allowed use of excess cell material for research purposes. The generation of TILs was described in detail before.[102] In short, fragmentation, enzymatic digestion, fine needle aspiration, and tissue remnant culture techniques were used to isolate TILs and melanoma cells from surgically resected metastatic lesions.

TILs were cultured in complete medium containing 10% human serum (BioIVT, Cat#HUMANABSRMP-HI-1), 25 mmol/l HEPES (Gibco, Cat#15630-056), 100 U/ml penicillin and 100 μg/ml streptomycin (Gibco, Cat#15140-122), 50 μg/ml gentamicin (DANHSON, Cat#SN: VC253LV3L4CHN7, Gentamicin DS), and 0.5 μM 2-mercaptoethanol (Gibco, Cat#31350-010) in RPMI 1640 (Gibco, Cat#21875-034). Melanoma cells were cultures in MEL medium contained 10% FBS (Gibco, Cat#A5256801) vesicles free, 25 mmol/l HEPES, 100 U/ml penicillin and 100 μg/ml streptomycin, 2 mM L-glutamine (Gibco, Cat#25030-024), and 1 mM sodium pyruvate (Sartorius, Cat#03-042-1B) in RPMI 1640. TILs were cultured in 24-well plates, and complete medium with 3,000 IU/ml IL-2 (Proleukin) (Megapharm, Cat#HM5420Y) was added every 2–3 days to keep the cell concentration at 0.5–2 $\times$ 10^6 cells/ml.

Melanoma specimens

Human tissue samples from different stages of melanoma (*in situ*, vertical, and metastasis) were obtained from Wolfson and Sourasky Medical Center BioBank under ethical approvals WOMC 0039-18 and 16-660-TLV-7. Samples were from both male and female patients.

Mice

All animal experiments were performed in accordance with the guidelines of the Tel Aviv University Institutional Animal Care and Use Committee with institutional policies and approved protocols (IACUC permit: 01-21-047). All the animals were maintained in the Tel-Aviv University SPF animal house for 12 h dark/12 h light phases with 22 ± 1 °C temperature and 32–35% humidity with *ad libitum* water and food. Female wild-type C57BL/6J mice (7-8 weeks old) were purchased from Envigo and were allowed to acclimatize for 1 week after arrival. OT1 TCR C57BK/6 CD45.1$^+$ mice expressing the transgenic T cell receptor designed to recognize ovalbumin peptide residues 257-264 were a kind gift from the lab of Professor Steffen Jung (Weizmann Institute of Science). gp-100 mice expressing the transgenic Pmel 17 TCR (in C57BL/6J background) specific for a 9-mer epitope (25-32), a kind gift from Professor Michal Lotem (The Hebrew University of Jerusalem), were housed and bred in-house under an approved protocol (IACUC permit: 01-19-086).

Cell culture

3T3-L1 fibroblasts (gender unknown), B16-F10 wild-type cells (male), B16-F10 MHC-I knock-out cells (male), B16-F10 cells stably expressing luciferase and *mCherry* (male), B16-F10 OVA cells (male), B16-F10 DN cells stably expressing luciferase (male), B16-F10 tyrosinase knock-out cells stably expressing luciferase (male), MC-38 cells (female), MC-38 cells stably expressing luciferase (female), MNT-1 (male), WM3526 (male), WM1716 (gender unknown), WM3682 (gender unknown), WM3314 (female) were cultured in DMEM (Gibco, Cat#41965-039) supplemented with 10% heat-inactivated FBS, 2 mM L-glutamine, and 100 μg/mL penicillin and 100 μg/mL streptomycin.

METHOD DETAILS

In vivo tumor growth models

All the animal experiments were conducted according to the guidelines of the Tel Aviv University Institutional Animal Care and Use Committee (IACUC permit: 01-21-047). For *in vivo* tumor growth, cultured tumor cells suspended in PBS (Gibco, Cat#14190-094) at 5.0 $\times$ 10^5 cell/50 μl for MC-38 and *B16* cells, 5.0$\times$ 10^5 cells/50 μL for *B16-OVA* cells. An aliquot of 50 μl was injected subcutaneously into the shaved area on the dorsal side of the mouse. The height and width of the subcutaneous tumors were measured twice a week using calipers. Tumor size was calculated as volume (in mm^3). Mice were sacrificed when the tumors reached 1.5mm^3. Tumors were monitored and quantified twice a week by *in vivo* imaging beginning 7 days post subdermal injection.

Please cite this article in press as: Chemla et al., HLA export by melanoma cells decoys cytotoxic T cells to promote immune evasion, Cell (2026), https://doi.org/10.1016/j.cell.2025.11.020

Bioluminescent assays

A fresh stock solution of D-luciferin, potassium salt (Biovision, Cat#AB-ab143655-1-B) was prepared at 15 mg/mL in sterile PBS (X1) and sterilized through a 0.2-μm filter. For *in vivo* imaging, mice were anesthetized using 2.5% isoflurane (Piramal) and administered 150 mg/kg D-luciferin by intraperitoneal injection 10 to 15 minutes prior to imaging. *Ex vivo* imaging of resected tumors was performed after sacrifice. The average radiance (photons/s/cm^2/sr) was calculated using an IVIS Lumina III system (PerkinElmer). After the acquisition, a photographic image was taken.

In vivo tumor treatment

C57BL/6J Mice were intratumorally injected every other day with either 30 μL of 150 mg/mL kojic acid (Sigma-Aldrich, Cat#501-30-4), or 30 μL of control vehicle (DMSO) (Sigma-Aldrich, Cat#67-68-5). Additionally, mice were intraperitoneally injected every 4 days with 200 μg for the first injection, 100 μg in all other injections of αCD8 antibody (Cat#BE0061, Bio X Cell, Lebanon, NH, USA), or IgG as control (Cat#BE0090, Bio X Cell, Lebanon, NH, USA).

Primary cell isolation

Excised tumor samples were homogenized in Hank's balanced salt solution (Gibco, Cat#14-025-092) supplemented with 2% FBS and 5 mmol/L EDTA (Bio-Lab, Cat#009012233100) and were isolated through a 70-μm strainer (Corning). Tumors were digested in RPMI 1640 with 2 mg/mL collagenase IV (Worthington-Biochem, Cat#LS004188), 2000 U/mL DNase I (Worthington-Biochem, Cat#LS002006) for 30 min at 37 °C and then homogenized and strained through a 70-μm strainer.

Survival curve

Mice were subcutaneously injected with B16 melanoma as described before. Intertumoral injections of vehicle control (DMSO) or Kojic acid began a week after injection. When the tumor reached 1.5 cm3 in volume, mice were sacrificed as per the ethical approval. The sacrifice date was taken into survival curve analysis. Significance was determined using Gehan-Breslow-Wilcoxon long-rank test.

In vitro CD3 activation

Activation of TILs with anti-CD3 antibody was performed as described.[79,103] First, 96-well flat-bottom tissue culture plates were coated with anti-CD3 antibody OKT3 (Miltenyi, Cat#170-076-124). OKT3 was diluted in PBS to a final concentration of 1 μg/mL (1:1000 dilution). A volume of 200 μL was added to each well, with some wells left uncoated to serve as controls for a final concentration of OKT3 of 10 ng/mL. The plates were incubated for 2 h at 37 °C, the antibody solution was removed, and the wells were washed twice with PBS. Cells were seeded at a density of 100,000 cells per well, typically in triplicate, then incubated overnight at 37 °C in a 5% CO2 incubator. IFNγ secretion was measured using ELISA as described below (BioLegend, Cat#430104; Cat#430105).

Melanosome isolation

To isolate melanosomes of mouse origin, B16-F10 or B16-F10 OVA cells were plated at 2 x 10^6 cells per 15-cm plate and incubated for 72 h at 37 °C at 5% CO_2. All cells seeded for EVs isolation were cultured in vesicles free medium containing FBS serum that centrifuged at 100,000 xg for 2 h at 4 °C. All steps of the procedures after media collection were performed at 4 °C. The cell-culture media was centrifuged at 300 xg for 15 min. The resulting supernatant was centrifuged at 1000 xg for 30 min. The resulting supernatant was centrifuged at 10,000 xg for 1 h. The resulting melanosomal pellet was resuspended in 1 ml of sterile PBS and centrifuged at 10,000 xg for 20 min. The resulting pellet was resuspended in the desired amount of sterile PBS. The melanosomes were quantified using the Bradford assay. Freshly isolated melanosomes were used for all the experiments.

To isolate melanosomes of human origin, MNT-1, WM3682, or WM3526 cells, or the primary patient melanoma cells were plated at 5 x 10^6 cells per 15-cm plate and incubated for 72 h at 37 °C at 5% CO_2. All steps of the procedures after media collection were performed at 4 °C. The media was centrifuged at 300 xg for 15 min. The resulting supernatant was centrifuged at 1000 xg for 30 min. The resulting supernatant was centrifuged at 20,000 xg for 1 h. The resulting melanosomal pellet was suspended in 1 ml of sterile PBS and centrifuged at 10,000 xg for 20 min. The resulting melanosomes pellet was suspended in PBS and quantified using the Bradford assay. Freshly isolated melanosomes were used for all the experiments.

Exosome isolation

Wild-type B16-F10, B16-F10 OVA, and MNT-1 cells were plated 2 x 10^6 cells per 15-cm plate and incubated for 72 h at 37 °C at 5% CO_2. All cells seeded for EVs isolation were cultured in vesicles free medium containing FBS serum that was centrifuged at 100,000 xg for 2 h at 4°C. All steps of the procedures after media collection were performed at 4 °C. The resulting supernatant was centrifuged at 2000 xg for 10 min. The resulting supernatant was centrifuged at 10,000 xg for 30 min. In the next step, the resulting supernatant was filtered through a 0.22-μm filter to remove large vesicles and then centrifuged at 100,000 xg for 2 h. The resulting exosomal pellet was resuspended in sterile PBS. The exosomes were quantified using the Bradford assay. Freshly isolated exosomes were used for all the experiments.

Please cite this article in press as: Chemla et al., HLA export by melanoma cells decoys cytotoxic T cells to promote immune evasion, Cell (2026), https://doi.org/10.1016/j.cell.2025.11.020

Labeling of melanosome and exosome membranes

The pellets of melanosomes or exosomes were labeled with membrane-labeling dye PKH67 or PKH26 (green and red fluorescent dyes, respectively) as per the manufacturer's instructions (Sigma-Aldrich, Cat#PKH67GL; Cat#MINI67; Cat#PKH26GL; Cat#MINI26). In brief, the pellets were resuspended in 1 mL of Dilutent C (provided in labeling kit) and 6 μL of dye was added and gently mixed. After incubation at room temperature for 5 min, BSA (Thermo-Fisher. Cat#134731000) was added to quench the reaction, and the residual dye was removed by separation over 0.971 M sucrose gradient (Sigma-Aldrich, Cat#S0389-5KG) via centrifugation at 100,000 xg for 2 h at 4 °C with slow deceleration. The resulting pellet was suspended in PBS for downstream applications.

Mouse melanoma model

Under inhalable anesthesia, female C57BL/6J mice were injected subcutaneously on the dorsal side after hair removal with 0.5 x 10^6 B16-F10 luciferase *mCherry* cells suspended in 100 μl of sterile complete DMEM. After 7 days, under inhalable anesthesia, mice were injected with either DMSO or Kojic acid (300 mg/kg of body weight[104]) every other day (8 total injections) for 16 days intratumorally using a 30G sterile syringe.

Mice were imaged weekly after injection with 150 μl of freshly prepared D-luciferin using the IVIS Spectrum imaging system (Perkin Elmer). Images were quantified for the intensity of the luminescence as average radiance [p/s/cm^2/sr]. Tumor volumes were measured by Vernier caliper every week for the duration of the experiment. The tumor volume was calculated using the formula V = ½ (Length × $Width^2$). After sacrificing the mice, tumors were excised with a margin of 5 mm from all sides and were weighed on an analytical balance (MRC Laboratory).

Tumor Pigmentation Level Analysis

Excised tumors were placed on a 70-μm filter placed inside a petri dish with 5-10 ml of media (0.1 g BSA, 0.02 g collagenase-II (Worthington-Biochem, Cat#LS004176), 0.02 g collagenase-IV, and 0.001 g DNAse-I (Worthington-Biochem, Cat#LS002006) in 20 ml DMEM) and minced. Tumor fragments were placed in a 50-ml conical tube and incubated at 37 °C in a water bath for 20-30 min with stirring every 5 min. 20 ml of DMEM with 10% FBS was added, and the sample was centrifuged at 700 xg for 7 min at room temperature. Then, to the pellet 6 ml of RPMI 1640 with 10% FBS was added. Samples were again centrifuged at 700 xg for 7 min the cellular pellet was resuspended in 100 μl of 1 M NaOH (Sigma-Aldrich, Cat#72068-100ML) at 70°C for 2 h. The dissolved melanin was calculated by the mean of the melanin absorbance at 405 nm.

Isolation and activation of mononuclear cells from mouse spleens

Spleens were excised and washed with sterile PBS. Spleens were homogenized in RPMI 1640 medium supplemented with 10% FBS and 1% pen-strep. Cells were then centrifuged at 800 xg for 5 min at 4 °C. The pellet was suspended in 6 ml RPMI 1640 followed by the addition of 6 ml of Histopaque-1077 (Sigma Aldrich, Cat#H8889-100ML). Cells were centrifuged at 800 xg for 20 min at room temperature with acceleration "0" and deceleration "0". After centrifugation, the white buffy layer at the interface containing mononuclear cells were collected, washed by adding 10 mL of RPMI 1640 medium, and centrifuged at 700 xg for 10 min at 18 °C.

T cell enrichment and activation

To enrich $CD8^+$ cells, the pellet was re-suspended in MACS buffer (0.5% BSA, 2 mM EDTA in PBS). To 10 x 10^6 cells was added 10 μl $CD8^+$ mouse magnetic MicroBeads (Miltenyi Biotech, Cat#130-116-478), and samples were incubated for 15 min at 4 °C, and 500 μl of MACS buffer was added. Samples were placed on LS Columns (Miltenyi Biotech) prepared by equilibrating with 500 μl of MACS buffer. The flow-through was collected and this step was repeated. The column was then washed with 2 ml of MACS buffer to eliminate the unbound cells, and this step was repeated twice. The columns were placed in new 15-ml conical tubes, and 2 ml MACS buffer was injected onto the columns to elute the $CD8^+$ enriched cells.

For activation, these $CD8^+$ T cells were cultured in RPMI 1640 supplemented with 1% penicillin-streptomycin, 10% heat-inactivated FBS, 1% sodium pyruvate (Sartorius, Cat#03-042-1B), 1% MEM-Eagle non-essential amino acids (Biological Industries, Cat#M7145-100ML), 1% insulin-transferrin-selenium liquid Media Supplement (Sigma-Aldrich, Cat#I3146-5ML), and 50 μM β-mercaptoethanol (Gibco, Cat#31350-010) For T cell activation, culture dishes were pre-coated with 0.5 μg/mL Purified anti-mouse CD3 (BioLegend; Clone: 17A2; Cat#100201) and 0.5 μg/mL Purified anti-mouse CD28 (BioLegend; Clone: 37.51; Cat#102101) LEAF antibodies in PBS and were supplemented with 1,000 IU/mL recombinant murine IL-2 (PeproTech, Cat#212-12) overnight.

Image analysis of melanoma Tissue Micro Array (TMA)

Samples were fixed with 4% PFA (Electron Microscopy Sciences, Cat#15710) and stained for melanin with Fontana Masson as per the manufacturer's protocol (Abcam, Cat#ab150669) and as we did before.[105] In brief, the stained TMA was scanned in an Aperio Digital Pathology Slide Scanner (Leica Biosystems), and the images were extracted from the Aperio ImageScope software (Leica Biosystems) and were manually analyzed by board-certified pathologists.

Hematoxylin and eosin staining

Formalin-fixed paraffin-embedded tissue sections were stained using hematoxylin (Sigma-Aldrich, Cat#H3136-25G) and eosin (Sigma-Aldrich, Cat#318906-500ML). Sections were mounted using the DPX mountant (Sigma-Aldrich, Cat#06522-100ML). Images were acquired using the Aperio Slide Scanner microscope (Leica Biosystems) at 20X magnification.

Please cite this article in press as: Chemla et al., HLA export by melanoma cells decoys cytotoxic T cells to promote immune evasion, Cell (2026), https://doi.org/10.1016/j.cell.2025.11.020

Immunofluorescence analyses

Tissue samples were stained as describe previously.[106] In brief, slides were incubated with primary antibodies: human anti-HMB45 (Abcam, Cat#ab732; dilution 1:100), human anti-GPNMB (R&D Systems, Cat#AF2550; dilution 1:25), and human anti-CD8 (Cell Marque, Cat#108M-95; dilution 1:100). Samples were then incubated with appropriate fluorophore-conjugated secondary antibodies: Secondary antibody Alexa Fluor 488 (Invitrogen, Cat#A-11055; dilution 1:1000), Secondary antibody Alexa Fluor 594 (Invitrogen, Cat#A-21207; dilution 1:1000), Secondary antibody Alexa Fluor 647 (Invitrogen, Cat#A-31571; dilution 1:1000). VECTASHIELD® Antifade Mounting Medium with DAPI (Vector Laboratories, Cat#H-1200-10) was used as the nuclear stain. Images were obtained at the desired magnifications using a Nikon fluorescence microscopy. High-resolution microscopy was performed on a Leica sp8 microscope.

Nanosight analyses

Isolated melanosome and exosome samples were quantified by nanoparticle tracking analysis (NTA), using a Nanosight NS300 (Malvern Instruments). Data were analysed with the NTA 3.0 software. Melanosome stocks were diluted with PBS to a concentration between 10^8 and 10^9 particles ml^{-1}. Each sample was analysed five times for 60 s; the mean values were used for further calculations.

Transmission electron microscopy analyses

Cells and melanosomes were co-cultured in suspension overnight and were collected by centrifugation. Cells were fixed in 2.5% glutaraldehyde (Sigma-Aldrich, Cat#G7651) and 2% paraformaldehyde (Sigma-Aldrich, Cat#158127) in 0.1 M Sodium cacodylate Buffer (Sigma-Aldrich, Cat#97068; pH 7.4) for 6 h at room temperature and then rinsed four times for 10 min each time in cacodylate buffer, post fixed, and stained with 1% osmium tetroxide (Sigma-Aldrich, Cat#75632), 1.5% potassium ferricyanide (Sigma-Aldrich, Cat#702587) in 0.1 M cacodylate buffer for 1 h. Cells were then washed four times in cacodylate buffer, followed by dehydration in increasing concentrations of ethanol (30, 50, 70, 80, 90, and 95%, 10 min at each step, followed by three 20-min washes with 100% anhydrous ethanol). After each wash, the cells were spun down for a few seconds, and the supernatant was removed. Following dehydration, the cells were infiltrated with increasing concentrations of agar 100 (Sigma-Aldrich, Cat#05040) resin in propylene oxide (Sigma-Aldrich, Cat#56671) (25, 50, 75, and 100% resin; vendor needed) for 16 h at each step. The cells were then embedded in fresh resin and allowed to polymerize at 60 °C for 48 h. Blocks were sectioned at 80 nm with a diamond knife on Leica Reichert Ultracut S microtome, and sections were collected onto 200-mesh thin-bar copper grids. After sequential staining with uranyl acetate and lead citrate for 10 min each, sections were imaged with a Phillips Tecnai 12 TEM 120kV equipped with Phurona camera and RADIUS software (Emsis).

Negative staining

Samples were adsorbed on formvar/carbon coated grids and stained with 2% aqueous uranyl acetate (EMS, CAS#541-09-3). Samples were examined using JEM 1400plus transmission electron microscope (Jeol, Japan). Images were captured using SIS Megaview III and iTEM the Tem imaging platform (Olympus).

Scanning electron microscopy

Melanosomes from B16-F10 and B16-F1-OVA cells labeled with PKH67. were co-cultured with OT-1 splenocytes cells (20 μg/ml melanosomes per 3 x 10^6 cells) overnight at 37 °C. Splenocytes were stained with the anti-CD8 antibody (Miltenyi Biotec, Cat#130-118-946 (PE 594), Clone 53-6.7; dilution 1:50) as per the manufacturer's instructions, and the OT-1 cells bound to labeled melanosomes were separated by FACS (BD FACSAria II) into 1) $CD8^+$ cells with B16-F10 OVA melanosomes, 2) $CD8^+$ cells with B16-F10 melanosomes, and 3) $CD8^+$ cells without melanosomes. Cells were seeded on B16-F10 OVA cells overnight on 24-well cell culture plate. Samples were then washed with sterile PBS three times (5 min per wash) and were fixed with Karnovsky fixative buffer (2.5% (w/v) paraformaldehyde, 2.5 % glutaraldehyde, and 0.1 M cacodylate buffer) (EMS, Cat#15720) for 1 h at room temperature and then left overnight at 4 °C. Next, the samples were washed three times using PBS, then three times with doubly distilled water (5 min per wash). Samples were then dehydrated in increasing concentrations of ethanol (30, 50, 70, 95, and 100%, two 15-min washes each) and then incubated with 100% hexamethyldisilazane (Sigma-Aldrich, Cat#440191-100ML) for 5 min and then air dried. Scanning electron microscopy images were acquired in the Nanocenter at TAU using a Zeiss GeminiSEM300. Imaging conditions: high vacuum mode at $8x10^{-7}$ mbar, 3 KV beam landing energy, and the InLens as well as the standard Everhart Thirnley SE2 detectors.

Mass spectrometry

Mouse and human melanosomes and exosomes were analyzed in the Smoler Proteomics Center at Technion, Israel, by mass spectroscopy.

The exosomes samples were brought to 2% SDS, 10mM DTT, 100mM TRIS pH 8. The samples were boiled 95°C for 5 min, sonicated twice (90%, 10-10, 5'), and centrifuged (10,000g, 10'). The samples were precipitated and washed 3 times with cold 80% acetone. The proteins were reduced in 3mM DTT100mM, ammonium bicarbonate and 8M Urea, modified with 10mM iodoacetamide in 100mM ammonium bicarbonate and 8M Urea (room temperature 30 min in the dark) and digested in 2M Urea, 25mM ammonium

bicarbonate with modified trypsin (Promega), overnight at 37oC in a 1:50 (M/M) enzyme-to-substrate ratio. The tryptic peptides were desalted using Oasis HLB 96-well μElution Plate (Waters)/homemade C18 stage tip, dried and re-suspended in 0.1% Formic acid in 2% acetonitrile.

The resulting peptides were analyzed by LC-MS/MS using a Q Exactive HFX, Q Exactive HF mass spectrometer (Thermo) fitted with a capillary HPLC (easy nLC 1200, Thermo-Fisher) or Exploris 480 fitted with Evosep One.

The peptides were loaded in solvent A (0.1% formic acid in water) on a homemade capillary column (30 cm, 75-micron ID) packed with Reprosil C18-Aqua (Dr. Maisch GmbH, Germany, Cat#r10.9aqua.), resolved with a 5 to 28% linear gradient of solvent B (99.99% acetonitrile with 0.1% formic acid/ 60/ minutes followed by gradient of 15 minutes of 28 to 95%/ 80% and 15 minutes at 95% solvent B at flow rates of 0.15 μl/min. Mass spectrometry was performed in a positive mode (m/z 300–1800, resolution 60,000for MS1 and 15,000 for MS2 using repetitively full MS scan followed by high collision dissociation (HCD, at 27 normalized collision energy) 18 most dominant ions (>1 charges) selected from the first MS scan. In the experiments that were analysed by the Exploris 480, the peptides were loaded onto a 15cm, ID 150μm, 1.9-micron Performance column EV1137 (Evosep). The peptides were eluted with the built-in Xcalibur 15 SPD (88 min) method. Mass spectrometry was performed in a positive mode using repetitively full MS scan (m/z 350–1200) followed by High energy Collision Dissociation (HCD) of the 20 most dominant ions (>1 charges) selected from the full MS scan. A dynamic exclusion list was enabled with exclusion duration of 30s.

The mass spectrometry data was analyzed using the MaxQuant software version 2.1[107] for peak picking and identification using the Andromeda search engine, searching against the human monocytogenes proteome from the Uniprot database and specific sequences with mass tolerance of 4.5 ppm for the precursor masses and 20 ppm for the fragment ions. Oxidation on methionine and protein N-terminus acetylation were accepted as variable modifications and carbamidomethyl on cysteine was accepted as static modifications. Minimal peptide length was set to seven amino acids and a maximum of two miscleavages was allowed. The data was quantified by label free analysis using the same software. Peptide- and protein-level false discovery rates (FDRs) were filtered to 1% using the target-decoy strategy. Protein table was filtered to eliminate the identifications from the reverse database and common contaminants.

Flow cytometry

Cells or melanosomes were stained with antibodies in 100 μl FACS buffer (1% (v/v) FBS, 1 mM EDTA in PBS) and incubated for 30 min on ice in the dark. For MHC-I analyses, cells or melanosomes were incubated with the anti-MHC-I antibody (Abcam, Cat#ab95571, clone 34-1-2S; dilution 1:50). For HLA-A,B,C analyses, melanosomes or exosomes were incubated with the FITC anti-human HLA-A,B,C antibody (BioLegend, Cat#311404, clone W6/32; dilution 1:20). For H2-Kb analyses, B16-F10-OVA cells and melanosomes were centrifuged and the pellet was pulsed with 25 μM of OVA^{257}-^{264} (SIINFEKL) peptide (Sigma-Aldrich, Cat#A5503-1G) for 1h at 37°C and then washed once with the FACS buffer and stained with the antibody to OVA^{257}-^{264} peptide bound to H-2Kb (eBioscience, Cat#12-5743-82, clone 25-D1.16; dilution 1:50). Cells were also stained with DAPI (4′,6-diamidino-2-phenylindole; Thermo Fisher Scientific, Cat#D1306). Subsequently, 1 ml FACS buffer was added to each sample, and the samples were centrifuged at 700 xg for 7 min and then suspended in 100 μl FACS buffer. For T cells–melanoma/melanosome co-culture analyses, T cells from human melanoma patient were incubated with PKH67-labeled autologous melanoma cells or melanosomes at 1:4 ratio at 37°C and 5% CO_2 for 30 min and 4 h. Samples were centrifuged at 5000 xg for 15 min, and pellets were washed with FACS buffer (PBS with 1% FBS vesicle free) and stained with the anti-CD4 (BioLegend, Cat#300552, clone RPA-T4; dilution 1:50) and anti-CD8 (BioLegend, Cat#344712, clone SK1; dilution 1:50) antibodies. Samples were centrifuged at 5000 xg for 15 min and then suspended in 100 μl FACS buffer. FACS analyses were performed on Beckman Coulter CytoFLEX 4 or 5 instruments. Cells were initially gated for the areas of the forward and side scatter, the gated population was gated for the singlet cells and then gated for the $DAPI^-$ cells (live cells). The live cells were further gated for the fluorescence intensity of the desired fluorophore. All gatings were performed in reference to the unstained and IgG control antibody for the specific fluorophores. The data are shown as the % gated of cells or melanosomes from the total population determined. The FACS density plots are means of experimental repeats.

Analyses of TILs from mouse tumors

Mice were sacrificed, and tumors were excised and prepared as described above. Equal amounts of cells were stained for CD45 (Miltenyi Biotec, Cat#130-110-798, APC, clone REA737; dilution 1:50) and CD8 (Miltenyi Biotec, Cat#130-118-946, PE 594, Clone 53-6.7; dilution used 1:50) followed by FACS as described above.

Immunopeptidome sample processing and LC-MS/MS

MHC-I-peptide complex purification was done as previously described.[66] Briefly, cell pellets consisting of $200*10^6$ cells and secreted melanosomes collected from the media $400 x10^6$ cell (50 flasks of 25ml, seeded with $3.5x10^6$ each and collected 4 days post seeding) were homogenized and lysed with lysis buffer (containing 0.25% sodium deoxycholate (Sigma-Aldrich, Cat#D6750), 0.2mM iodoacetamide (Sigma-Aldrich, Cat#I6125), 1mM EDTA (Promega, Cat#V4231), protease inhibitor cocktail (Sigma-Aldrich, Cat#P8340), 1mM PMSF (Sigma-Aldrich, Cat#78830) and 1% octyl-β-D-glucopyranoside (Sigma-Aldrich, Cat#O8001) in PBS) and incubated at 4°C for 1 hour. Lysates were cleared by centrifugation at 4°C, 48,000 x g for 45 minutes and passed through a pre-clearing column containing Protein A/ G resin beads (GenScript, Cat#L00210; Cat#L00209); Human-derived HLA-peptide complexes were then immunoaffinity purified from the cleared lysate using pan-HLA antibody (W6/32 antibody purified from HB95 hybridoma cells),

covalently bound to Protein A Resin (Genescript). For the mouse-derived MHC complexes, two anti-MHC-I antibodies - M28 (HB27) 28-14-8S and M20 (HB11) 20-8-4S (ATCC, HB-27 ™)- were covalently bound to Protein-G sepharose beads (Genscript; the same beads were used for the pre-clear step) at a 1:1 ratio. MHC-peptide complexes were eluted with 1% trifluoracetic acid (TFA; Sigma-Aldrich, Cat#302031), followed by purification of the peptides by Sep-Pak tC18 100mg Sorbent 96-well plate (Waters). Elution of the peptides was done with 28% acetonitrile (ACN; Bio-Lab, Cat#000120410100) in 0.1% trifluoracetic acid TFA.

In preparation for LC-MS/MS analysis, MHC-peptides were dried by vacuum centrifugation and resolubilized with 0.1% formic acid. For Orbitrap MS/MS experiments, peptides were separated using reversed-phase chromatography using the nanoAquity system (Waters), with a Symmetry trap column (180 × 20 mm) and HSS T3 analytical column, 0.75 × 250 mm (Waters), mobile phase A: H_2O+0.1% formic acid, B: acetonitrile+0.1% formic acid. The peptides were separated with a linear gradient over 2h from 5 to 28% B, 28 to 35% in 15min, 35% to 95% in 15min, maintained at 95% for 10min and back to initial conditions, at a flow rate of 0.35μl min−1.

The LC was connected online via a nano-electrospray ionization source (FlexIon, Thermo Scientific) using an emitter (Fossil) to a Quadrupole Orbitrap MS (Q-Exactive-Plus, Thermo Scientific). Data were acquired using a data-dependent method, fragmenting the peptides by higher-energy collisional dissociation (HCD). On the Q-Exactive-Plus, full-scan MS spectra were acquired at a resolution of 70,000 at 200 m/z with automated gain control (AGC) value of 3×10^6 ions, mass range of 300 to 1800 Th and maximum injection time of 100msec. MS/MS scans were acquired with an AGC target value of 10^5 with a maximum injection time of 150 msec, isolation of 1.7 Th, normalized collision energy was set to 25%, and MS/MS resolution was 17,500 at 200 m/z. Fragmented m/z values were dynamically excluded from further selection for 20s.

For timsTOF (TTU) experiments, the peptides were resolubilized with 0.1% trifluoroacetic acid and 5mM TCEP before LC-MS/MS analysis. 5μL of each sample was loaded using the nanoElute2 (Bruker, Germany) liquid chromatography. Mobile phase A was 0.1% formic acid in water. B was 0.1% formic acid in acetonitrile. Peptides were separated using the Aurora Ultimate C18 nano column, 0.075x250mm (IonOptiks, Australia), using a gradient of 2% B to 29% B in 80min, then 0.5min to 95% B, maintained 95%B for 2.9min at flow of 300nL/min. The column was placed in the column toaster and connected to a CaptiveSpray Electrospray ionization source. The column was maintained at 50°C. Data was acquired with a timsTOF Ultra (Bruker) in data-dependent-acquisition-parallel-accumulation-serial-fragmentation (DDA-PASEF) mode with the following parameters: capillary voltage of 1600v, temperature of 180°C, mass range of 100-1,700 Th, ion mobility 0.6-1.57 1/K0, tims ramp time of 300msec, number of PASEF MS/MS scans 10, target intensity of 20,000 with threshold of 2,500, charge range 0 to 5, collision energy of 20 at 0.6 1/K0 and 59 at 1.6 1/K0.

Immunopeptidome data analysis

RAW files were analyzed using FragPipe v.22[108,109] with default parameters for HLA peptides discovery (searched with the human Ensemble v.109) as previously described.[110] NetMHCpan v.4.1[111] was utilized to predict peptide binding affinity (binder <2% rank).

Retention time and Hydrophobicity index

Hydrophobicity values for total PSM peptides were predicted with R package protViz version 0.7.7[69] (https://CRAN.R-project.org/package=protViz) were plotted against the experimental retention time.

Tumor-associated antigens identification

A Tumor Associated Antigen (TAA) reference database (TAAs-refDB) was compiled based on melanoma-associated antigens described by Pitcovski et al.[112] Gene and protein annotations were retrieved using the org.Hs.eg.db and biomaRt packages[113,114] to map aliases, gene symbols, and descriptions. A custom pipeline was used to merge peptide-related information from human alias databases and FASTA headers extracted from the Ensembl protein database. The presence of peptides in experimental conditions (cells or melanosomes, with and without IFNγ stimulation) was determined by filtering for MS/MS-detected sequences and cross-referencing Protein IDs. Known TAAs were identified by matching against two reference datasets: the Benign HLA Ligand Atlas[70] and the Immune Epitope Database (IEDB). Peptides found in either database were labeled. TAA-to-canonical peptide ratios were calculated per replicate and condition.

Whole-exome sequencing and neoantigen identification

Whole Exome Sequencing (WES) was performed on the WM3526 cutaneous melanoma cell line by IDT-V2 enrichment kit at Hadassah Medical Center. Raw sequencing reads in FASTQ format were mapped to the human reference genome (GRCh38) using the BWA aligner[115] (GEO: PRJNA1322090). Duplicate reads were removed using Picard tools (https://github.com/broadinstitute/picard). Aligned BAM files were then processed, and variants were called using GATK Mutect2,[116] producing a VCF file that was filtered by quality scores. After variant calling, the variants were translated into protein sequences using Annovar.[117] For each mutation, 13 amino acids upstream and downstream of the mutation were extracted and stored in a FASTA file for further analysis. Variants were then marked using allele frequencies from the gnomAD database[118] and/or dbSNP (link: https://www.ncbi.nlm.nih.gov/snp/), and variant allele frequency (VAF) was calculated for each variant in the sample data.

Non-synonymous mutations were further analyzed for neoantigen identification by searching the immunopeptidomic data using a proteogenomic approach. We utilized the group-specific false discovery rate (FDR) search feature in FragPipe[110,119] with 1% FDR for both the canonical database (PE=1) and the non-synonymous mutation database (PE=2), followed by a stringent data processing pipeline as previously described.[110] Identified peptides were further filtered to remove variants with allele frequency > 1% in gnomAD as previously described[120] and to have VAF > 0.1 in the sample data. Neopeptides that passed the variant confidence filtration process were further examined for peptide-spectrum match (PSM) confidence by visualizing mirror plots of the identified spectrum versus the predicted one using the PDV tool and Unweighted Spectral Entropy (USE) scoring.[121]

Please cite this article in press as: Chemla et al., HLA export by melanoma cells decoys cytotoxic T cells to promote immune evasion, Cell (2026), https://doi.org/10.1016/j.cell.2025.11.020

Hydrophobicity analyses

The SpecL R package was used to calculate the hydrophobicity index using ssrc_2004. For each sample separately, the hydrophobicity index and retention time were modeled using a linear regression model. Absolute-sign residual distribution was used to calculate the interquartile range. Any peptide associated with a residual greater than 1.5 times the interquartile range was considered an outlier.

Heatmaps and principal component analyses

The DEP R library package was used to analyze the LFQ-intensities of the proteins (derived from proteinGroups MaxQuant output file). The normalize_vsn function was applied to the data. Imputation of missing data was performed using random draws from a Gaussian distribution centered around a minimal value (q = 0.01; 1st percentile of the intensities). All possible test comparisons of samples were analyzed to obtain significant proteins (p value < 0.05 and |Log2 fold change| > 1.5). The correlation matrix between samples was calculated, and a heatmap was generated. The heatmap shows that the samples first separate into IFNγ-treated versus control samples. Within the IFNγ-treated cluster, melanosome-associated replicates show specific subgroups of proteins relative to whole-cell.

Co-culture survival assay of CD8$^+$ T cells

CD8$^+$ T cells from the splenocytes of the gp-100 mice were activated as described above and seeded at 0.02 x 10^6 cells/well in a U-bottom cell culture plate and cultured with or without melanosomes (at a final concentration of 25 μg/ml) and incubated at 37 °C and 5% CO_2 for 96 h. Samples were stained to quantify apoptosis of the CD8$^+$ T cells at 24, 48, 72, and 96 h. The samples were stained with the CellEvent Caspase-3/7 Green (Invitrogen, Cat#C10423; dilution 1:1000) for 30 min at 37 °C and 5% CO_2 followed by FACS analysis. Percent apoptotic CD8$^+$ cells and percent CD8$^+$ cells were determined.

Melanosome CD8$^+$ T cells binding assay

CD8$^+$ T cells from mouse splenocytes activated as described above were seeded at 0.02 x 10^6 cells/well in a U-bottom cell culture plate with PKH67-labeled melanosomes and incubated at 37 °C and 5% CO_2 overnight. Samples were centrifuged at 700 xg for 7 min, and pellets were washed with PBS and stained with anti-CD8 antibody (Miltenyi Biotec, Cat#130-123-781, clone REA601; dilution 1:50) for 20 min. Samples were analyzed using FACS. The percentage of CD8$^+$ T cells (PE$^+$) co-localized with labeled melanosomes was determined.

Killing assay

CD8$^+$ T cells or mouse splenocytes were activated or not and were with or without melanosomes (20 μg/ml) at 37 °C and 5% CO_2 overnight. Simultaneously, melanoma cells were plated (0.02 x 10^6 cells/well) in a 96-well flat-bottom plate and incubated at 37 °C with 5% CO_2 overnight. CD8$^+$ T cells or splenocytes (with or without melanosome treatments) were incubated with the seeded melanoma cells at a 1:1 ratio and monitored in the IncuCyte Live Cell Analysis System (Sartorius) for up to 48 h. A random image was snip-extracted using the IncuCyte S3 2019A software at 0, 224, and 48 h. The number of melanoma cells were counted using ImageJ software. For each time point, data were normalized to day 0.

ImageStream cytometry

PKH67-labeled vesicles were added to cells and were shaken gently to disperse the vesicles. After 24 h, cells were trypsinized (Gibco, Cat#25200056) and imaged using the ImageStreamX markII flow cytometer (Luminex Corporation). Fluorescence intensity of the labeled vesicles was measured in channel 2 of the cytometer (480 nm excitation, 560 nm emission). An X60 magnification was used for all samples. Between 1500 and 2,000 cells were collected for each sample, and the data were analyzed using a dedicated image analysis software (IDEAS 6.2; AmnisCorp) to determine co-localization or cellular uptake (internalization) of vesicles. To eliminate dead cells and debris, cells were first gated for positive nuclear staining, using the area and aspect ratio features of the DAPI-labeled nuclear image. At least 105 focused images of single 'recipient' live cells were collected from each sample. The pattern and intensity of the 'recipient' cells served as a reference for defining the physical parameters for gating the correct cell population. Images were compensated for fluorescent overlap by using cells from each cell line as a control. Cells were gated for single cells using the area and aspect ratio features and for focused cells using the Gradient RMS feature. The internalization of exosomes or melanosomes was calculated by the internalization feature (i.e., the ratio of the intensity inside the cell to the intensity of the entire cell), mapped to a log scale. To define the internal region of the cell, the object mask of the bright-field image was eroded by 4 pixels. Cells with internalization scores higher than 0.5 were gated as cells with internalized vesicles.

Apoptosis assay

CD8$^+$ T cells (from C57BL/6J mice activated as described above) or B16-F10 melanoma cells were seeded at 0.02 x 10^6 cells/well in a U-bottom cell culture plate and incubated at 37 °C and 5% CO_2. Samples were stained to evaluate apoptosis at 24, 48, and 72 h. The samples were stained with the CellEvent Caspase-3/7 Green (Invitrogen, Cat#C10423; dilution 1:1000) for 30 min at 37 °C and 5% CO_2 followed by FACS analysis.

Please cite this article in press as: Chemla et al., HLA export by melanoma cells decoys cytotoxic T cells to promote immune evasion, Cell (2026), https://doi.org/10.1016/j.cell.2025.11.020

Proliferation assays

CD8$^+$ T cells from C57BL/6J mice were activated as described above and were labeled with CFSE Cell Division Tracker Kit (BioLegend, Cat#423801) as per the manufacturer's instructions. Briefly, the cells were seeded (0.02 x 10^6 cells/well) in a U-bottom cell culture plate and incubated at 37 °C and 5% CO_2. FACS was performed at 24, 48, and 72 h to determine the percentage of gated CFSE$^+$ (non-proliferating) and CFSE$^-$ (proliferating) CD8$^+$ T cells.

B16-F10 and MC-38 cells were seeded at 0.02 x 10^6 and 0.007 x 10^6 cells/well respectively in a flat-bottom cell culture plate in complete DMEM medium and incubated at 37 °C and 5% CO_2. The proliferation was evaluated using the CyQUANT™ XTT Cell Viability Assays (Invitrogen, Cat#X12223) as per the manufacturer's instructions.

RNA sequencing

Aliquots of 500 ng total RNA from the paired co-culture of human TILs with human melanosomes were used for RNA-seq library preparation. Libraries were prepared using the NEBNext Ultra II Directional RNA Library Preparation kit (New England BioLabs, Cat#E7760S) with the NEBNext Poly(A) mRNA Magnetic Isolation Module (New England BioLabs, Cat#E7490), according to the manufacturer's protocol. During amplification, 10 PCR cycles were performed. Library quality and quantity were assessed using TapeStation 4200 system (Agilent) and Qubit 3.0 Fluorometer (Invitrogen). Libraries were sequenced with a NextSeq 500/550 High Output Kit v2.5 (75 Cycles) kit (Cat#20028870) on a NextSeq 500 system, according to the manufacturer's instructions (Illumina). Both library preparation and sequencing were performed at the Genomics Research Unit, Life Sciences Inter-Departmental Research Facility Unit, Tel Aviv University.

Analyses of secreted IFNγ levels

The conditioned medium from the co-culture of CD8$^+$ T cells from OT-1 mouse spleenocytes with B16-F10 or B16-F10-OVA melanoma cells was centrifuged at 1000 xg for 15 min and subjected to IFNγ ELISA (Boster Bio, Cat#EK0375) as per the manufacturer's instructions. The conditioned medium from the co-culture of human CD8$^+$ TILs from melanoma patient tissue biopsies incubated with or without paired melanosomes for 24 h and with paired melanoma cells for an additional 24 h was centrifuged at 1000 xg for 15 min and subjected to IFNγ ELISA (Human IFNγ ELISA MAX Deluxe Sets, BioLegend, Cat#430105) as per the manufacturer's instructions.

Analyses of secreted GranzymeB levels

The conditioned medium from the co-culture of human CD8$^+$ TILs from melanoma patient tissue biopsies incubated with or without paired melanosomes for 24 h and with paired melanoma cells for an additional 24 h was centrifuged at 1000 xg for 15 min and subjected to GranzymeB ELISA (Human Granzyme B ELISA MAX Deluxe Set, BioLegend, Cat#439204) as per the manufacturer's instructions.

T cell interaction with melanoma or melanosomes assays

TIL, melanoma, and melanosome co-culture

T cells from four human patients (Sheba) were co-culture in a 15 ml tube with PKH67-labeled autologous melanoma cells or melanosomes at 1:4 ratio at 37 °C and 5% CO_2 for 4 h. Samples were centrifuged at 5000 xg for 15 min, and pellets were washed with FACS buffer (PBS with 1% FBS vesicle free) and stained with the anti-CD8 antibody (BioLegend, Cat#344712, clone SK1; dilution 1:50) and the anti-CD4 antibody (BioLegend, Cat#300552, clone RPA-T4; dilution 1:50) for 15 min in room temperature. Samples were centrifuged at 5000 xg for 15 min, resuspend in FACS buffer and stained with DAPI. Flow cytometry was performed on the BD FACSAria III Cell sorter or BD FACSymphony S6, using a 100-μm nozzle, analyzed with BD FACSDIVA software (BD Biosciences) and FlowJo software.

T cell Sorting

For sorting, to discriminate live and dead cells, DAPI was added immediately prior to analysis. Dead cells (DAPI$^+$) were excluded from downstream gating strategies. To identify the target populations, we first gated on viable (DAPI$^-$) cells and then used the APC channel as a dump to exclude unwanted populations from a PE panel. Specifically, APC+ cells (CD4+ T cells) were excluded to enrich for PE-Cy7$^+$ cells (CD8$^+$ T cells). From the DAPI$^-$/APC$^-$/ PE-Cy7$^+$ population (CD8$^+$ T cells), we subsequently gated for FITC expression (PKH67-labeled melanoma cells or melanosomes). Two subsets were defined: FITC$^+$ (CD8$^+$ T cells attached to melanoma cells or melanosomes) and FITC$^-$ cells (CD8$^+$ T cells). These subsets were sorted separately into collection tubes containing FBS-coated sorting buffer and immediately processed for downstream applications. Appropriate single-stain controls were included for all fluorophores to ensure accurate compensation and gating.

Single-cell RNA and TCR sequencing

Sorted cells were washed and resuspended in PBS supplemented with 0.5% BSA to achieve optimal concentration of approximately 1400 cells/uL. Cells were manually counted on hemocytometer and viability assessed with Trypan Blue. 20,000 cells were loaded on GEM-X Chip v3 (10x Genomics, Cat#PN-1000699). Libraries were prepared at the Single-Cell Genomics Core, Research Infrastructure Core Facilities, Gray Faculty of Medical & Health Sciences, Tel-Aviv University, using the 10x Genomics Chromium X instrument in conjunction with the single cell 5′ v3 kit, protocol revision A (CG000733). The concentration of the libraries was determined by Qubit assay, and the size distribution was assessed using Agilent 4200 TapeStation system. Sequencing was performed on Illumina

NovaSeq X Plus and NextSeq2000, following the manufacturer's instructions outlined in the 10X Genomics user guide. Single-cell RNA-seq can be found at GEO: GSE309733, and TCR-seq can be found at ENA: PRJEB102639.

Bioinformatic analysis

The Seurat package in R[122] was used for downstream analysis and visualization. Log normalization was used to normalized the reads. Dimension reduction was done using PCA. Clustering was done using KNN graph and visualization and non-linear reduction was done using UMAP. Marker genes were found by performing differential expression based on the non-parametric Wilcoxon rank sum test (Seurat default).

Single-cell gene signature scoring

Single-cell gene signature scoring was done as described previously.[123] Briefly, as an initial step, to remove bias towards highly expressed genes, the data was scaled using z-score across each gene. For a given gene signature (list of genes), a cell-specific signature score was computed. Scores were computed by first sorting the normalized scaled gene expression values for each cell followed by summing up the indices (ranks) of the signature genes.

Statistical analysis and visualization of TCR-seq

Statistical analysis was performed using R Software. We used the following packages: 'scRepertoire' (), 'ggpubr'(), 'ggplot2'(),'ggvenn'(), 'dplyr'() for TCRseq visualization.

Cryo Electron Microscopy

Plunge Freezing

FACS-sorted CD8+ T cells coupled with melanosomes from patients (3.5 μl) were mixed with 1 μl of gold beads (15 nm) and applied to glow-discharged holey carbon R2/2 Cu 200-mesh grids with a SiO_2 support (Quantifoil, Q2100R2S) pre-coated with Type I collagen (Rat Tail; EMD Millipore 08-115) to promote cell adherence. The grids were then blotted and vitrified by rapid plunging into liquid ethane using a Leica EM GP automatic plunger (Leica Microsystems), under controlled conditions of 4°C and 90% humidity. The frozen grids were stored in liquid nitrogen until further use.

Cryo Transmission Electron Microscopy

Data were acquired on a Titan Krios G3i (Thermo Fisher Scientific) operated at 300 kV with a K3 direct electron detector (Gatan) in counting mode. The nominal magnification yielded a calibrated pixel size of 1.60 Å/pixel and a target defocus range of 3–5 μm.

Confocal microscopy

Confocal 4-chamber plate was coated with poly-L-lysine (PLL; Sigma, Cat#P1399-25MG), incubated at 37°C for 1 hour, washed twice with DPBS (Gibco, Cat#14190-094), and stored at 4°C until use. Unsorted and sorted samples of TILs from human patients (anti-CD8 antibody, BioLegend, Cat#344712, clone SK1; dilution 1:50) (anti-CD4 antibody, BioLegend, Cat#300552, clone RPA-T4; dilution 1:50) that were co-cultured with PKH67-labeled autologous melanoma cells or melanosomes were plated in the pre-coated 4-chamber plates and centrifuged at 300 × *g* for 10 minutes at room temperature. After centrifugation, the medium was replaced with 2% paraformaldehyde (PFA) in DPBS, and cells were fixed for 30 minutes. Following fixation, cells were washed twice with DPBS and stored in PBS in 4°C in dark until imaging. Imaging was performed using a Zeiss LSM800 confocal laser scanning microscope, and data were analyzed using ZEN software (Carl Zeiss Microscopy). In the pictures $CD8^+$ T cells were marked in red, CD4+ T cells in blue, and melanoma cells or melanosomes cells were marked in green.

Confocal microscopy Image analysis for unsorted and sorted human samples

Image analysis was performed using ZEN software (Carl Zeiss Microscopy). To enhance clarity, color correction and contrast adjustments were applied to improve the identification of T cells and melanosomes. CD4+ and $CD8^+$ cells were manually counted based on the following criteria: cells with a clearly defined oval shape and a darker center were included, while partially cropped cells were excluded unless they contained at least one attached melanosome. Each counted cell in every image was assigned an ascending number. After the initial count, each cell was re-evaluated to determine the number of cells attached by melanosomes, and this number was recorded alongside the cell's identifier. Cells that did not meet the inclusion criteria upon re-evaluation were marked with a "X". Melanosomes were considered as attached if they appeared as distinct, bright green dots that conformed to the circular shape of the T cell and remained visible even after contrast reduction. For statistical analysis, a total of 5, 3, and 2 images were analyzed for patients #129, #96, and #34, respectively. ****p <0.0001; Kruskal-Wails test.

Image analysis for Immunofluorescence analyses

One representative image was used per patient, for a total of three images, each containing an average of 40 cells. The images included staining for $CD8^+$ (red), HMB45 (pink), GPNMB (green), and DAPI (blue). Manual cell counting was conducted based on the following criteria: (1) Presence of a red oval or circular shape, (2) A blue DAPI-stained nucleus at the center of the shape, (3) A high concentration of green signal overlapping with red (appearing as yellow) was considered indicative of an $CD8^+$ cell interacting with melanosomes, (4) Cells partially cropped by the image boundaries were excluded, unless at least one attached melanosome was present. In each image, each cell was marked with individual number according to the criteria mentioned above. After the initial count, each cell was re-evaluated and circled in yellow. Cells that did not meet the inclusion criteria upon re-evaluation were crossed out. ****p <0.0001; Kruskal-Wails test.

Please cite this article in press as: Chemla et al., HLA export by melanoma cells decoys cytotoxic T cells to promote immune evasion, Cell (2026), https://doi.org/10.1016/j.cell.2025.11.020

Quantification of melanosomes secretion amount

Human melanoma cells from melanoma patients were counted and seeded in a T75 flask containing vesicle-free melanoma medium. After four days of culture, conditioned medium was collected, and the melanoma cells were detached and counted again to determine final cell numbers. Melanosomes were isolated from the conditioned medium, and their concentration (particles/mL) was measured using nanoparticle tracking analysis (NanoSight). To calculate the melanosomes secretion rate for each patient, a normalization formula was applied that accounted for the initial and final cell counts, assumed exponential growth, incubation time, and vesicle concentration. The final output was expressed as the number of vesicles secreted per cell per day.

Vesicle secretion was calculated with the following assumptions:

Cells grow exponentially in a dish for 4 days

$$N(t = 0) = 7 \times 10^6$$

$$N(t = 4) = 14 \times 10^6$$

Total number of vesicles after 4 days V_{Tot} is measured to be $\sim 10^7$

We assume that cell cells secrete vesicles at a constant rate of $S \frac{vesicles}{cell \cdot day}$

Hence, the total number of vesicles is simply the sum (or integral) over all cells multiplied by the secretion rate, namely:

$$\int_0^4 N(t) S dt = V_{Tot}$$

The growth rate can be estimated from the doubling time, which for 4 days is. This rate is:

$$r = \frac{ln\ 2}{4}$$

From the growth rate and the total number of vesicles, the secretion rate can be extracted. S is constant and can be taken out of the integral:

$$S = \frac{V_{Tot}}{\int_0^4 N(t) dt}$$

Assuming exponential growth:

$$N(t) = N_0 e^{rt}$$

The expression becomes:

$$\int_0^4 N(t) dt = \frac{1}{r} N_0 \left(e^{4r} - 1\right) = \frac{ln\ 2}{4} \cdot 7 \times 10^6$$

And the secretion rate is:

$$S = \frac{10^7}{\frac{ln\ 2}{4} 7 \times 10^6} = \frac{40}{7\ ln\ 2} \cong 8.2\ \frac{vesicles}{cell \cdot day}$$

Expression of activation and exhaustion markers in TIL

To verify TIL activation and exhaustion levels, we co-cultured them with autologous or HLA-A*02:01-matched melanoma cells, as well as with mismatched melanoma cells. Co-cultures were also performed with and without melanosomes from the corresponding melanoma cells. Cells were co-cultured for 24 and 72 hours at 37°C at a 1:1 effector-to-target (E:T) ratio (1x10^5 cells each in a total of 200 μL of vesicle-free MEL medium). Following incubation, cells were collected, washed, and resuspended in running buffer (BioLegend). They were then incubated with antibodies for 30 minutes on ice, washed again, and analyzed using a MACS Quant FACS cytometer (Miltenyi Biotec). Data were analyzed using FlowJo software (FlowJo LLC, Ashland, Oregon).

The antibodies for exhaustion markers were CD3 (Pacific Blue, clone: SK7, Cat#344824), CD8 (PE/Cy7, clone: SK1, Cat#344712), CD25 (APC, clone: BC96, Cat#302610), CD28 (APC, clone: CD28.2, Cat#302912), CD223 (LAG-3) (FITC, clone: 11C3C65, Cat#369308), CD279 (PD-1) (FITC, clone: EH12.2.H7, Cat#329904) and CD366 (TIM-3) (PE, clone: F38-2E2, Cat#345006). The antibodies for activation markers were CD3 (Pacific Blue, clone: SK7, Cat#344824), CD8 (PE/Cy7, clone: SK1, Cat#344712), CD134 (OX-40) (FITC, clone: Ber-ACT35 (ACT35), Cat#350006) and CD137 (4-1BB) (APC, clone: 4B4-1, Cat#309810). All the antibodies we used are from BioLegend.

Please cite this article in press as: Chemla et al., HLA export by melanoma cells decoys cytotoxic T cells to promote immune evasion, Cell (2026), https://doi.org/10.1016/j.cell.2025.11.020

IFNγ Release Assay

TILs were co-cultured overnight with autologous melanoma cells in 96-well plates at a 5:1 effector-to-target (E:T) ratio (1x10^5 TILs and 2x10^4 autologous melanoma cells) with or without melanosomes in a total of 200 μL of MEL medium, or as indicated. Cells were centrifuged at 1500 rpm for 5 minutes. Supernatants were collected and diluted if necessary. Secreted IFNγ levels were determined by sandwich enzyme-linked immunosorbent assay (ELISA) according to the manufacturer's instructions (BioLegend, Cat#430104). Measurements were performed in triplicate.

Cell-Mediated Cytotoxicity Assay

TILs were co-cultured overnight with autologous melanoma cells at 37°C at a 5:1 effector-to-target (E:T) ratio (1x10^5 TILs and 2x10^4 autologous melanoma cells) with or without melanosomes in a total of 200 μL of MEL medium. Triplicate cultures of melanoma cells and TILs alone were also included for each patient to assess high and low lactate dehydrogenase (LDH) secretion. Cells were centrifuged at 1500 rpm for 5 minutes, and supernatants were collected. LDH, a stable cytosolic enzyme released upon cell lysis, was measured using the CytoTox 96® Assay according to the manufacturer's instructions (Promega, Cat#G1780). Measurements were performed in triplicate.

CRISPR

The CRISPR/Cas9-mediated knockout of Tyrosinase KO in B16-F10 cells was using the D10A Cas9 mutant to avoid off-target effects (Nikase system). B16-F10 cells were transfected with Tyrosinase Double Nickase Plasmid (m): sc-423566-NIC (Santa cruz biotechnology), and UltraCruz Transfection Reagent (sc-395739).

sc-423566-NIC Tyrosinase Double Nickase Plasmid (m)- A:
GCCCACCATGGATGGGTGAT
sc-423566-NIC Tyrosinase Double Nickase Plasmid (m)- B:
TGCCAACAAGTTCTTAGAGG

Transfected cells were selected in medium containing 2 μg/ml puromycin for 72 h. The surviving cells were then expanded in puromycin-supplemented medium before being sorted and plated as single cells in 96-well plates without antibiotics. After clonal expansion, loss of Tyrosinase expression was first assessed by western blot analysis.

In addition, genome editing was validated by Sanger sequencing as detailed:

(1) Genomic DNA Extraction and PCR Amplification: Genomic DNA was extracted using the DNeasy Blood & Tissue Kit (Qiagen, Cat#69504). To validate genome editing at the target site, a primer pair (5'-GCCTTCTGTGGAGTTTCCAG-3'; 5'-CCCTCCA TATTTCAGAGCCC-3') was designed to amplify a 567 base pair (bp) region encompassing the CRISPR-Cas9 cleavage site, including the PAM sequence. PCR amplification was performed using a DNA Taq polymerase (PCRBIO Taq Mix Red; PCRBIOSYSTEM, Cat#PB10.13-02) under the following conditions: initial denaturation at 98°C for 30 seconds; 35 cycles of 98°C for 10 seconds, 60°C for 30 seconds, and 72°C for 30 seconds; with a final extension at 72°C for 5 minutes.

(2) Cloning and Sanger Sequencing: PCR amplicons were purified using the QIAquick PCR Purification Kit (Qiagen, Cat#28104) and subsequently cloned into a TA cloning vector (e.g., pCR™2.1-TOPO®, Thermo Fisher Scientific) according to the manufacturer's instructions. Recombinant plasmids were transformed into E. coli competent cells, and individual colonies were picked and cultured for plasmid extraction. Purified plasmids containing cloned inserts were then subjected to Sanger sequencing using vector-specific primers. Sequence data were aligned to the reference genome to identify insertions or deletions (indels) at the CRISPR-Cas9 target site. Successful editing was confirmed by the presence of sequence disruptions at or near the predicted cut site. Clones were selected upon complete absence of wild-type Tyrosinase alleles and were cultured for 10 days (five passages) at sub-confluency in antibiotic-free medium before being used for subsequent assays.

CyTOF

Staining Procedure for Mass Cytometry

Purified antibodies were obtained from commercial vendors and labeled with metal isotopes using the MAXPAR™ X8 chelating polymer kit (Standard BioTools, Cat#201144A) following the manufacturer's instructions. A full list of antibodies, their elemental isotope tags, clone, and source are listed in the key resources table.

Tumors were dissected and broken down into a single cell suspension with approximately 3 million cells per sample were used for staining with isotope-labeled antibodies. For viability staining, cells were washed with CSM and incubated for 15 min in 500 μl of 250 nM Rhodium solution (Standard BioTools, Cat#201103A) at RT, following washing. The antibodies to surface proteins were added in a total reaction volume of 100 μl; the cells were incubated at RT for 30 min. Following incubation, cells were fixed with the Foxp3/Transcription Factor Staining Buffer Set (eBioscience, Cat#00-5523-00) as per manufacturer's instructions. The samples were then stained intracellularly for 60 min, washed and fixed in 1.6% PFA for 10 additional min. Thereafter, washed and resuspended in 125nM Ir DNA intercalator (Standard BioTools, Cat#201192B), incubated overnight at 4 °C. Prior CyTOF acquisition, samples were

Please cite this article in press as: Chemla et al., HLA export by melanoma cells decoys cytotoxic T cells to promote immune evasion, Cell (2026), https://doi.org/10.1016/j.cell.2025.11.020

washed once in CSM, and twice more in Cell Acquisition Solution (Standard BioTools, Cat#201240). Next passed through a cell strainer and spiked each sample with internal metal isotope normalization beads and acquired on a Helios mass cytometer (Standard BioTools) at a rate of 250-300 events per second.

Preliminary data filtration

Acquired data was signal normalized and concatenated using the Helios Software (Standard BioTools) and uploaded into Cytobank (Cytobank Inc.) for further QC data processing. Gaussian parameters of the Helios system were used for doublet exclusion, Ir+ and Rh- were used for gating out of dead cells and normalization beads. Data was transformed using an arcsinh(X/5) transformation. Single live intact cells were then used for data analysis.

Mass Cytometry

Data were acquired using a CyTOF mass cytometry system (Fluidigm) and uploaded to the Cytobank web server. $CD45^+$ live cells were analyzed, and the gated cells were segregated into subpopulation clusters by expression markers. Data analysis was performed using UMAP and FlowSOM algorithms for unsupervised analysis and a traditional flow cytometry gating strategy for supervised analysis on the Cytobank server. After removal of dead cells, $CD45^-$ cells, and low-quality events, the $CD45^+$ population was divided into Myeloid cells (CD45+/CD11b+/IgM-/CD3-) and Lymphocytes (CD45+/CD11b-/CD11c-/GR1-). Each group was then divided into the major immune cells populations (T cells, B cells, Dendritic cells, Macrophages and other cells). Supervised analysis was performed for each sub-population using only markers relevant for each cell type (See Key Resources Table) and visualized using the UMAP dimensional reduction algorithm. Additionally, un-supervised analysis was performed on both myeloids and lymphocytes using the FlowSOM clustering algorithm, then visualized using UMAP.

Mitochondrial activity assay

Mitochondrial activity and mass were assessed by flow cytometry. Mitochondrial membrane potential was measured using TMRE staining (Abcam, Cat#ab113852), and mitochondrial mass was measured using MitoTracker™ Green FM (Thermo Fisher Scientific, Cat#M7514) staining. The ratio of TMRE to MTG Mean Fluorescence Intensities (MFI) was calculated for each sample to represent mitochondrial activity per mitochondrion.

Spatial proteomics

Spatial proteomics of sentinel lymph nodes was taken from Amitay et al.[101] A total of 18 patients with lymph node metastases were taken for the analysis. For each patient, we quantified the mean normalized expression of MelanA and SOX10 in all tumor cells, and the mean normalized expression of TIM-3 in all $CD8^+$ T cells residing within the tumor macroenvironment. The tumor macroenvironments were defined by Amitay et al. Tumor macroenvironments containing less than 100 cells or less than 10 infiltrating $CD8^+$ T cells were excluded from the analysis. Correlation and corresponding p-values were calculated using Pearson correlation.

QUANTIFICATION AND STATISTICAL ANALYSIS

Statistics

Statistical analyses were performed using GraphPad Prism version 10.0.0 for Windows, GraphPad Software, Boston, Massachusetts USA, www.graphpad.com. Specific statistical analyses employed are indicated in figure legends.

Immunopeptidomics statistical analyses

All immunopeptidomic statistical analyses were performed with R. All statistical tests used in the study were two-sided tests. Assumptions and multiple comparisons corrections were tested (or corrected) for each reported statistic by the Shapiro test, Levene's test, and Bonferroni correction, as described above. Standard errors of the mean are shown as error bars. Null hypothesis testing statistics are described in the figure legend, while confidence intervals and estimation of effect size (calculated by Cohen's D for FS reporter experiments) are not shown.

Proteomics Gene Ontology enrichment analysis

The filtered peptidomics data were used to generate the lists of genes for enrichment analysis. Any peptide identified in melanosome-IFN sample at least once and not in melanosome-control was kept. Subsequently, redundancy was removed between the associated genes of these peptides. The same process was applied to the whole-cell IFN versus control samples. The final two list of genes were used to identify GO enrichment using "enrichplot" library in R.

The differentially expressed gene list (2366 genes) in responders versus non-responders between pre- and on-therapy of nivolumab (from Riaz et al.[27]) was taken and the top 200 genes (up-regulated in non-responders) and bottom 200 genes (down-regulated genes in responders) were subjected to GO enrichment analysis (https://maayanlab.cloud/Enrichr/). The graphs represent the top six biological processes or cellular components for the indicated list. The details of the GO term, p-value, and the genes associated with the particular GO term appear in Table S2.

Please cite this article in press as: Chemla et al., HLA export by melanoma cells decoys cytotoxic T cells to promote immune evasion, Cell (2026), https://doi.org/10.1016/j.cell.2025.11.020

RNA-seq data analysis

Total RNA was extracted using TriZol (Invitrogen). Raw read quality was analyzed using FASTQC (Babraham Bioinformatics – FastQC, 2022 [https://www.bioinformatics.babraham.ac.uk/projects/fastqc/]. Adaptors were trimmed using Trimmomatic[124] with default parameters. Sequences were aligned to the human genome build GRCh38 using STAR aligner,[125] generating raw read counts and RPKM normalized matrixes.

Melanogenesis-related gene enrichment

Riaz et al. used the gene expression from the melanoma patients before and after anti-PD1 therapy with history of anti-CTLA4 or naive to anti-CTLA4 therapy.[27] Hugo et al. evaluated the gene expression profile from melanoma patients given anti- PD1 therapy.[100] The pigmentation gene list (Table S1) represents a comprehensively cross-species list of 650 genes associated with pigmentation phenotypes that was established by Baxter et al.,[126] by extensive manual curation of entries from OMIM, MGI, ZFIN, and GO. The resulting dataset includes genes both intrinsic and extrinsic to integumentary pigment cells.

TCGA data

All 469 samples from the TCGA melanoma dataset were split into two groups based on the mean gene expression level of 384 genes that are enriched for melanogenesis. The genes were identified by clustering of the 2000 most variable genes. The threshold for splitting the samples into two groups was the mean of its 5th and 95th expression percentile for the gene cluster mean.

MHC-I peptidomics immunogenicity analyses

Raw peptide sequences from HLA-peptidomics were mapped to the *Mus musculus* reference genome (GRCm39, release M27) using DIAMOND (v.0.9.14)[127] with recommended parameters. Unique peptides were identified as those exclusive to a specific condition. Up to 7 mismatches were allowed for mismatch analysis, and proteins corresponding to peptides for each mismatch level were extracted. A stacked bar plot and statistical analyses (Chi-square test) were generated using GraphPad Prism (v.8.4.3). Immunogenicity was assessed by evaluating peptide binding to MHC class I alleles using NetMHCpan (v.4.1)[111] with default settings. Peptides with %Rank scores < 0.5 were considered strong binders. Predictions were conducted for all *Mus musculus* alleles. GraphPad Prism (v.8.4.3) was used for plotting and statistical tests.

CellPress
OPEN ACCESS

Supplemental figures

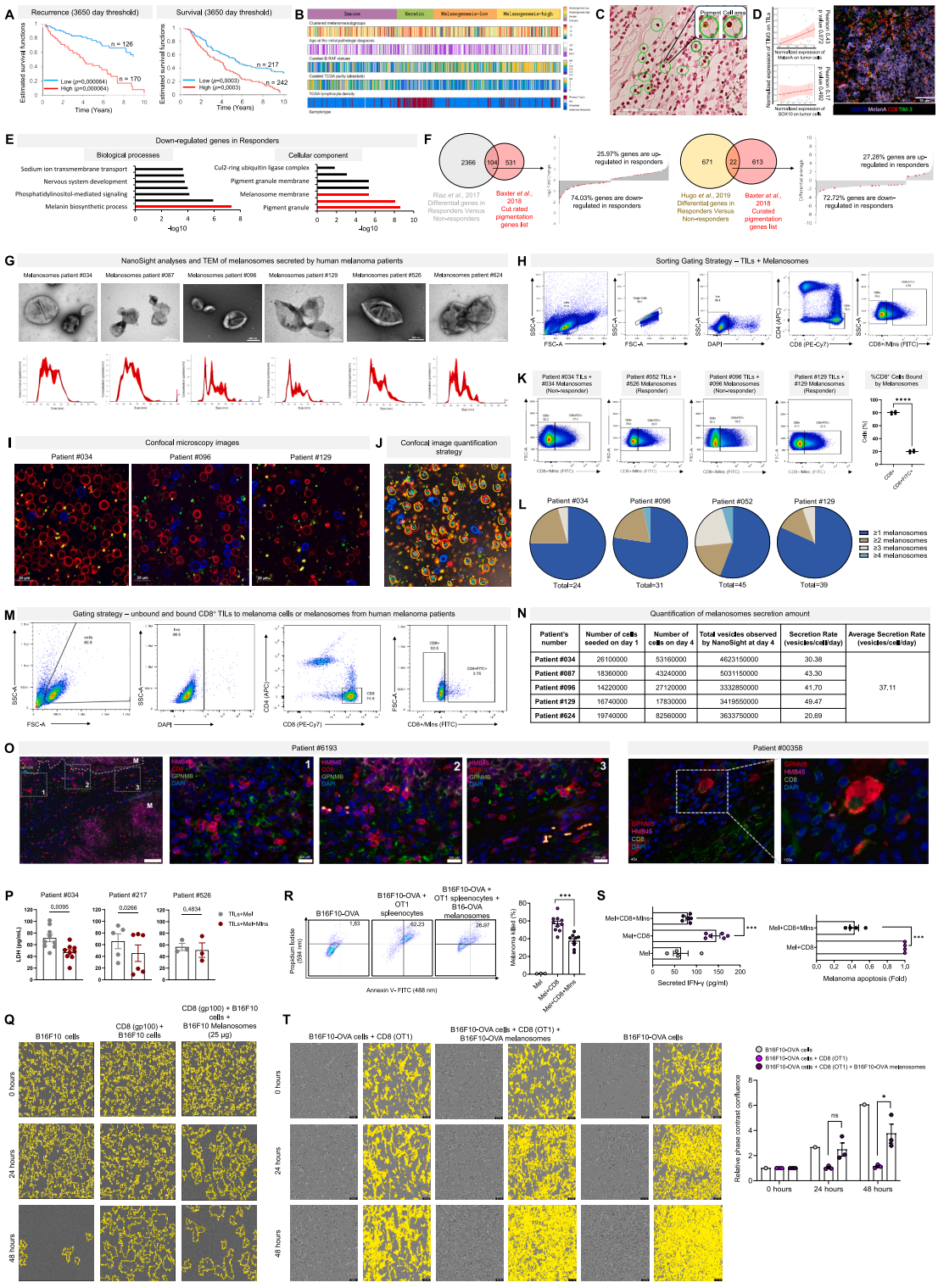

Patient's number	Number of cells seeded on day 1	Number of cells on day 4	Total vesicles observed by NanoSight at day 4	Secretion Rate (vesicles/cell/day)	Average Secretion Rate (vesicles/cell/day)
Patient #034	26100000	53160000	4623150000	30.38	37.11
Patient #087	18360000	43240000	5031150000	43.30	
Patient #096	14220000	27120000	3332850000	41.70	
Patient #129	16740000	17830000	3419550000	49.47	
Patient #624	19740000	8256000	3633750000	20.69	

(legend on next page)

Figure S1. The presence of melanosomes correlates with poor prognosis, lack of response to immunotherapy, and decreased T cell cytotoxicity, related to Figure 1

(A) Left: estimated disease reassurance for melanoma patients with high and low levels of expression of 384 melanogenesis-related genes. Right: 10-year survival estimates for melanoma patients grouped by high or low levels of expression of 384 melanogenesis-related genes. Data are from TCGA. Log-rank test.

(B) Clustering TCGA's RNA-seq of 469 melanoma samples (matrix columns) into four groups based on the 2,000 genes with the most variable expression profiles (matrix rows) using the k-means algorithm (using k = 4 for the samples and k = 5 for the genes).

(C) Representative image of the melanin and cell size quantification method.

(D) Left up: correlation between the normalized mean expression of Melan-A (melanosome marker) on tumor cells (*x* axis) and TIM-3 on CD8 T cells inside the tumor macroenvironment (*y* axis). *n* = 18 patients. Left down: the same as for Melan-A was done for $SOX10^+$ (neural crest marker) on tumor cells. Right: representative image of TME expressing Melan-A (purple) with CD8 T cell (red) infiltration expressing TIM-3 (green). Pearson correlation test.

(E) GO enrichment analysis of differentially expressed genes (2,366 genes) in responders versus NR to nivolumab (from Riaz et al.[27]). The graphs represent the top biological processes (left) and cellular components (right) for the genes downregulated in responders. Melanogenesis-related processes are marked in red.

(F) Right: overlap of genes differentially expressed in melanoma responders versus NR to immunotherapy (Riaz et al.[27]) and genes related to pigmentation (Baxter et al.[126]) and direction of change in responders for overlapping genes. Left: overlap of genes differentially expressed in melanoma responders versus NR (Hugo et al.[100]) and genes related to pigmentation (Baxter et al.[126]) and direction of change in responders for overlapping genes.

(G) NanoSight analyses and transmission electron microscopy of melanosomes secreted by human melanoma patients.

(H) FACS plots showing the gating strategy for isolation of $CD8^+$ T cells bound by melanosomes (MIns) ($CD8^+FITC^+$) and $CD8^+$ T cells ($CD8^+$) (related to Figures 1C and 5B). *n* = 4 patients.

(I) Representative confocal microscopy images of human $CD8^+$ T cells (red) and $CD4^+$ T cells (blue) co-cultured with autologous melanosomes (green). Scale bar, 20 μM.

(J) Representative confocal microscopy image showing the analysis strategy of quantifying the percent of melanosomes per $CD8^+$ T cell. $CD8^+$ T cells (red), $CD4^+$ T cells (blue), and melanosomes (green).

(K) Left: FACS plots showing $CD8^+$ T cells bound to melanoma cells or melanosomes ($CD8^+FITC^+$) and unbound $CD8^+$ T cells ($CD8^+$) populations. Right: percent of $CD8^+$ T cells attached by melanosomes. *n* = 4 patients. $^{****}p < 0.0001$; two-tailed unpaired *t* test.

(L) Confocal microscopy image analysis: distribution of melanosomes bound to $CD8^+$ T cells per patient.

(M) FACS plots showing the gating strategy for isolation of $CD8^+$ T cells bound to melanoma cells or melanosomes and $CD8^+$ T cells only from human melanoma patients after 30 min and 4 h. Related to Figure 1E.

(N) Melanosome secretion rate per cell per day of human melanoma patients.

(O) Image of melanoma specimen from a human patient stained for CD8 (T cell, red), HMB45 (melanoma cells, pink), GPNMB (melanosomes, green), and DAPI (nuclei, blue). Different regions are shown in higher magnification. Scale bar, 200 μM.

(P) Fold change in LDH (pg/ml) secretion from melanoma cells co-cultured with autologous TILs isolated from melanoma biopsy in the presence (TIL+Mel+mIns) or absence of melanosomes (TIL+Mel). Plotted are means ± standard deviations of three independent experiments. Statistical analysis performed via unpaired *t* test; error bars ± SEM.

(Q) Images of B16F10 melanoma cells co-cultured with $CD8^+$ cells of gp-100 mice (1:5 cell ratio) with or without melanosomes. Areas with no adherent cells are outlined in yellow and were used for confluency measurements.

(R–T) $CD8^+$ cells of OT1 mice were incubated with or without B16F10-OVA melanosomes (MIns) and co-cultured with B16F10-OVA melanoma cells (Mel) at a ratio of 5:1.

(R) Left: analysis of dead cells stained with propidium iodide and annexin V using FACS. Right: percent melanoma cells killed. Statistical analysis performed via unpaired *t* test; *** $p < 0.001$. Error bars ± SEM.

(S) Left: amount of secreted IFNγ. Right: fold increase in melanoma cell apoptosis relative to melanoma cells cultured alone. *n* = at least 4 per group. $^{***}p < 0.001$; two-tailed paired *t* tests. Error bars ± SEM.

(T) Left: images of B16F10-OVA melanoma cells co-cultured with $CD8^+$ cells of OT1 mice (1:5 cell ratio) with or without melanosomes for the indicated time points. Right: confluence, measured as relative phase contrast, as a function of time for indicated cultures. *n* = 3 replicates. ns indicates not significant, * $p > 0.05$; two-tailed paired *t* tests. Error bars ± SEM.

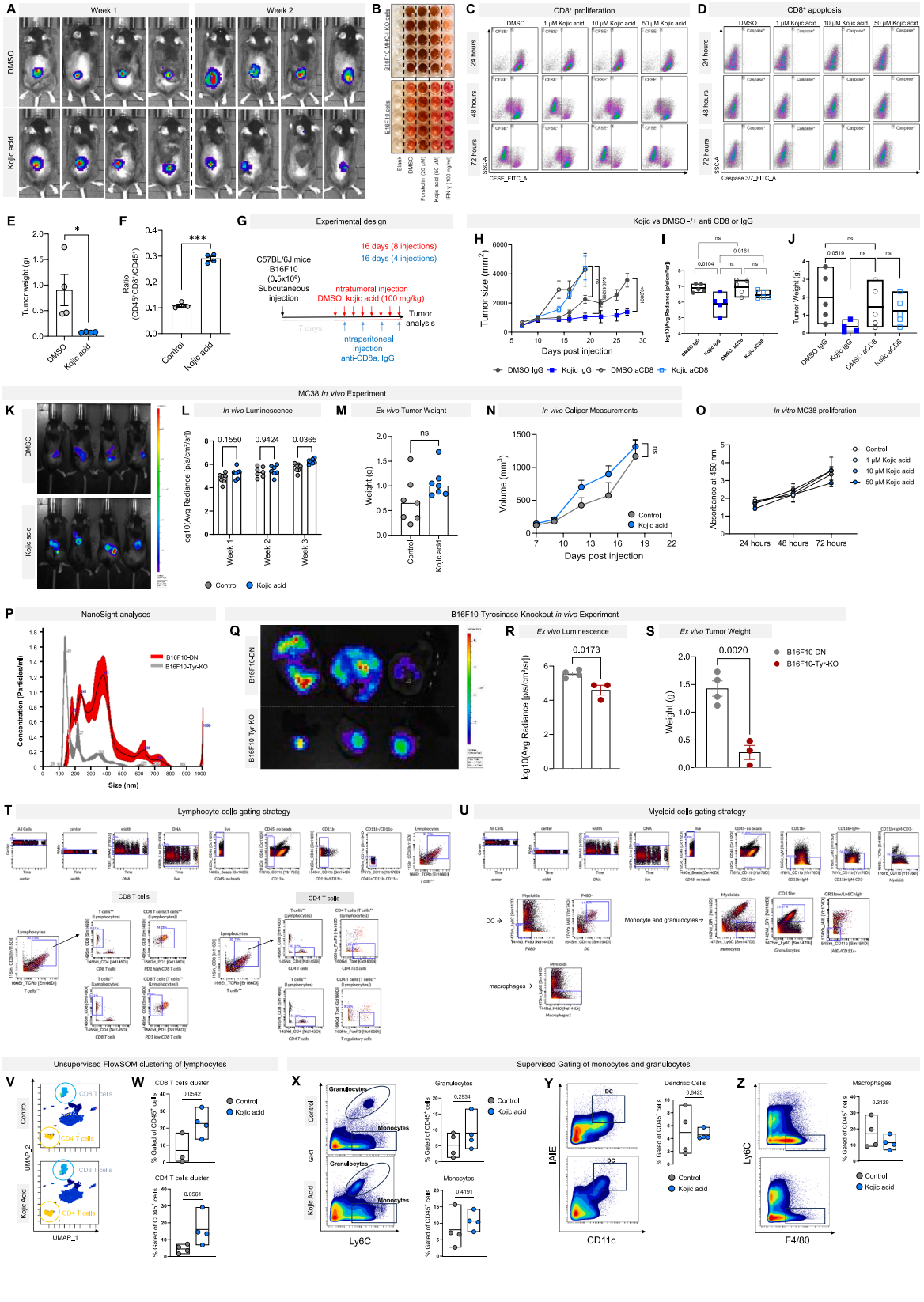

(legend on next page)

Figure S2. Inhibition of melanoma melanosome secretion blocks tumor progression and induces infiltration of CD8$^+$ T cells, related to Figure 2

(A) Images of each mouse's *in vivo* luminescence intensity at 1 and 2 weeks after tumor cell implantation.
(B) Photographs of wells containing conditioned medium from B16F10 melanoma cells or B16F10 cells lacking MHC class I upon indicated conditions for 72 h.
(C) FACS analyses of CFSE-stained CD8$^+$ T cells after indicated treatments and time points.
(D) FACS analysis for caspase-stained CD8$^+$ T cells after indicated treatments and time points.
(E) Mean weight of the primary tumors excised from mice treated as indicated. $n = 4$. *$p < 0.05$, two-tailed unpaired *t* test. Error bars ± SEM.
(F) Ratio of CD45$^+$/CD8$^+$ cells to CD45$^+$ cells isolated from tumors of mice treated as indicated. $n = 4$. ***$p < 0.001$; two-tailed unpaired *t* tests. Error bars ± SEM.
(G) Experimental scheme of Figures 2M–2O. $n = 6$ mice per group.
(H–J) Similar procedure as in (G). $n \geq 4$ mice per group.
(H) Tumor size (mm^2) measured across 3 weeks post injection. two-tailed equal variance *t* test. ns indicates not significant. Error bars ± SEM.
(I) Photon quantification of bioluminescence via IVIS of tumors *ex vivo* over the experimental time plotted as $\log_{10}$ of the average radiance. two-tailed equal variance *t* test. ns indicates not significant. Error bars ± SEM.
(J) Harvested tumor weight. two-tailed equal variance *t* test. ns indicates not significant. Error bars ± SEM.
(K–N) Mice injected with MC38 cells and treated as in (G). $n = 7$ mice per group.
(K) Representative bioluminescent images *in vivo* of mice injected subdermally with MC38 cells and then injected intratumorally with either DMSO or kojic acid.
(L) Photon quantification *in vivo* over the experimental time, plotted as $\log_{10}$ of the average radiance per mouse. Error bars ± SEM.
(M) *Ex vivo* tumor weight quantification. Statistical analysis performed via unpaired *t* test; ns indicates not significant. Error bars ± SEM.
(N) Calculated average tumor volume per group over the experimental time. Statistical analysis performed via unpaired *t* test; ns indicates not significant. Error bars ± SEM.
(O) Proliferation of the MC38 colon adenocarcinoma cells as monitored by mean absorbance over time under indicated conditions. $n = 3$. Error bars ± SEM.
(P) NanoSight analyses of melanosomes secreted by B16F10-DN and B16F10-Tyr-KO cells.
(Q–S) Mice injected with B16F10-tyrosinase double negative (DN) or B16F10-tyrosinase knockout (KO) treated as in (G). $n \geq 3$ mice per group.
(Q) Representative bioluminescent images of tumors *ex vivo* taken from mice subdermally injected with either B16F10-tyrosinase DN or B16F10-tyrosinase KO.
(R) Photon quantification of bioluminescence *ex vivo* via IVIS plotted as average radiance. Statistical analysis performed via unpaired *t* test; error bars ± SEM.
(S) *Ex vivo* tumor weight quantification. two-way ANOVA with Tukey's correction for multiple comparisons. Error bars ± SEM.
(T) Gating strategy of lymphocyte cells taken from the CyTOF.
(U) Gating strategy of myeloid cells taken from the CyTOF.
(V) Representative UMAPs of unsupervised FlowSOM clustering of lymphocyte population (CD45$^+$/CD11b-/CD11c-/GR1-/Ly6C-) (CD8 T cells in light blue; CD4 T cells in yellow).
(W) Percentage of CD8 T cells (top) from CD45$^+$ population and CD4 T cells (bottom) from CD45$^+$ population. Statistical analysis performed via unpaired *t* test.
(X–Z) Representative dot plot showing changes in granulocytes (X), monocytes (X), dendritic cells (DCs) (Y), and macrophages (Z) as a percentage of CD45$^+$ cells. $n = 4$ mice per group. two-tailed t test.

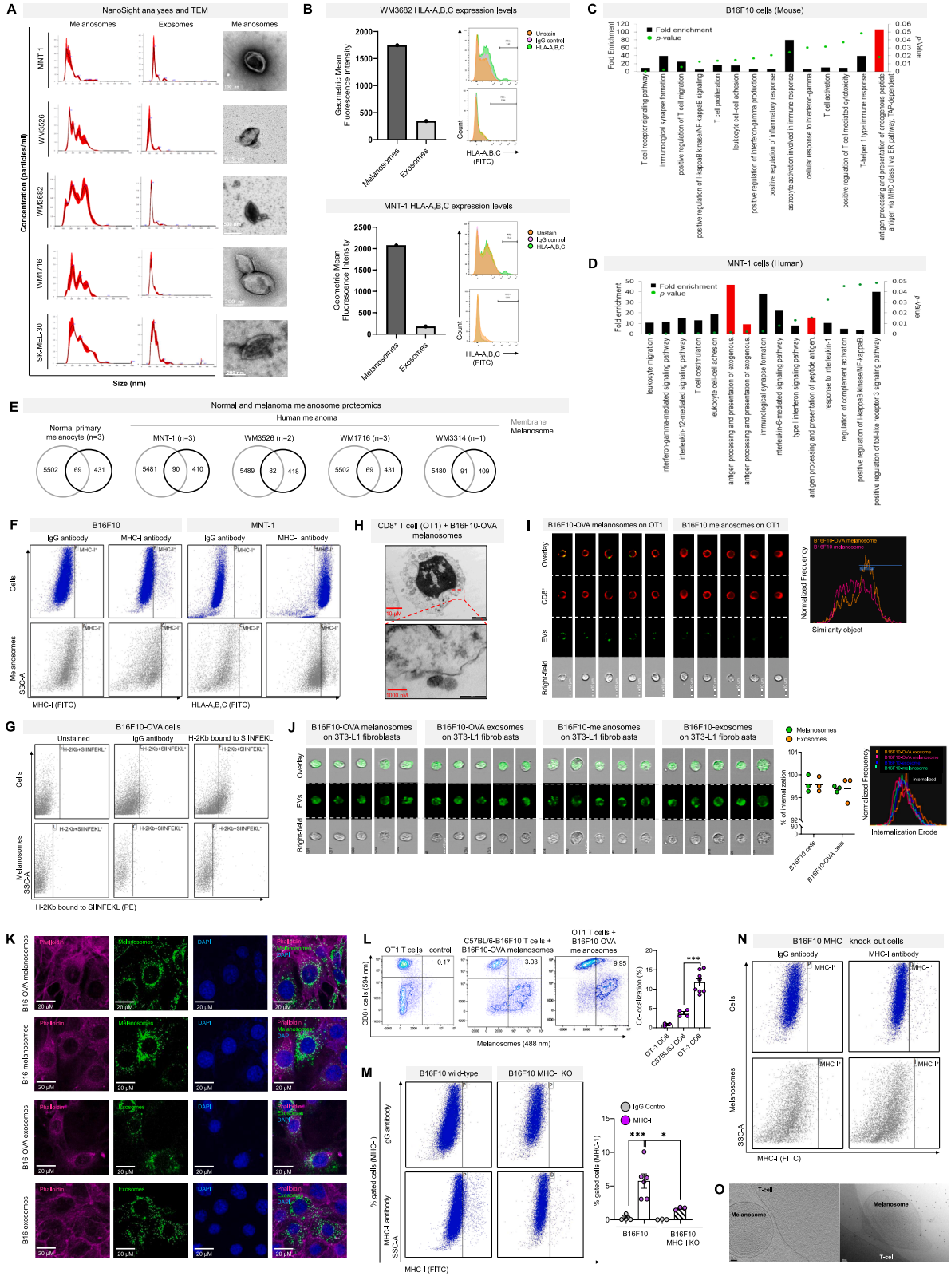

(legend on next page)

Figure S3. MHC class I on melanosome membranes binds to the TCR on CD8$^+$ T cells, related to Figure 3

(A) NanoSight analyses of melanosomes and exosomes and transmission electron microscopy of melanosomes secreted by human melanoma cell lines.

(B) Flow cytometry analysis of HLA-A, -B, and -C expression levels in melanosomes and exosomes from human melanoma cell lines.

(C and D) Fold enrichment based on GO annotation analysis of the genes that encode proteins from melanosomes secreted by (C) B16F10 and (D) MNT-1 cells and membrane genes taken from GeneCards. Green dots indicate p values < 0.05.

(E) Venn diagram of melanosomes' proteome (top 500) crossed with predicted membrane protein genes from The Human Protein Atlas (5,571 genes).

(F) Mean density plots from FACS analyses of indicated cells and melanosomes stained for the IgG (control) and anti-MHC class I or anti-HLA-A, -B, and -C antibodies (related to Figure 3D).

(G) Mean density plots from FACS analysis of B16F10-OVA cells and melanosomes incubated with OVA257-264 (SIINFEKL) peptide stained for the IgG (control) and the antibody that recognizes H-2Kb bound to SIINFEKEL (related to Figure 3E).

(H) Transmission electron microscopy of CD8$^+$ T cells from OT1 mice co-cultured overnight with melanosomes isolated from B16F10-OVA cells. Scale bars, 1 μM (upper) and 1,000 nM (lower).

(I) Left: images of melanosomes (green) isolated from B16F10-OVA (left) or B16F10 (right) cells co-cultured overnight with CD8$^+$ T cells (red) from OT1 mice. Right: co-localization frequency.

(J) Left: images of indicated EVs (green) co-cultured overnight with 3T3-L1 fibroblast cells. Right: quantification of percent intracellular or membrane localization of melanosomes. n = 3.

(K) Immunofluorescence images of 3T3-L1 fibroblasts (phalloidin, red) co-cultured overnight with melanosomes or exosomes (green) isolated from B16F10-OVA or B16F10 cells. Nuclei were stained with DAPI (blue). Scale bar, 20 μM.

(L) Left: representative FACS analyses of T cells from OT1 or wild-type mice co-cultured overnight with melanosomes secreted from B16F10 cells. Right: percent co-localization of T cells and melanosomes under indicated conditions. ***p < 0.001; two-tailed unpaired t tests. Error bars ± SEM.

(M) Left: FACS analyses of B16F10 cells or B16F10 cells lacking MHC class I stained for IgG (control) and MHC class I. Right: percentages of gated cells or melanosomes stained for IgG (gray) and MHC class I (pink). n > 3 independent samples for each experimental condition. *p < 0.05, and ***p < 0.001; two-tailed unpaired t tests. Error bars ± SEM.

(N) FACS analyses of B16F10 cells lacking MHC class I and their melanosomes stained for IgG (control) and MHC class I.

(O) Representative high-resolution microscopy image of CD8$^+$ T cell interacting with a melanosome isolated from human melanoma biopsy tissue. Scale bar, 50 nM.

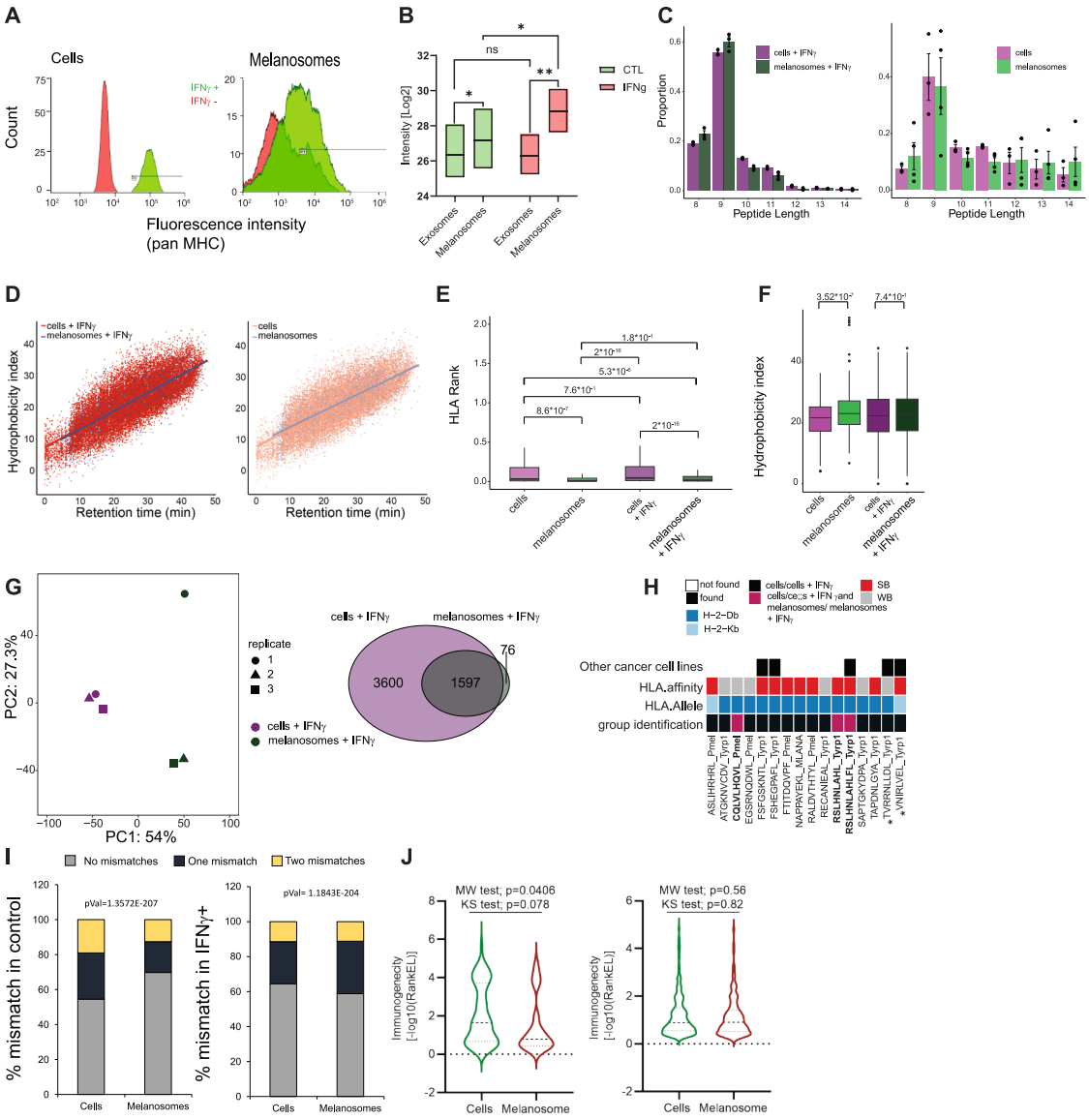

Figure S4. Immunopeptidome characterization of B16F10 melanoma cells and their secreted melanosomes, related to Figure 4

(A) Histograms depicting MHC class I surface levels on B16F10 cells (left) and derived melanosomes (right), measured by flow cytometry.

(B) Proteome analysis of HLA-A, -B, and -C presence in melanosomes and exosomes from human melanoma cell lines (WM1716, WM3526, and MNT-1). $^{*}p < 0.05$, $^{**}p < 0.01$; paired *t* test.

(C) Bar charts presenting the length distribution of MHC class I-bound peptides identified in IFNγ-treated B16F10 cells and their derived melanosomes (left; $n = 3$ biological replicates per group) and in untreated samples (right; $n = 3$ biological replicates per group). Mean ± SEM.

(D) Scatterplots of retention time versus hydrophobicity index of MHC class I-bound peptides identified in IFNγ-treated B16F10 cells and their derived melanosomes (left; r = 0.82 for both) and in untreated samples (right; r = 0.81 and r = 0.78, respectively).

(E) Boxplots presenting the rank percent of peptides predicted to bind the MHC class I alleles presented by B16F10 cells and their derived melanosomes. *p* values were obtained using pairwise *t* test followed by Bonferroni correction. Boxes represent the interquartile range (IQR) and median rank percent, and whiskers extend to ±1.5 IQR.

(F) Boxplots of the hydrophobicity index of each peptide detected in B16F10 samples. *p* values were obtained using pairwise *t* test followed by Bonferroni correction. Boxes represent the IQR and median rank percent, and whiskers extend to ±1.5 IQR.

(G) Principal-component analysis (PCA) of IFNγ-treated B16F10 cells ($n = 3$) and their derived melanosomes ($n = 3$; left) and Venn diagram showing the overlap of peptides identified in the two sample groups (right).

(H) Heatmap of tumor-associated antigen (TAA)-derived peptides identified in B16F10 samples. Each column represents a peptide. The top annotation row indicates prior detection in other cancer cell line immunopeptidomics datasets (black, detected; white, not detected), and asterisks mark peptides also identified in healthy tissues (murine MHC Atlas). The bottom annotation row indicates whether peptides were detected in B16F10 cells only (black) or in both cells and

(legend continued on next page)

melanosomes (magenta). The main heatmap shows the best predicted MHC class I allele for each peptide (color-coded) and predicted binding affinity (strong binders [SBs] in red; weak binders [WBs] in gray).

(I) Number of peptides isolated from B16-F10 cells and melanosomes treated with IFNγ or vehicle with indicated numbers of mismatches to the mouse genome. Significance was determined by the chi-squared test.

(J) Peptide immunogenicity evaluated by non-parametric analysis as the mean of ranks. $p = 0.068$ as analyzed by the Mann-Whitney test and $p = 0.03$ as analyzed by the Kolmogorov-Smirnov test.

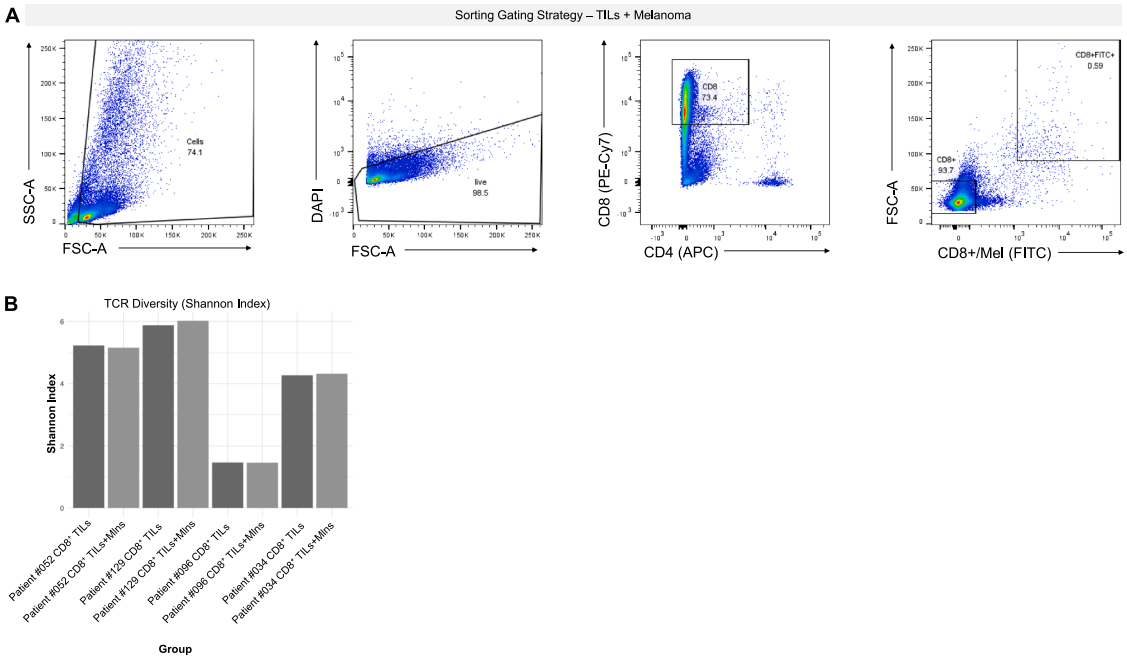

Figure S5. The majority of melanosome-bound CD8$^+$ TILs' TCRs are shared with those of melanoma-bound CD8$^+$ TILs, related to Figure 5

(A) FACS plots showing the gating strategy for isolation of CD8$^+$ T cells bound by melanoma (Mel) cells (CD8$^+$FITC$^+$) and CD8$^+$ T cells (CD8$^+$) (related to Figure 5B). n = 4 patients.

(B) Bar plot showing TCR diversity of CD8$^+$ TILs that were bound by melanosomes (CD8$^+$ TILs+MIns) or free (CD8$^+$ TILs), shown per patient.

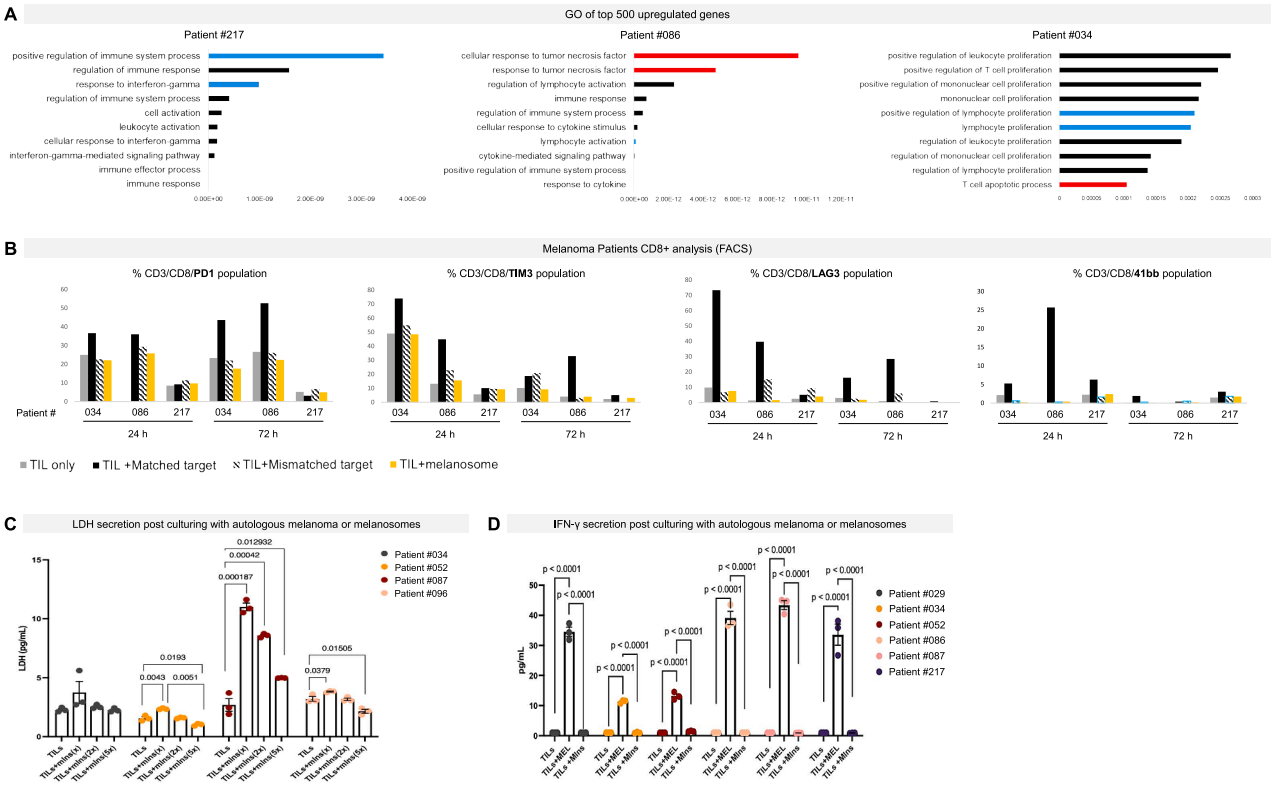

Figure S6. Melanosome binding to CD8$^+$ T cells induces a non-optimal transcriptional profile, reduces TCR signaling and mitochondrial activity, and leads to apoptosis, related to Figure 6

(A) Gene Ontology enrichment of the top 500 differentially expressed genes in melanosome-treated TILs demonstrating positive (blue) and negative (red) regulation of the immune response of each patient.

(B) Percent of CD8$^+$ T cells expressing the indicated markers post incubation with autologous melanosomes isolated from human melanoma biopsy. n = 3 patients.

(C) LDH secretion (pg/ml normalized to fold change) by human TILs treated with a decreased dose of autologous melanosomes (MIns). Two-way ANOVA. Error bars ± SEM.

(D) IFNγ secretion (pg/ml normalized to fold change) by human TILs treated with autologous melanoma (MEL) or melanosomes (MIns). Two-way ANOVA. Error bars ± SEM.